UNIVERSITÉ DU QUÉBEC À CHICOUTIMI

MÉMOIRE PRÉSENTÉ À

L'UNIVERSITÉ DU QUÉBEC À CHICOUTIMI

COMME EXIGENCE PARTIELLE

DE LA MAÎTRISE EN INGÉNIERIE

PAR

Ying Huang

PROTECTION OF METAL AND ALLOY SURFACES USING

CORROSION RESISTANCE NANOSTRUCTURED

SUPERHYDROPHOBIC COATINGS

JANVIER 2012

PROTECTION DES SURFACES MÉTALLIQUES ET D'ALLIAGES EN UTILISANT UNE RÉSISTANCE À LA CORROSION DE REVÊTEMENTS NANOSTRUCTURÉS SUPERHYDROPHOBES

RÉSUMÉ

Les surfaces superhydrophobes, lesquelles démontrent une forte déperlance de l'eau, sont récemment devenues un domaine très populaire en raison de leur importance scientifique et technologique ainsi que leur large gamme d'applications dans divers domaines. La préparation des surfaces nanostructurées superhydrophobe nécessite à la fois une rugosité optimale et une faible énergie de surface et, par conséquent, les surfaces superhydrophobe sont classiquement préparées employant deux étapes: une surface rugueuse et abaissant son énergie de surface.

Dans notre travail actuel, le processus de fabrication de surfaces de cuivre superhydrophobe est simplifié en une simple étape. L'application d'une tension continue entre deux plaques de cuivre immergé dans une solution diluée d'acide stéarique éthanolique transforme la surface de l'électrode de cuivre anodique en superhydrophobe due à la formation de micronanofibres de stéarate de cuivre à faible énergie de surface, tel que confirmé par rayons X diffraction (XRD) et microscopie électronique à balayage (MEB). L'augmentation du potentiel de modification, ainsi que la temps de modification conduit à l'augmentation de la valeur de la faible énergie de surface des micronanostructures ainsi que l'augmentation de la superhydrophobicité des surfaces telle que mesurée par l'angle de contact de l'eau.

Les surfaces nanostructurées superhydrophobes en alliage d'aluminium ont également été préparées par une procédure semblable comme il a été effectué sur les surfaces en cuivre. Cependant, les surfaces en alliage d'aluminium modifiées à l'acide stéarique n'ont pas montré les propriétés superhydrophobes. Par conséquent, les surfaces en aluminium sont d'abord revêtues de films en cuivre suivi par la modification électrochimique avec une solution d'acide stéarique. Le cuivre se développe que sur les surfaces des micropointes d'Al d'alliage AA6061. Les densités de surface des micropoints sont augmentées avec l'accroissement des potentiels négatifs. D'autre part, leurs tailles ainsi que les distances entre les micropointes sont réduites avec l'augmentation des potentiels négatifs du dépôt.

L'angle de contact des surfaces, les rugosités du film de cuivre électrodéposé suivi par la modification électrochimique augmentent à l'augmentation des potentiels négatifs de dépôt de cuivre. Les films de cuivre modifiés à l'acide stéarique déposés à -0.6 V fournissent une rugosité de surface de 6.2 μm avec un angle de contact de l'eau de 157 ° offrant des propriétés superhydrophobes des surfaces en alliage d'aluminium AA6061.

La prévention de la corrosion des surfaces superhydrophobes des alliages de cuivre et d'aluminium a été ensuite analysée par tests en laboratoire de corrosion ainsi que par les courbes de polarisation des surfaces avec différentes propriétés superhydrophobes. La diminution de la densité de courant de corrosion ainsi que l'augmentation de la résistance de polarisation montre que la surface du cuivre superhydrophobe est plus stable par rapport à la surface de cuivre dans l'environnement corrosif. Les deux Cu superhydrophobes et les surfaces en alliage Al AA6061 montrent propriétés anticorrosion. Toutefois, les surfaces en cuivre superhydrophobe sont plus

stables que les surfaces superhydrophobe alliage Al AA6061 tel que préparé dans nos études.

ABSTRACT

Superhydrophobic surfaces, which demonstrate high water-repellency, have recently become a very popular field because of its scientific and technological importance and wide range of applications in diverse areas. Preparation of nanostructured superhydrophobic surfaces requires both an optimum roughness and low surface energy; therefore, superhydrophobic surfaces are conventionally prepared employing two steps: roughening a surface and lowering its surface energy.

In our present work, the fabrication process of superhydrophobic copper surfaces is simplified as just one-step. The application of a direct voltage between two copper plates immersed in a dilute ethanolic stearic acid solution transforms the surface of the anodic copper electrode to superhydrophobic due to the formation of micro-nanofibors low surface energy follower-like copper stearate as confirmed by X-ray diffraction (XRD) and scanning electron microscope (SEM), respectively. The increase of the modification potential as well as the modification time leads to the increase of the amount of the low surface energy micro-nanostructures as well as the increase of the superhydrophobicity of the surfaces as measured by water contact angle.

The nanostructured superhydrophobic aluminum alloy surfaces have also been prepared by the similar procedure as it was performed on copper surfaces. However, stearic acid modified aluminum alloy surfaces didn't show the superhydrophobic properties. Therefore, the aluminum surfaces were firstly coated with copper films followed by electrochemical modification with stearic acid solution. The copper grows as microdots on AA6061 Al alloy surfaces. The surface densities of the microdots increase with the increase of the negative deposition potentials. On the other hand

their sizes as well as the distances between the microdots reduce with the increase of the negative deposition potentials. The surface roughness and water contact angle of electrodeposited copper film followed by electrochemical modification in ethanolic stearic acid solution increase with the increase in negative copper deposition potentials. The stearic acid modified copper films deposited at -0.6 V provides a surface roughness of 6.2 μm with a water contact angle of 157 ° providing superhydrophobic properties of AA6061 aluminum alloy surfaces.

The corrosion prevention of the superhydrophobic copper and aluminum alloy surfaces were then analyzed by home-made corrosion tests as well as the polarization curves of surfaces with different superhydrophobic properties. The decrease of the corrosion current density as well as the increase of the polarization resistance shows that the superhydrophobic copper surface is more stable as compared to copper surface in the corrosion environment. Both superhydrophobic Cu and AA6061Al alloy surfaces show anti-corrosion properties. However, superhydrophobic copper surfaces are more stable than superhydrophobic AA6061 Al alloy surfaces as prepared in our studies.

谨以此文献给我亲爱的父母

ACKNOWLEDGMENTS

To start with, I would like to express my sincere and special thanks to my director, Prof. Dilip Sarkar, for his patience, guidance, encouragement and support of my research work. He always has plenty of good ideas to solve problems and I have always gained a lot of knowledge whenever I talked with him. I am so proud and privileged to work with him and learn from his expertise throughout my Masters studies.

I am extremely grateful to my co-director Prof. X.-Grant Chen, for his continuous support during my research work Thanks to his valuable instructions technical discussions and suggestions throughout this project.

Both technical and scientific discussions with Prof. Sarkar and Prof. Grant Chen made me extremely successful in demonstrating my presentation skills in conferences where the fruit of labor of my directors came out in prizes for best poster and best oral presentation winner in national conferences such as REGAL's students day.

I am also grateful to Dr. Danick Gallant as well as Yumei Han, who have offered me their time and help for the corrosion tests. I sincerely appreciate their generosity in sharing their knowledge and expertise to make me feel comfortable with this part of my thesis work.

I would like to express my sincere appreciation to Prof. Duygu Kocaefe for being present and providing her valuable comments and during my evaluation seminars as well as for providing access to measure the water contact angle in her laboratories which has an enormous contribution to my thesis completion. My sincere thanks to Xianai Huang and Sudeshna Saha, who helped me learn to use the contact angle goniometer at the early stages of my research.

I would also like to thank all my colleagues, professors and technicians in Cural for their continuous support and help throughout my Masters study. Those include Dr. Zhan Zhang, Martin Bouchard, Émélie Brideau, Pascal Vandal, Dany Racine, Emad Elgallad, Ehab Elsharkawy, Jing Lai, Mehand Tebib, Junfeng Guo, Kun Liu, Gaofeng Li, Pierre-Alexandre Minier, Peng Shen, Jian Qin, Mohammad Shakiba and Lei Pan.

I would like to specially thank Dr. Zhan Zhang, Dr. Danick Gallant, Prof. Dilip. Sarkar and Prof. X.-Grant Chen for taking their precious time off to be present in my examination committee in spite of their busy schedules.

I would also like to thank Dr. A. M. Samuel, who with lot of patience took her time to explain me things in the course works I took with her. In addition to being my class room Prof., she also continuously encouraged me in terms of developing English language skills as well as in the subject throughout my course.

I would like to specially appreciate Dr. N. Saleema who gave me plenty of support throughout my Masters research. She did so much work on the modification of my seminar reports and

presentations and showed me her experience in the experiment, which helped me feel more comfortable with the new research field that I was into for this Master study.

Also I sincerely appreciate Jean-Denis Brassard for his help in the French learning, during my research period and for correcting the French abstract of my thesis.

I would like to express my warmest and deepest appreciation to my dear parents, my father and my mother for their never-ending support, understanding and patience in all the situations. Whenever I came across any kind of difficulties, they always say "you can do it" to encourage me.

Cangji Shi, my forever love, is a very important contributor to the successful completion of my thesis. Thanks for his suggestion during the research, his encouragement, his affection, and his love. Thanks for everything he did for me.

TABLE OF CONTENTS

LIST OF FIGURES

LIST OF TABLES

LIST OF EQUATIONS

CHAPTER 1

INTRODUCTION

This chapter provides an introduction to the superhydrophobicity on the metal surfaces. The hypothesis and objectives of the research project and the methodologies employed to achieve the objectives will be outlined in the following sections.

1.1   Introduction of Superhydrophobicity

The morphology and chemical composition of the solid surfaces play an important role on the corrosion resistance, and the right combination of surface properties can dramatically lower the ability of water drops to stick [1] and hence the possible enhancement of corrosion resistance. In the review on "Non-sticking drops", by David Quéré [1] details the requirements for a water drop to slide on an inclined surface on the basis of the water contact angle (CA, see section 2.1.3) and the contact angle hysteresis (CAH). The CAH is defined as the difference between the advancing and receding CAs of water obtained on a surface during the motion of a water drop in one direction [1]. Quéré states that a water drop can slide off a surface if CA is greater than 160 ° even when the CAH is higher, due to the lower contact area between the liquid and the solid. He concluded that "non-sticking" drops must therefore be observed on surfaces with CA > 160 ° and such surfaces are termed "superhydrophobic". Superhydrophobicity is observed on certain natural tissues such as lotus leaves. The so-called "Lotus effect" is due to the presence of a rough micro-nanostructure covered with waxy materials which are poorly wetting, resulting in a water contact angle greater than 150 ° [2]. The rough micro-nanostructure allows the entrapment of air beneath the water drop in the pores (troughs) of the rough structure and the waxy coating, which has a low surface energy,

1

helps to reduce the interaction of the surface with water.

Studies have been carried out in an attempt to understand the role of superhydrophobicity on corrosion prevention [3,4]. Learning from nature, a superhydrophobic surface can be obtained by creating an optimum surface roughness followed by passivation with a low surface energy coating leading to a very low area of contact between the solid surface and the liquid, causing a water drop to roll off the surface. As the contact area of water on a superhydrophobic solid surface is negligible, such surfaces would effectively reduce the contact area of water. Therefore, the superhydrophobic film can resist corrosion and protect the metals.

It is well known that, copper and its alloys have been one of the important materials in industry owing to its high electrical and thermal conductivities, mechanical workability and its relatively noble properties. It is widely used in many applications in electronic industries and communications as a conductor in electrical power lines, pipelines for domestic and industrial water utilities including seawater, heat conductors and heat exchangers [5]. Thus, corrosion of copper and its inhibition in a wide variety of media, particularly when they contain chloride ions, have attracted attention of a number of investigators [6,7,8]. In addition to copper, aluminum and its alloy are also widely used in Aerospace, marine applications, automotive applications and so on for their low density, favorable mechanical properties and relatively good corrosion resistance. Aluminum and its alloy have a natural corrosion protection from its oxide layer, but if exposed to aggressive environments it may corrode [9].

The appropriate coatings on copper, aluminum and their alloys may be reliable and add longer service life. In this work, therefore, we have fabricated superhydrophobic copper and aluminum

alloy surfaces and studied their morphological, chemical as well as their corrosion prevention properties.

The detailed background study with an expanded literature review will be provided in Chapter 2.

1.2   Hypothesis

Based on the background and literature (see chapter 2), it is well known that superhydrophobic surfaces are traditionally prepared via a two-step process: (i) creation of surface roughness (ii) passivation of the rough surfaces. However, if the creation of surface roughness and surface passivation can be accomplished simultaneously in one-step, it could simplify the complexity of using two different procedures as used in the conventional two-step method in making surfaces superhydrophobic. In this research project, one-step process was used to prepare superhydrophobic copper surfaces and two-step processes comprising electrochemical deposition and electrochemical modification were used to prepare superhydrophobic aluminum surfaces.

Corrosion behavior on surfaces caused mainly by their contact with wet environments can be effectively reduced or even eliminated completely by making the surfaces superhydrophobic where water wouldn't stick, thereby repelling wet corrosive substances.

1.3   Main objectives

Based on the background, the superhydrophobic copper and aluminum surfaces will be fabricated and the feasibility of the corrosion prevention of the superhydrophobic surfaces will also

be explored. The main objectives of this research project are as follows:

Preparation of superhydrophobic copper surfaces by one-step process via a chemical route under the influence of electric field;

Electroplating of copper on aluminum surfaces and their electrochemical modification to obtain superhydrophobic aluminum surfaces.

To characterize these surfaces by surface morphological and compositional studies as well as to study their wetting characteristics;

To study the dynamics of corrosion behavior on the superhydrophobic surfaces as compared with their hydrophilic counterparts.

1.4   Methodology

The major procedures of this research work consist of the following steps:

Fabrication of nanostructured superhydrophobic copper surfaces: A one-step process of electrochemical deposition technique is applied to fabricate superhydrophobic surface on copper substrates, a method where Cu substrates are immersed in stearic acid solution for a certain period of time in the application of DC voltage.

Fabrication of nanostructured superhydrophobic aluminum surfaces: The similar methodology to fabricate superhydrophobic copper surface is applied on aluminum substrates to obtain superhydrophobic aluminum substrates.

Fabrication of nanostructured superhydrophobic copper-plated aluminum surfaces: Copper deposited on aluminum substrates under certain potential as the first step followed by electrochemically modification copper-plated aluminum surface with stearic acid as the second step.

The prepared superhydrophobic surfaces will be exposed to corrosive environments (3.5 wt. % NaCl solution) in a simulated off-shore and atmospheric conditions to which many industrial and aeronautical structures are exposed. In the test, different parameters such as the superhydrophobicity of the surfaces, solution concentration, exposure time, etc., will be controlled. The potentiodynamic polarization curve is also used to investigate how different superhydrophobicity of surfaces affect the corrosion protection by means of polarization curves and polarization resistance. A visual analysis with supporting digital images of the various surfaces following exposures at varying time-frame will be performed to monitor the corrosion behavior. In addition, morphological and chemical compositional studies will also be carried out using SEM/EDS. The wettability of the surface before and after corrosion will be compared by using water contact angle measurement.

The detailed description of the experimental procedures is provided in Chapter 3.

CHAPTER 2
LITERATURE REVIEW

As part of the tasks of this Master's research project, a detailed literature review up to date has been performed on, preparation superhydrophobic coatings and their applications among which, a literature review on corrosion performance of certain materials has also been performed after the main review on the superhydrophobicity. The corrosion studies on superhydrophobic surfaces are only a kind of feasibility exploration as one of the applications of superhydrophobicity.

2.1   Wettability and Superhydrophobicity

2.1.1   Superhydrophobicity phenomena in nature

Superhydrophobicity is a technologically important property which describes the non-wetting characteristics of solid surfaces when the solid surfaces come in contact with water. The superhydrophobic properties or non-wetting properties are commonly observed on surfaces of many natural plants and insects [1,10]. Figure 2.1 shows their photos and microstructure. One of the commonly cited examples is the lotus leaf shown in figure 2.1(a). The so-called "Lotus effect", is due to the presence of a binary structure with numerous papillae, with diameters in the range between 3 to 10 μm, providing a rough micro-nanostructure (figure 2.1(b)), which in turn is covered with low surface energy waxy materials with a high degree of resistance to wetting, resulting in a water contact angle above 150 ° [11]. The rough surface enhances the entrapment of large amount of air in the gaps of the rough structure resulting in a heterogeneous composite structure and the low surface energy waxy coating reduces the affinity of water to the surface, weakening the water-solid interaction. Cassie-Baxter and Wenzel models are the two classic mathematical models which

explain the influence of roughness on wettability [12,13]. These models will be explained in detail later in the section of 2.1.4.
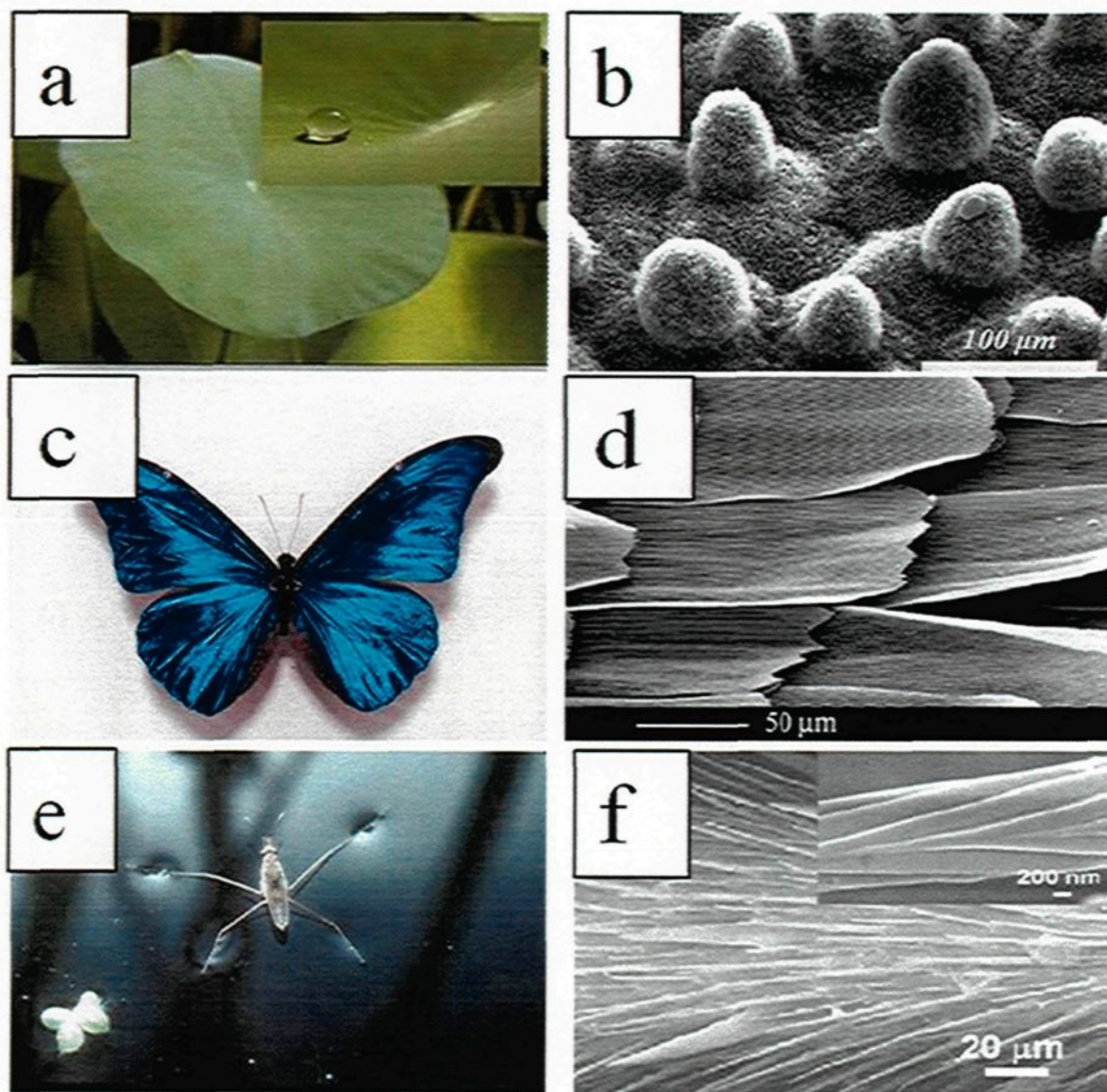
Figure 2.1(a) Water drop on a lotus leaf; (b) Microstructure of a lotus leaf; (c) A colorful picture of a butterfly and (d) the microstructure of a butterfly wing; (e) Water strider on water surface and (f) the microstructure of a water strider leg showing the special hierarchical arrangement of large numbers of oriented tiny hairs (microsetae) with fine nanogrooves coated with waxy materials.

On the surfaces of animals and insects which exhibit superhydrophobic properties, the water droplets easily roll off. For examples, butterfly wings (fig. 2.1(c)) have the special ability of

7

superhydrophobicity resulting from the direction-dependent arrangement of flexible nano-patterns on ridging nano-stripes and micro-scales overlapped on the wings at the one-dimensional level (fig. 2.1(d)) [14]. Water striders are also commonly known as shown in fig. 2.1(e), as they can easily stand and walk on water due to the special non-wetting feature of their legs. The water repellency of their legs, according to Gao and Jiang [10], is due to the special hierarchical structure of the legs, as they are covered with large numbers of oriented tiny hairs with fine nanogrooves coated with waxy materials. The microstructure of the water strider leg is shown in fig. 2.1(f).

2.1.2   The surface energy

Wetting phenomena happen where all the three states (solid, liquid and gas) are in contact, including the behaviors of intersection of three interfaces, solid-liquid, solid-vapor, and liquid-vapor. An interface is the boundary between two phases, and when one side is a vapor or gas, the other is called a surface. One important property of the surface is the extra energy associated with the surfaces, also known as surface energy.

There are two main types of solid surfaces with which liquids can interact. Traditionally, solid surfaces have been divided into high energy solids and low energy types. The relative energy of a solid has to do with the bulk nature of the solid itself. Solid such as metals, glasses, and ceramics are known as "hard solids" because the chemical bonds those hold them together (e.g. covalent, ionic, or metallic) are very strong. Thus, it takes a large input of energy to break these solids so they are termed "higher energy". Most molecular liquids achieve complete wetting with high-energy surfaces. The other type of solids is weak molecular crystals (e.g. fluorocarbons, hydrocarbons, etc.) where the molecules are held together essentially by physical forces (e.g. van der waals and

hydrogen bonds). Since these solids are held together by weak forces it would take a very low input of energy to break them, and thus, they are termed "low energy" [15].

The wettability of a surface is determined by the outermost chemical groups of the solid. Differences in wettability between surfaces that are similar in structure are due to differences in packing of the atoms. For instance, if a surface has branched chains, it will have poorer packing than a surface with straight chains.

2.1.3 Water contact angle and contact angle hysteresis

Wettability is one of the most important properties of a solid surface. Many practical applications depend on the wetting or non-wetting characteristics of the solid surface. When a water drop comes in contact with a surface, the surface is either wet or not wet depending on the hydrophilicity or hydrophobicity of the surface, respectively. Wettability is assessed by the water contact angle (CA) or θ formed by the liquid and the substrate. The degree of wetting is characterized by the angle of contact the water drop makes with the surface which is the angle at which the liquid-vapor (LV) interface meets the solid-liquid (SL) interface and the solid-vapor (SV) interface (fig. 2.2). If the surface is hydrophilic, the water drop is strongly attracted to the surface and will spread on the surface providing a contact angle close to 0 °. Less strongly hydrophilic surfaces can have a contact angle up to 90 °. If the surface is hydrophobic, the interaction forces between the water drop and the solid are weaker and the water drop will have a tendency to form a compact droplet on the surface. The contact angle on such surfaces is usually greater than 90 °. The contact angle, therefore, is determined by the strength of the interfacial forces between the water drop and the solid surface. These interfacial forces are sometimes denoted as interfacial tensions or

interfacial free surface energies.

A very basic and commonly used relation (eq. 2.1) describing wettability with respect to the contact angle of a drop in equilibrium with a solid surface was given by Young [16]. It relates the interfacial free energies of the three interfaces where drop comes into contact with, when placed on a solid surface, namely the solid/liquid (γ_{SL}), solid/vapor (γ_{SV}), and liquid/vapor (γ_{LV}) interfaces. The line of contact with the three co-existing phases of the system makes an angle of contact, θ, with the surface, as shown in figure 2.2.

$$\cos \theta = \frac{\gamma_{SV} - \gamma_{SL}}{\gamma_{LV}}$$ (Equation 2.1)
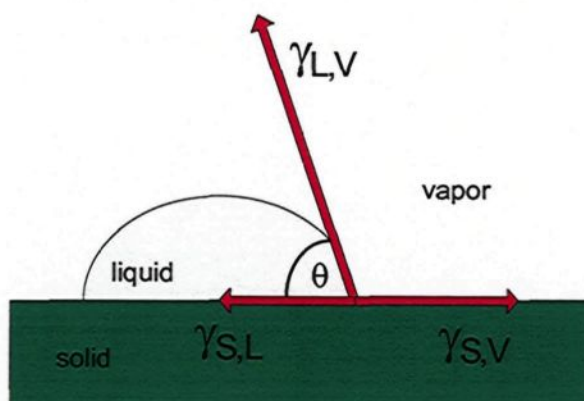
Figure 2.2 A water drop in equilibrium state on a surface, as presented by Young.

The measurement values of CA provide information regarding the bonding energy of the solid surface and the surface tension of the droplet. Because of its simplicity, CA has been broadly accepted for material surface analysis related to wetting, adhesion, and absorption. For a given liquid, a high-surface-energy solid tends to be wetted in contrast to a low-energy surface solid which does not absorb the liquid.

10

When there is a relative movement between the droplet and the surface, for instance because of the movement of the needle, as shown in figure 2.3, there will be a change in the contact angles. The contact angle hysteresis is defined as the difference between the advancing angle (θ adv) and the receding angle (θ rec), shown in eq. 2.2.

$$CAH = \theta_{adv} - \theta_{rec}$$
(Equation 2.2)
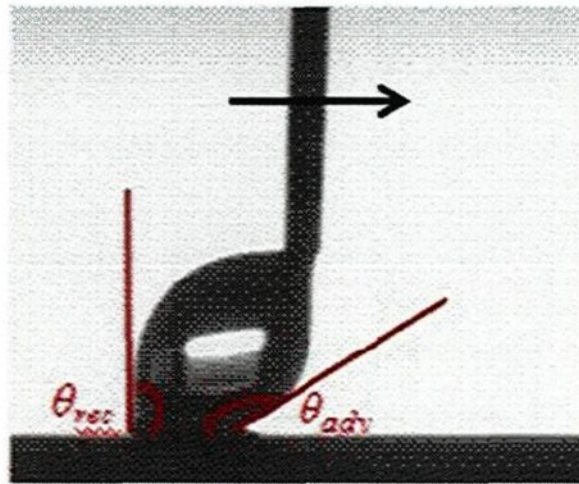
Figure 2.3 The schematic of contact angle hysteresis

2.1.4 Effect of roughness on the wettability of the surfaces

To reach contact angle values greater than 150 °, which is necessary for achieving superhydrophobicity, surface roughness is often added to enhance the hydrophobicity of the solid surface. The surface topography effects have been mathematically expressed by the Wenzel and the Cassie-Baxter equations. The Wenzel equation is expressed as:

$$\cos \theta' = R_w \cos \theta$$
(Equation 2.3)

11

where the roughness factor Rw is the ratio of the true and apparent (geometric) surface areas. According to the Wenzel model as shown in fig. 2.4(a), when the true contact angle θ of water on a smooth surface is less than 90 °, the apparent contact angle θ' is less than the true contact angle θ on a rough surface, and when the true contact angle θ is greater than 90 °, the apparent contact angle θ' is greater than the true contact angle θ on a rough surface. It has been shown that the contact angle and the contact angle hysteresis increase as the roughness factor increases [17]. However, it has also been demonstrated that the contact angle continues to increase when the roughness factor exceeds a certain level, whereas the hysteresis starts to decrease. This decrease in the CAH is attributed to a transition from the Wenzel regime to the Cassie-Baxter regime where the water drop does not penetrate the surface irregularities; rather, it stays suspended on the tips of the rough crests due to the entrapment of air pockets in those crests.
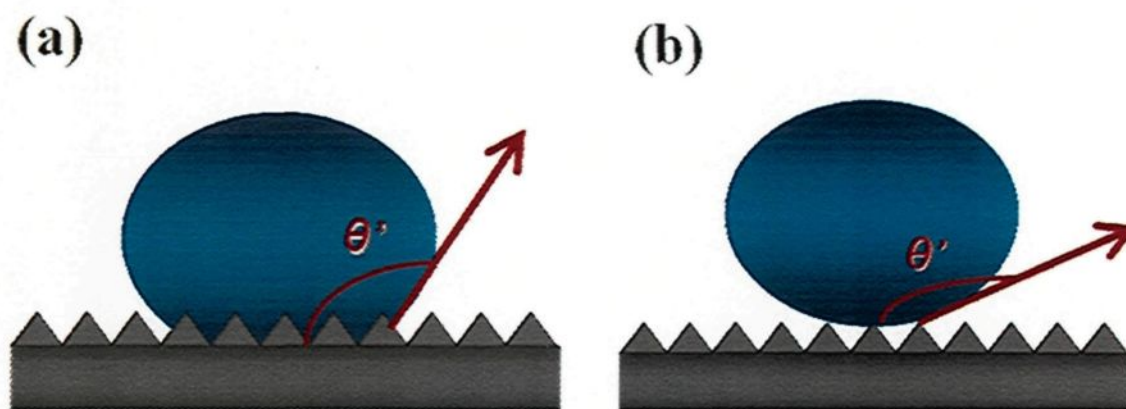
Figure 2.4 Surface topography effects on water contact angle by (a) Wenzel Model; (b) Cassie-Baxter Model.

The Cassie-Baxter model shown in fig. 2.4(b), describes the effect of roughness on chemically heterogeneous structures where the apparent contact angle is mathematically derived from the Cassie equation, as follows:

$$\cos \theta' = f_1 \cos \theta_1 + f_2 \cos \theta_2 \qquad \text{(Equation 2.4)}$$

where θ' is the contact angle of the composite surface consisting of two components with contact angles θ_1 and θ_2, and their corresponding area fractions f_1 and f_2. In such a composite system, f_1 is assumed to be the area fraction of the solid surface and f_2 is assumed to be that of air, where θ_2 is 180 °. As $f_1 + f_2 = 1$, equation 2.4 can be further modified as:

$$\cos \theta' = f_1 (\cos \theta_1 + 1) - 1 \qquad \text{(Equation 2.5)}$$

This equation explains why, on a rough surface with a large amount of air entrapment in the surface irregularities, one can obtain a highly superhydrophobic surface with a very small area fraction f_1 of the surface in contact with the water drop.

2.1.5 Applications of superhydrophobicity

A number of products using the lotus effect are already commercially available or in the process of development. Most of these applications use the high water repellent effect, especially of glasses (for architecture, automotive, optical sensor and other applications), roof tiles and other architectural materials [18]. Additionally, sprays and paints that create clean surfaces (e.g. graffiti-resistant) have been proposed, as well as self-cleaning textiles.

Some agricultural applications were also discussed, such as antibiofouling paints for boats [19], bio-chips [20], biomedical applications [21], microfuidics [22], corrosion resistance [23], eyeglasses, self-cleaning windshields for automobiles [1], stain resistant textiles [24], antisticking of snow for antennas and windows [25], expected inhibition of adherence of snow, oxidation, current

13

conduction [26] and many others. The following section includes how superhydrophobic coatings are used to improve the performance of some applications by surface modification.

2.1.5.1 Anti-icing applications

Ice buildup on overhead transmission and distribution lines may lead to mechanical line failure or insulator flashovers, entailing both power outages and often major costs. As a matter of fact, the ice storm that hit Eastern Canada in January 1998 caused several billions of dollars in damage to the power networks (fig. 2.5) and great hardship among hard-hit communities [27].

Figure 2.5 Image of fallen wood poles due to ice deposited on metal cables.

Sarkar et al. [27] mentioned that superhydrophobicity can help mitigate the ice accretion problem on power network equipment and other exposed structures by reducing ice-to-surface adhesion. As the contact area of water on a superhydrophobic solid surface is negligible, such surfaces would effectively reduce the contact area of ice as well. Therefore, ice adhesion would be significantly reduced on superhydrophobic surfaces.

2.1.5.2 Self-cleaning applications

Superhydrophobic substrates with a self-cleaning property are prepared mostly on the basis of the lotus effect of plants. As illustrated in figure 2.6, when a droplet of water rolls off the surface of a superhydrophobic substrate, it removes the dust, whereas the dust remains on the normal surfaces.
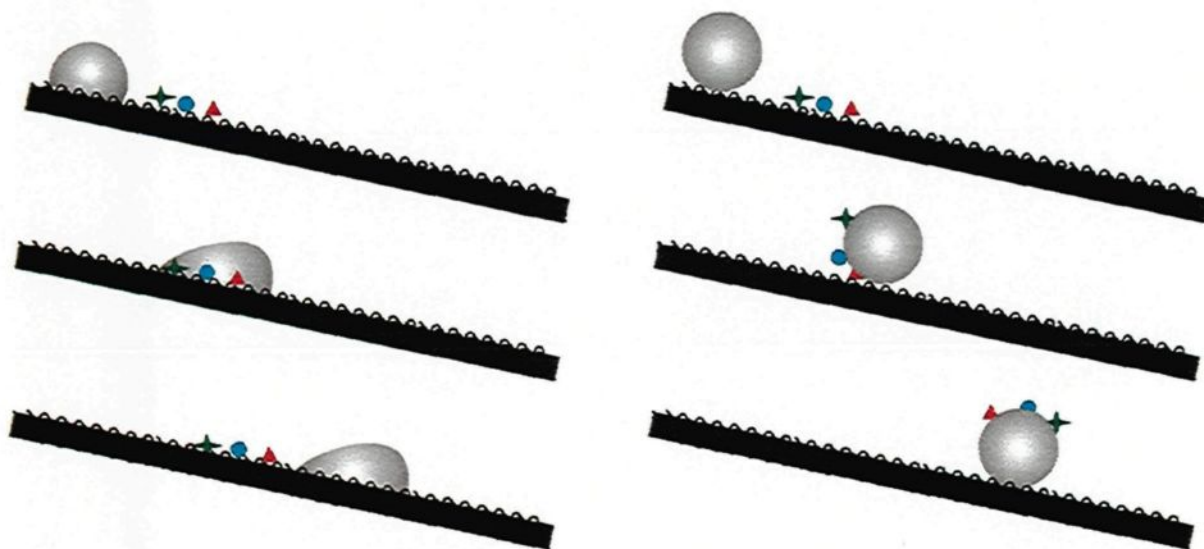
Figure 2.6 Water droplets rolling off substrates with a normal hydrophobic surface (left) and a self-cleaning superhydrophobic surface (right) through dust particles.

Superhydrophobic and self-cleaning surfaces with a high static contact angle above 150 ° and low contact angle hysteresis play an important role in technical applications ranging from self-cleaning window glasses to paints and textiles, and including low-friction surfaces for fluid flow and energy conservation [28,29,30,31].

2.1.5.3 Anti-biofouling applications

Biofouling of underwater structures and ships' hulls, in particular, increases operational and maintenance costs [32,33]. It can be reduced through underwater superhydrophobicity, i.e. forming

15

a hydrophobic rough surface that supports an air film between itself and the water [34]. The reduction of the wetted area minimizes the probability that biological organisms encounter a solid surface. The design of such surfaces should involve optimization between mechanical stability and minimal wetted area. The anti-biofouling properties of superhydrophobic coatings have been investigated [35]. Compared to normal substrates which fouled within a day, almost no micro-organisms attached to the superhydrophobic surfaces in the first weeks after immersion. Figure 2.7 shows the photo of devices under biofouling in ocean.

Figure 2.7 The photo of devices under biofouling in ocean.

2.1.5.4 Anti-corrosion applications

It is known the contact with wet environments is the most important reason which leads to the corrosion behavior happens, which can be effectively controlled by making the surface superhydrophobic, where the water is non-sticky, thereby repelling the wet corrosive substance. Figure 2.8 shows the boat which was corroded badly.

Figure 2.8 The boat where the metal has been corroded badly

2.1.5.5 Drag reduction

Turbulent flows of a liquid along a surface experience frictional drag, a macroscopic phenomenon that affects the speed and efficiency of marine vessels, the cost of pumping oil through a pipeline, and countless other engineering parameters. The drag arises from shear stress, the rate per unit area of momentum transfer from the flow to the surface. Superhydrophobic surfaces can be fabricated in order to reduce the drag based on its highly water repellent property and capable of forming a thin air film over an underwater surface which stops the surface from becoming wet. The air film formed over the surface has the property of being able to take in air supplied from outside because of the surface tension of the water. The superhydrophobic surfaces to reduce frictional drag have been used in ships. When air is supplied from the bow section to a ship's hull with superhydrophobic coatings, it becomes attached to the superhydrophobic surface and forms an air film on it. The frictional drag can thus be reduced by an air lubricant effect. Figure 2.9 shows some areas where superhydrophobic surfaces can be used to reduce their drag reduction.

Figure 2.9 The applications of superhydrophobicity- drag reduction.

2.2   Preparation techniques of superhydrophobic surfaces

Learning from nature, superhydrophobicity can be obtained by creating a surface with optimum roughness followed by passivation with a low-surface-energy coating. Therefore, superhydrophobic surfaces are traditionally prepared using a common two-step procedure where a micro-nanorough pattern is first created using various procedures such as lithographic and template-based techniques [36], laser ablation technique [37] and plasma treatment of the surfaces [38,39], self-assembly and self-organization [40], chemical bath deposition (CBD) [41,42], chemical vapor deposition (CVD) [43], and electrochemical deposition [44], etc. These surfaces are then passivated using low surface energy coatings such as use of stearic acid or fluoroalkyl-silane molecules or by use of Teflon coating by plasma techniques [45]. Some of these methods of preparing superhydrophobic surfaces will be elaborated in the following sections as part of literature review.

2.2.1 Electrodeposition technique to achieve superhydrophobicity

Superhydrophobic films can be made by immersing samples in some solutions via electrochemical deposition. Because of its cheaper, faster and easier in operation at lower temperatures, the electrochemistry is used extensively for the formation of nanostructured surfaces, either by applying certain external potential between the electrodes or simply by making use of the galvanic ion exchange reaction between a substrate and ions [46,47,48,49,50,51].

2.2.1.1 Galvanic exchange reaction (electroless deposition)

Safaee et al. [52] studied the superhydrophobic properties of the modified silver-coated copper surfaces. In their experiment, copper substrates were coated by immersing in a silver nitrate solution via a galvanic exchange reaction and then passivated with stearic acid dissolved in acetone or hexane. The galvanic exchange reaction of copper and Ag+ is as follow:

$$2 \ Ag^+ + Cu \rightarrow 2Ag + Cu^{2+} \hspace{3cm} \text{(Equation 2.6)}$$

The concentration of silver nitrate solution was found to influence the surface of deposited silver and hence the wetting properties after passivation. Variations of contact angle and contact angle hysteresis as a function of the coating time are shown in figure 2.10 [52]. When the concentration is 13.2 mM, the contact angle increases from 134 ° at 0.5 min to 150 ° at 10 min, and finally to 151 ° after 12h, while the contact angle hysteresis decreases correspondingly. On the other hand with the 50 mM solution, contact angle reduces from 155 ° to 147 ° and hysteresis increases from 5.1 ° to 10.3 ° at 0.5 and 10 min, respectively. Using the 24.75 mM solution, the highest contact angle, 156 °, is obtained at 1 min while the least hysteresis, 4.1 °, is achieved at 2 min.

19
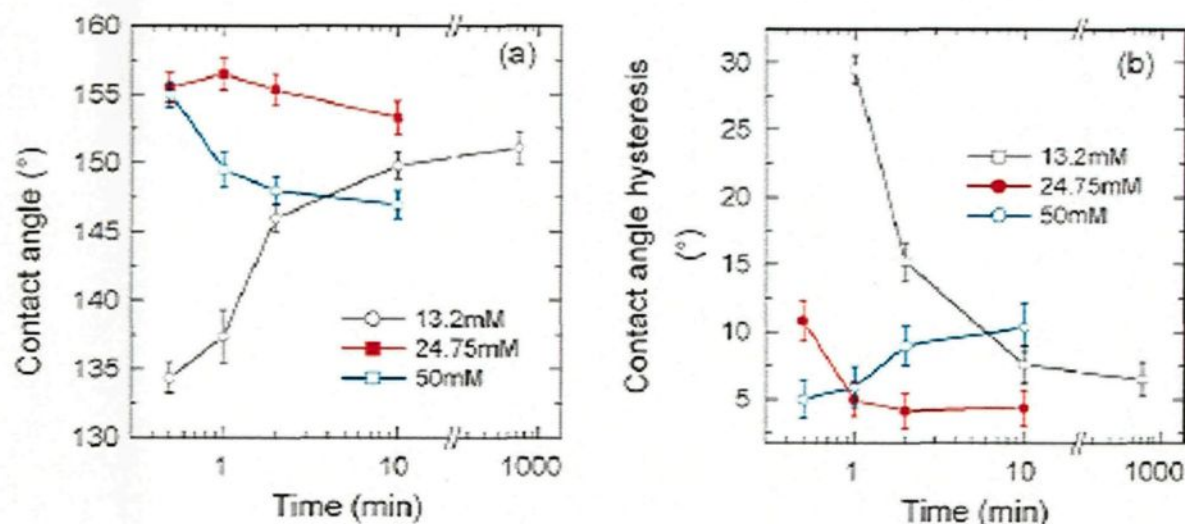
Figure 2.10 Variation of water contact angle and hysteresis with coating time.

The morphologies of the modified surfaces are shown by SEM measurement in figure 2.11 [52]. It can be seen from the 2.11 (a), (b) and (c) that various concentration of silver nitrate solution leads to various morphologies on the sample surfaces. When the concentration is low (13.2 mM), the film has tiny voids because the low Ag^+ concentration contributes to the slow reaction, as presented in fig. 2.11(a). Increasing the Ag^+ concentration to 24.75 mM (fig. 2.11(b)) and even to 396 mM (fig. 2.11(c)), however, the driving force of the galvanic exchange reactions is larger, so the reaction becomes faster and larger fractal-like structures of silver appear. Therefore, the size of the voids is more obvious than before, as compared with fig. 2.11(a). Figure 2.11(d) is a magnified fractal-like structure to (b). Due to their self-similarity, several nanometric empty spaces exist around the micrometric structures which are separated by voids.
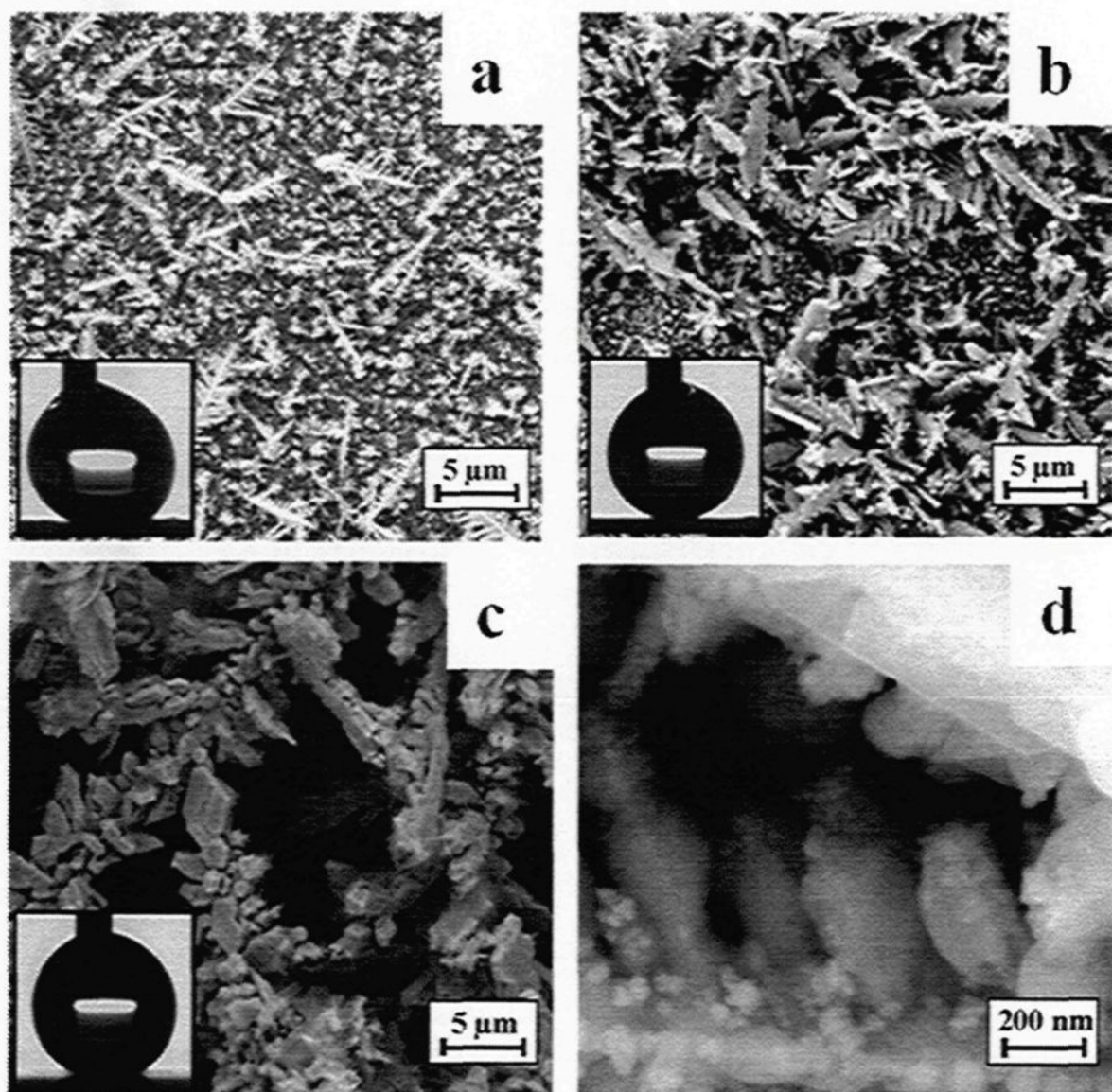
Figure 2.11 SEM images of samples prepared using three different initial Ag$^+$ concentrations of (a), 13.2 mM, (b) 24.75 mM and (c) 396 mM, respectively; and (d) a magnified section of (b); In the insets, the states of the droplets are shown.

Gu et al. [53] also applied galvanic reaction to fabricate superhydrophobic surfaces. In their study, galvanic replacement was adopted to grow cauliflower-like and dendrite coral-like silver films on commercial copper alloy substrates. The galvanic exchange reaction in their study is the same as that of Sarkar et al., as presented in eq. 2.6. However, the morphology of as-deposited silver crystals on the copper alloy substrates as a function of the reaction time is illustrated. The

21

insets shown in figure 2.12 are the corresponding SEM images with high resolution. After immersing for 5 s, abundant isolated silver particles with a size of about 50 nm and some nanoplates, having a length of 100-900 nm and a thickness of about 50 nm, are decorated loosely on the substrate, as shown in figure 2.12(a). The density of the nanoparticles and nanoplates increases with the reaction time. For the reaction time of 10 s, the nanoplates are interconnected to build a flower-like architecture, as shown in the inset of figure 2.12(b). When the reaction time is extended to 20 s, the interconnected silver nanoplates are transformed to microscopically coral-like silver aggregates shown in figure 2.12(c). The coral-like silver aggregates are expanded to bigger ones when prolonging the reaction time to 5min (see figure 2.12(d)). Furthermore, figure 2.12(f) shows that plenty of silver particles and plates with size of 100-500 nm have fully filled the intervals of the coral-like silver aggregates. Once some silver crystals have been deposited, further deposition is more likely on them than on the substrate because deposition on the flat substrate surface is generally less favorable due to the requirement of the formation of fresh metal nuclei [54]. Figure 2.12(e) gives the surface morphology of as-deposited silver films on the copper alloy substrate after 25 min reactions. It can be seen that dendrite silver crystals are emerged besides coral-like aggregates, nanoparticles, and nanoplates.
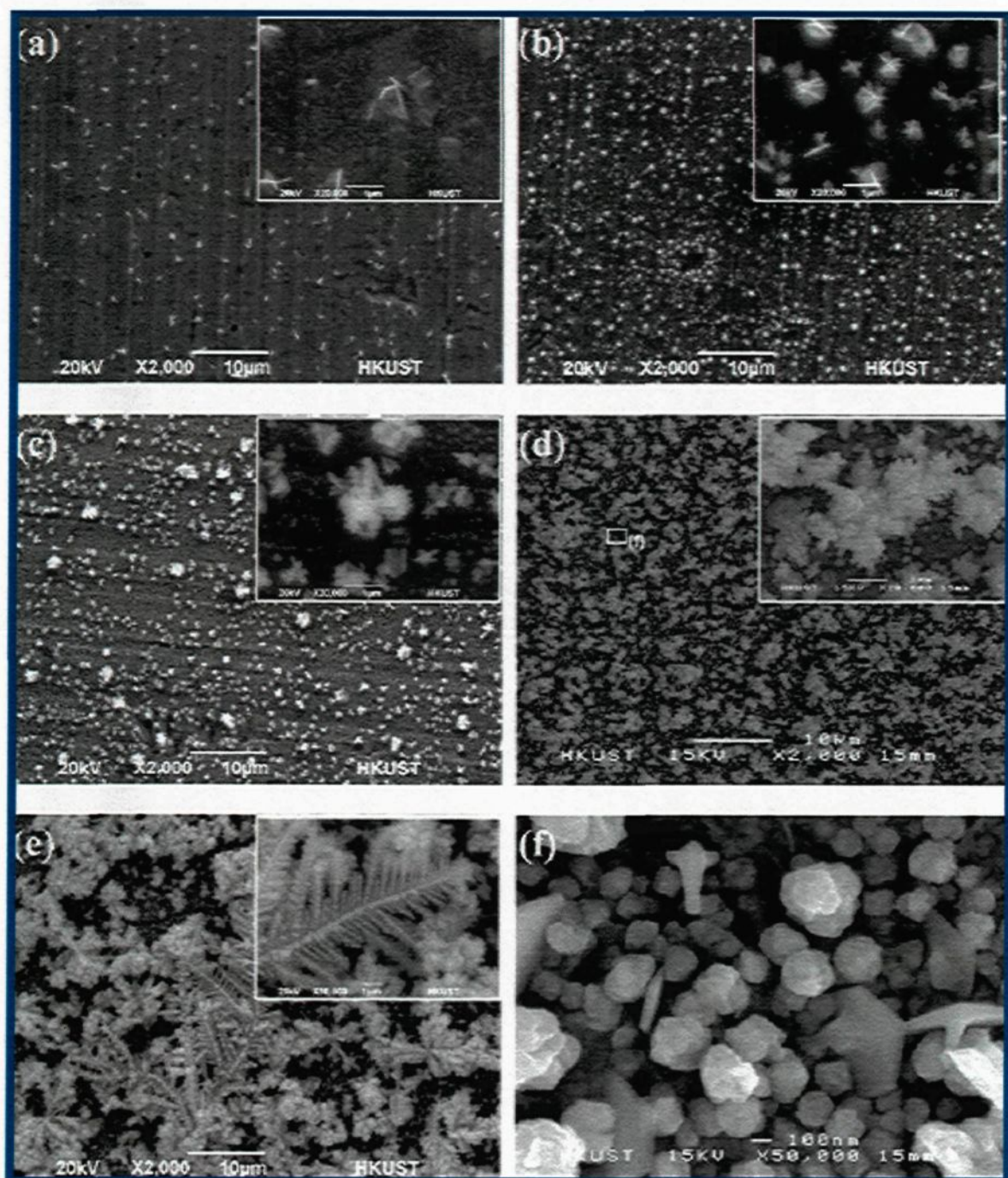
Figure 2.12 SEM images with different magnifications of as-deposited silver crystallites prepared in the 0.01 M AgNO₃ aqueous solution for reaction time of (a) 5 s; (b) 10 s; (c) 20 s; (d) 5min; (e) 25 min; (f) magnified image corresponding to the area indicated by the rectangle in panel (d).

Sarkar et al. [55] demonstrated that the superhydrophobic silver films on copper substrates can

be created in just a one-step process via galvanic reactions by immersing the copper substrates in

23

silver nitrate solution containing benzoic acid, simplifying the complexity of two different steps involved in the former method. Fig. 2.13 shows the X-ray diffraction (XRD) pattern of (a) copper substrates, (b) the silver films deposited on the copper substrates by the galvanic reaction in silver nitrate solution and (c) the silver films deposited on the copper substrates using silver nitrate solution in the presence of benzoic acid molecules. The characteristic peaks of Ag (1 1 1), Ag (2 0 0), Ag (2 2 0), Ag (3 1 1) and Ag (2 2 2) at 38.18 °, 44.38 °, 64.53 °, 77.48 ° and 81.65 °, respectively, confirming the silver deposition. The origin of the three peaks at 36.5 °, 42.35 ° and 61.43 ° are due to the formation of copper oxide (Cu_2O) crystalline phase, which is also complemented by the black colored appearance of the deposited films [56]. However, it has been observed from the pattern (c), which silver was deposited on copper substrate with the presence of benzoic acid molecules in the silver nitrate solution (fig. 2.13(c)), the three peaks of Cu_2O are completely disappeared. These films appeared to be pure silver as evident from the distinct peaks of Ag (1 1 1), Ag (2 0 0), Ag (2 2 0) and Ag (3 1 1) at 38.18 °, 44.38 °, 64.53 °, and 77.48 °, respectively [57].
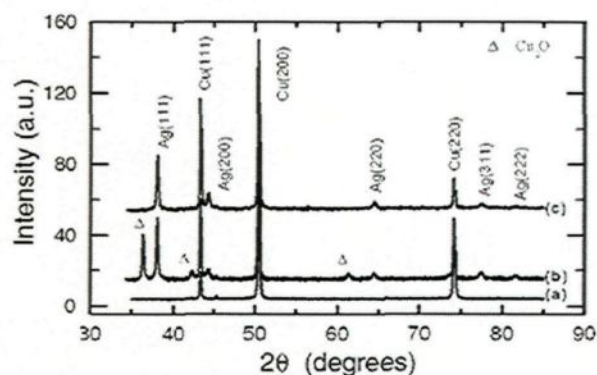
Figure 2.13 XRD patterns of (a) copper substrate, (b) the silver film deposited on galvanic exchange reaction on copper substrate in the silver nitrate solution, and (c) the silver film deposited on galvanic exchange reaction on copper substrate in the silver nitrate solution with benzoic acid molecules.

Furthermore, the chemical composition of the materials are analyzed by energy dispersive X-ray analysis (EDS) spectra of the silver films deposited on copper substrates (a) in silver nitrate solution and (b) in silver nitrate solution with benzoic acid molecules, as presented in fig. 2.14 [55]. The presence of oxygen in the EDS spectrum shown in fig. 2.14(a) is complemented with the observation of Cu_2O by XRD as shown in fig. 2.13(b). EDS spectrum of silver films prepared with the benzoic acid (fig. 2.14(b)) shows the presence of two distinct elements, namely, copper and silver with a trace of carbon. The absence of oxygen in this spectrum (fig. 2.14(b)) is well complemented with the XRD analysis (fig. 2.13(c)), confirmed the deposition of Cu_2O free pure silver films. The presence of carbon in this EDS spectrum confirms the incorporation of benzoic acid molecule in these films. The inset of fig. 2.14(b) shows the bonding characteristics of the carbon in these films by FTIR. The distinct peak at 1386 cm^{-1} is due to the presence of COO^- vibration bond with copper possibly resulting in the formation of copper-3-hydroxy benzoate ($C_7H_5CuO_3$) complementing the XRD analyses. The adsorption of benzoic acid on copper surfaces shows that the COO^- vibration bond varies from 1390 to 1405 cm^{-1} depending on the orientation of the benzoic acid with respect to the surface [58].

25
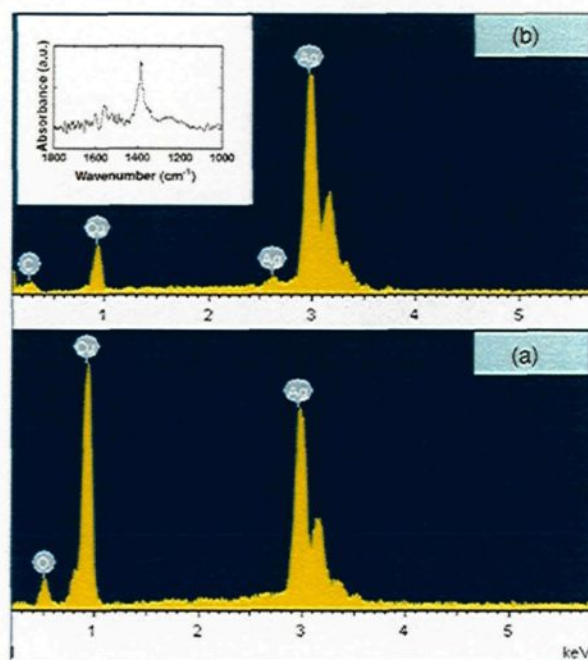
Figure 2.14 EDS spectra of silver films prepared in (a) silver nitrate solution and (b) silver nitrate solution with benzoic acid molecules. Inset shows the FTIR spectra of silver powder collected from the silver films prepared with the benzoic acid molecules.

2.2.1.2 Underpotential deposition

As mentioned in the previous section, galvanic exchange reaction is a kind of spontaneous reaction without external potential applied and some researchers studied the superhydrophobicity by electrochemical deposition without applied potential. In the electrochemical deposition methodology, underpotential deposition is another important type to achieve the deposition phenomena.

In Sarkar's study, the copper nanocrystals were deposited on thin polypyrrole films by the underpotential deposition [59]. Although he didn't investigate the superhydrophobic coatings in that work, the grow mechanism of the copper nanocrystals on the substrate by electrochemistry method is quite worthy to understand in order to convenience our studies in the master project.

26

Figure 2.15 compared the SEM micrographs of the copper nanostructures deposited on the 100-nm-thick polypyrrole substrates galvanostatically and potentiostatically [59]. In the galvanostatic mode (of copper deposition), 0.2 mA/cm^2 current density is passing through the electrodes. It is found that the potential on the electrode decreased 0 V to -1.9 V in less than 4 s, as shown in figure 2.15(a). Figure 2.15(b) shows the corresponding SEM micrograph for copper deposition obtained galvanostatically as shown in figure 2.15(a), revealed the presence of a number of remarkably different forms of nanostructures, including cubic nanocrystals (80 nm side length) individually or clustering together, nanowires, and microrods or clusters. Closer examination of an individual rod shows that it consists of near-perfect cubic copper nanocrystals. Figure 2.15(c) shows that copper nanostructures deposited at -0.4 V in the under-peak potential region correspond to fractal-like or dendrite structures. In contrast, uniformly dispersed near-perfect cubic nanocrystals (of 80 nm side length) are observed for copper deposition at -0.9 V in the under-peak potential region, as illustrated in figure 2.15(d). It is concluded that variation of the deposition potential may lead to the difference of the morphology as well as the size of the particles deposited on the substrates.
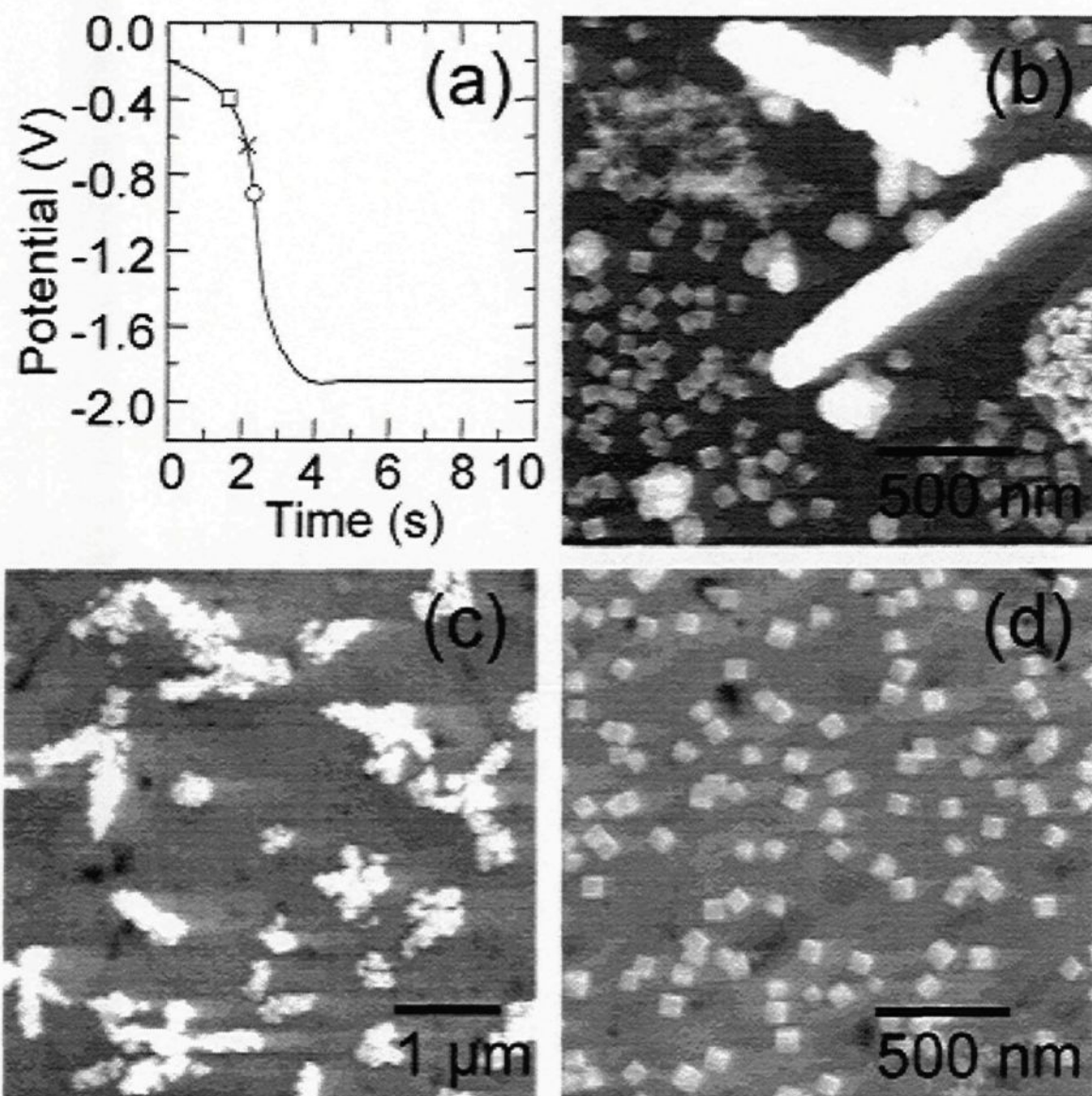
Figure 2.15(a) Change in the applied potential (V) as a function of time (s) in the galvanostatic mode for copper deposition on a 100-nmthick polypyrrole film. The cross at -0.56 V (versus AgCl/Ag standard potential) marks the peak potential for copper deposition obtained from a cyclic voltammetric scan for polycrystalline copper substrate. Potentials that are higher (e.g., open square at -0.4 V) and lower (e.g., open circle at -0.9 V) than -0.56 V are referred to as under-peak potential and over-peak potential, respectively. Panel b shows the corresponding SEM micrograph for copper deposition obtained galvanostatically as shown in panel a, depicting a variety of structures including nanowires, microrods, fractals, and cubic nanocrystals. Panels c and d show SEM micrographs for copper deposition obtained in potentiostatic mode at (c) under-peak potential (-0.4 V) and (d) overpeak potential (-0.9 V), depicting the changes in the predominant nanostructures from fractals to near-perfect cubic nanocrystals.

The chemical composition of these copper nanocrystals is then examined using XPS as a

function of depth (depth profiling), which confirmed the formation of Cu, CuO as well as Cu_2O.

Wang et al. have shown how the chain length of some organic molecules influences the water repellence of the surface [60]. In their work, copper coatings were prepared by a two-step electrochemical deposition approach, among which, a small potential was used to form the bare globe-shaped particles in the first step and the overpotential helped the particles to grow larger. Those copper coatings were further modified using different organic molecules with varying chain lengths. The relationship between water contact angle on the modified film and the second deposition time is shown in figure 2.16(a), and the water contact angle of smooth film and as-prepared film are influenced by the chain length of n-alkanoic acid (shown in figure 2.16(b)). It is clear to see that as the increasing of the chain length of the organic acid, the water contact angle increases even to over 150 °. Furthermore, the increase of the carbon number leads to the obvious increase of the as-prepared surface contact angle. When the rough films were modified by the short-chain acids, the disordered acid layer and the native copper leads to a high surface free energy and a low contact angle. On the other hand, when the films are modified by long-chain acids, the low-energy methyl groups become closed-packed on the top surface, which leads to a low surface energy and a higher contact angle. The chain length of the n-alkanoic acids of 8 is found to be necessary to obtain superhydrophobicity on the surfaces, where the water contact angle is higher than 150 °.
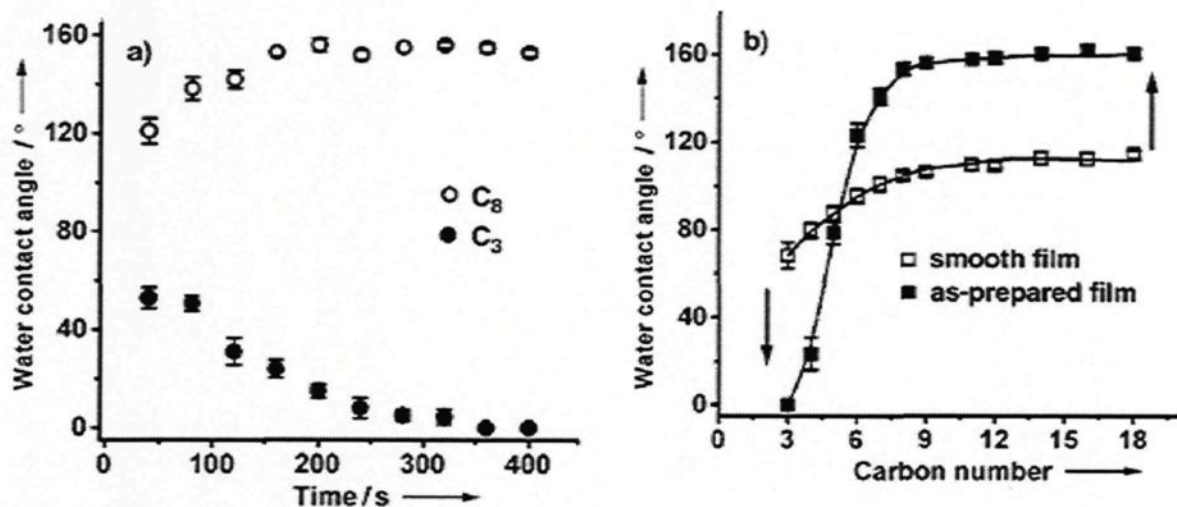
Figure 2.16(a) Relationship between water contact angle on the modified copper films and the second deposition time, C_3 and C_8 show different number of chain length; (b) Water contact angle on the modified copper films as a function of chain length of n-alkanoic acids.

2.2.2 Chemical etching technique to prepare superhydrophobic surfaces

It is known that surface roughness is important in obtaining superhydrophobic surfaces and the roughness of the surface can be created by chemical etching. The etching of aluminum surfaces has been performed using dilute hydrochloric acid and superhydrophobicity has been demonstrated following coating these surfaces further with ultrathin rf-sputtered Teflon as reported by D. K. Sarkar et al. [61]. These authors etched aluminum surfaces at different etching time as shown in figure 2.17(a). The influence of etching time on contact angles is presented in figure 2.17(b). It can be concluded that the increase of the etching time leads to the decrease of the thickness as well as the increase of water contact angle of the modified surfaces with Teflon.
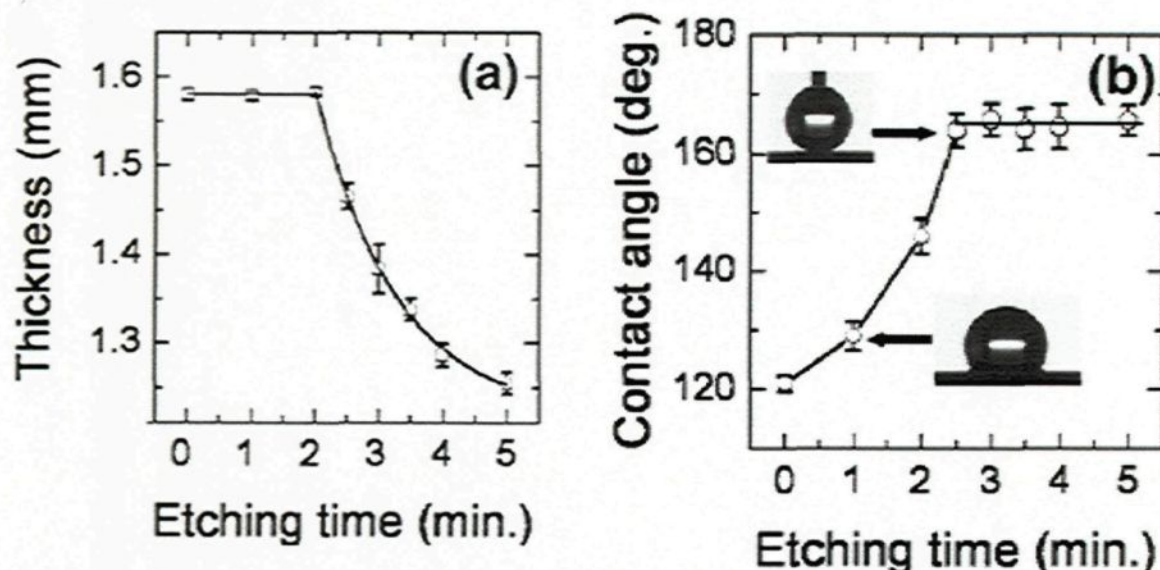
Figure 2.17(a) The variation of thickness of aluminum substrates with etching time; (b) Contact angle of water on ultrathin rf-sputtered Teflon coated aluminum substrates with etching time, inset shows the shape of water drop on 1min and 2.5 min etch surfaces.

Pan et al. [62] also studied the facile preparation of superhydrophobic copper surfaces by HNO3 etching technique with the assistance of CTAB and ultrasonication followed by modification with 1H, 1H, 2H, 2H- perfluorodecyltriethoxysilane (FDTES). It is found that the increase of the etching time leads to the obvious increase of the water contact angle the surfaces after modification with FDTES as shown in fig. 2.18, which is well agreement with the study by Sarkar et al. presented above.
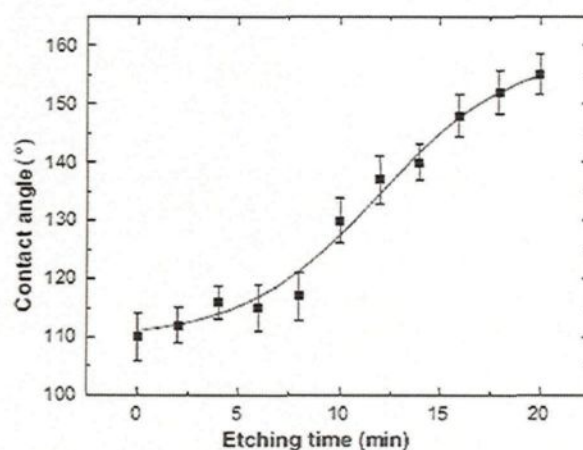
Figure 2.18 Influence of etching time on the contact angle of the copper wafer surface.

However, both Sarkar and Pan applied two-step process to fabricated superhydrophobic surfaces via chemical etching. In Saleema et al.'s study, a simple one-step process has been developed to modify the aluminum alloy surfaces to superhydrophobic by immersing the aluminum alloy substrates in a solution containing NaOH and fluoroalkyl-silane (FAS-17) molecules [63]. In their study, the SEM images are used to analyze the morphologies of the surface, the XPS figure is used to perform the surface chemical composition and the water contact angle analysis is used to verify the superhydrophobicity of the surfaces.

Fig. 2.19(b) shows the revealing of the craterlike microfeatures after the aluminum alloy surface treated with the NaOH in the presence of FAS-17 molecules at a F/OH ratio of 0.4, as compared to the cleaned aluminum alloy surface (fig. 2.19(a)) [63]. The formation of the rough surface due to immersing into NaOH etched solution as well as the modified surface chemistry arising from the adhesion of FAS-17 molecules, resulted in the creation of superhydrophobic properties. The insets show the shape of water drops on surfaces as well as the SEM image with higher resolution, respectively.
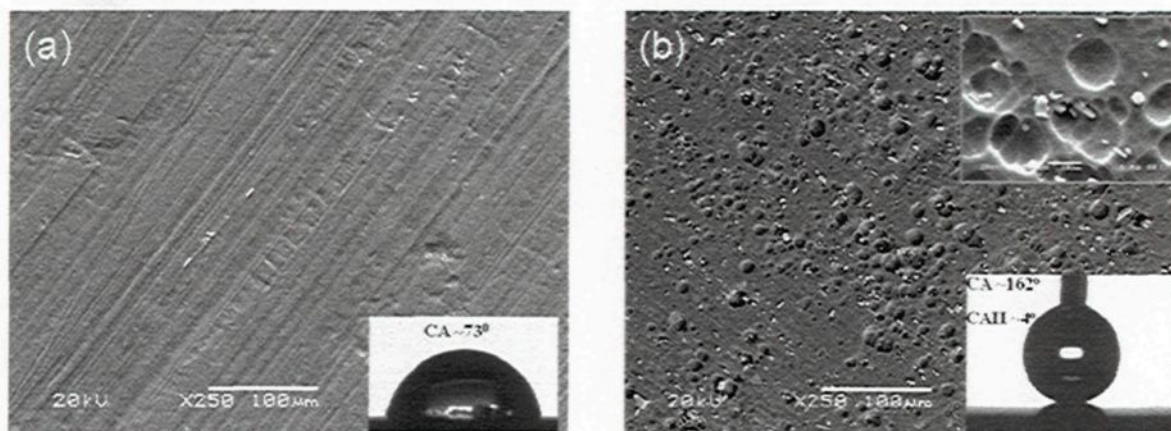
Figure 2.19 SEM images of aluminum surfaces (a) as-received (inset shows the water drop image on a) and (b) treated with NaOH and FAS-17 (inset shows a magnified SEM image of b as well as a water drop image on b).

Fig. 2.20 shows the XPS investigations of the aluminum surfaces treated with NaOH and FAS at different F/OH ratios revealed the presence of C, F, O, and Si with no treat of Na in the survey spectra [63]. The formation components, namely, $-CF_3$, $-CF_2$, $-CH_2-CF_2$, $-C-O$, $-C-C$, $-C-Si$ and $-C$-metals confirmed the formation of FAS-17 molecules on aluminum alloy surfaces. Among them, the CF_3 and CF_2 concentrations, which are 6.16 and 47.71 %, are slightly higher than the theoretical values obtained from that of FAS-17, indicating that the low surface energy components (CF_2 and CF_3) comprise the outermost surface contributing to superhydrophobic properties.
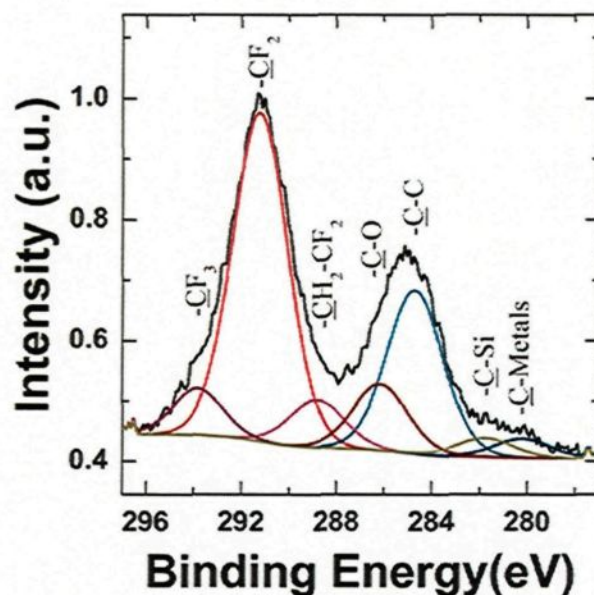
Figure 2.20 High-resolution C1s core level spectrum of FAS-17/NaOH treated Al surface.

The superhydrophobicity of the aluminum alloy surface after treatment by NaOH and FAS-17 mixed solution at different F/OH ratio is shown by water contact angle in fig. 2.21 [63]. The FAS/NaOH molar ratio of 0 presents the aluminum alloy surfaces immersed in 0.1 M NaOH without FAS-17, where the water contact angle is ~ 88 °, slightly higher than that of the aluminum alloy substrate. Further increase the F/OH molar ratio to 0.1 leads to the increase of the contact angle which is higher than 150 °, showing superhydrophobicity. The water contact angle on surfaces treated with F/OH ratios of 0.2 and 0.4 were found to be ~ 157 ° and 162 °, respectively, both showing superhydrophobic properties.
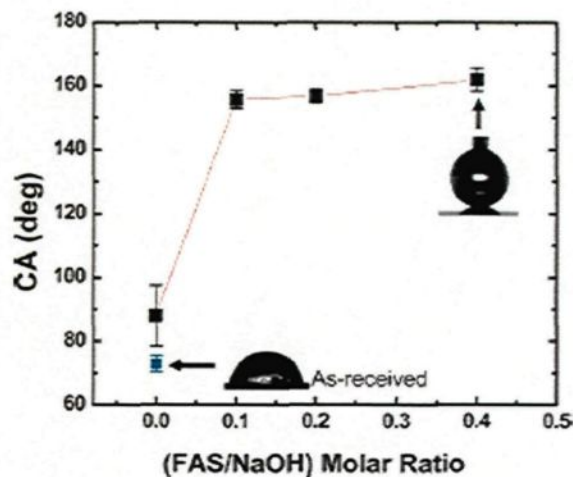
Figure 2.21 Water contact angle measured on aluminum surfaces treated with different FAS-17 concentrations.

2.2.3 Other techniques to achieve superhydrophobicity

2.2.3.1 Chemical bath deposition

The thermal desorption of stearic acid on superhydrophobic zinc oxide nanotowers has been investigated by Saleema et al. [45]. The cleaned silicon substrates were immersed in $Zn(NO_3)_2$ and NH_4OH mixed solution for the growth of ZnO nanotowers via chemical bath deposition (CBD) followed by passivation with stearic acid solution. Fig 2.22 displayed beautiful SEM images of ZnO nantowers after passivation in different magnification. The formation of randomly oriented hexagonal patterned ZnO nanotowers, the hexagonal patterns that have regular edges with an angle of 120 ° between adjacent sides are demonstrated in fig. 2.22 indicated the formation of rough binary structure with a combination of nanosteps on the nanotowers.

35
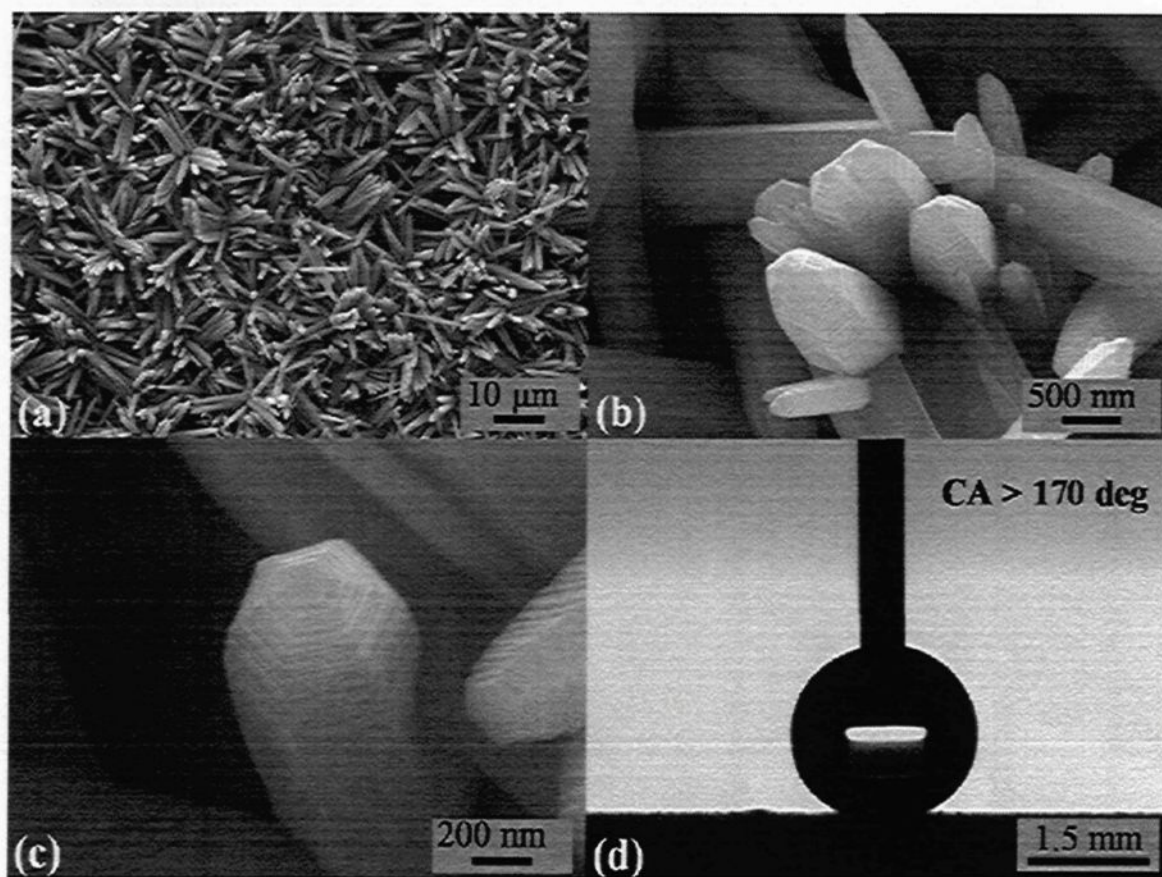
Figure 2.22 FESEM images of ZnO nanotowers at (a) low magnification (b) ZnO nanotowers at high magnification showing the hexagonal morphology; (c) close up view of a single nanotower showing the nanosteps; (d) image of a water drop on the surface of these nanotowers after SA passivation.

It is well known that the superhydrophobicity of a solid depends on both the roughness and the chemical composition of the surface. In Saleema's study, the chemical composition is confirmed by fourier transform infrared (FTIR) spectra. Fig. 2.23 shows the FTIR spectra of the samples [45], annealed at different temperatures, in the wavenumber range of 2550-3150 cm^{-1} showing only the $-CH_n$ peaks of stearic acid. The formation of the two peaks at wavenumbers 2919 and 2850 cm^{-1} confirmed the formation of the asymmetric and symmetric C-H stretching modes of $-CH_2$ groups of stearic acid, respectively, and the peak at 2958 cm^{-1} is ascribed to the asymmetric in-plane C-H stretching mode of the $-CH_3$ group. The appearance of the low surface energy methylated (CH_2 and

CH₃) components on the surface as well as the formation of the roughness structures as shown in fig.

2.22 results in the superhydrophobicity on the surface.
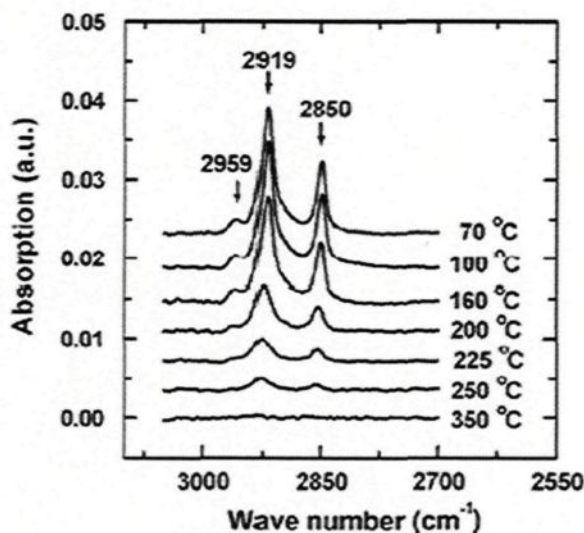
Figure 2.23 FTIR spectra showing –CHn peaks of stearic acid following annealing at various temperatures.

2.2.3.2   Sol-gel technology

In the sol-gel procedure, the 'sol' (or solution) gradually evolves towards the formation of a gel-like diphasic system containing both a liquid phase and solid phase whose morphologies range from discrete particles to continuous polymer networks. TiO_2 μ-donuts have been fabricated on glass and silicon by sol–gel technique using a mask of poly methyl methacylate (PMMA) nanopillars created by removing polystyrene (PS) from a spin-coated composite polymer of PS and PMMA by Saleema et al. [64]. Brassard et al. applied sol-gel process to obtain superhydrophobic aluminum alloy surfaces. [65]. In their study, monodispersive silica nanoparticles have been synthesized via the Stober process and further functionalized by adding fluorinated groups using fluoroalkylsilane in an ethanolic solution. Different size nanoparticles are prepared and used to

deposit thin films on aluminum alloy surfaces using spin coating processes. FAS-17 molecules are used for the fluorination of the silica nanoparticles. FTIR analysis confirmed the presence of C-F, C-H and Si-O bonds anticipated from the functionaliztion of silica nanoparticles by FAS-17 molecules. The roughness of the thin film as well as the superhydrophobicity of the surface is found to increase with the increase of the size of the fluorinated silica nanoparticles.

2.2.3.3   Plasma-enhanced chemical vapor deposition (PECVD)

Plasma-enhanced chemical vapor deposition (PECVD) is a process used to deposit thin films from a gas state (vapor) to a solid state on a substrate. Chemical reactions are involved in the process, which occur after creation of a plasma of the reacting gases. The plasma is generally created by RF (AC) frequency or DC discharge between two electrodes, the space between which is filled with the reacting gases. Sarkar et al. studied the depositing hydrocarbon and fluorinated-hydrocarbon coatings via plasma enhanced chemical vapor deposition (PECVD) technique using a mixture of Ar, CH4 and C_2F_6 gases. The micro-nanorough aluminum substrates demonstrated superhydrophobic properties upon coatings with fluorinatedhydrocarbon providing a water contact angle of 165 ° and contact angle hysteresis below 2 ° with water drops rolling off from those surfaces, due to the high fluorine content in the fluorinated-hydrocarbon coatings of ~ 36 at. %, as investigated by X-ray photoelectron spectroscopy (XPS), by lowering the surface energy of the micro-nanorough aluminum substrates [66].

2.2.3.4   Anodizing and some other techniques

Anodizing is an electrolytic passivation process used to increase the thickness of the natural

oxide layer on the surface of metal parts. Anodic aluminum oxide has been proposed as a suitable industrial process for use in the burgeoning field of nanotechnology [67] for developing nano-pore structure films with advantage of improvement of corrosion and wear resistance [68,69].

Laser ablation is the process of removing material from a solid surface by irradiating it with a laser beam. At low laser flux, the material is heated by the absorbed laser energy and evaporates or sublimates. Laser processing is one of the promising tools in non-contact material processing for industry applications, because it is fast and allows short processing time. It is clean to the environment and provides excellent control of the shape and size of the micro-dimples, which allows realization of optimum designs. By controlling energy density, the laser can safely process hardened steels, ceramics, and polymers as well as crystalline structures [70,71,72,73]. Romer et al. investigated the rippled nanostructures on steel which formed by laser pulses. They indicated that by controlling this structure, it is possible to control the hydrophobicity [74].

2.3   Corrosion properties of superhydrophobic surfaces

Corrosion is the decaying or destruction of a material due to chemical reactions with its surroundings. In other words, corrosion is the wearing away of metals due to a chemical reaction. The metals or alloys surfaces exposed to corrosive environments (humidity, salt, acid, base, etc.) along with pollution are not stable and can result in severe damages on the surfaces due to corrosion. Aluminum alloys corrode merely from exposure to moisture in the air, but the process can be strongly affected by exposure to certain substances such as salt, acid, corrosive gas (SO_2) etc. Corrosion sometimes starts on the surface forming pits or cracks which propagate into the material under continued exposure to the corrosive environment, ultimately resulting in serious damages.

Surface passivation or conversion coatings are being used to reduce surface corrosion processes. Very recently, superhydrophobicity is under research for protecting surfaces from corrosion [75,76,77]. A review on the corrosion studies on superhydrophobic surfaces is provided below.

Corrosion tests can often be done in many ways, such as in chloride containing solution [78,79,80], in hydrochloric acid (HCl) [81], Na_2HPO_4, $NaHCO_3$, KCl solution [82], deionized water et al. [83], etc., depending on the kind of intended application. In addition, corrosion resistance phenomenon can also be monitored via weight loss measurements [84,85,86] and neutron reflectivity [87]. The effects of corrosion resistance can also be seen from the potentiodynamic curves [88], electrochemical impedance spectroscopy (EIS), salt-spray and many other techniques.

2.3.1 The stability of the superhydrophobic surfaces

The stability of the superhydrophobic surfaces is always analyzed by immersing the surfaces in certain corroded solution, measuring by SEM, water contact angle and some other techniques.

In a study of Wang et al. [89], the durability of superhydrophobic copper surface was investigated using contact angle measurements. Fig. 2.24(a) presents the changes of contact angle of superhydrophobic film coated specimen (SS) as a function of immersion time in 3.5 wt. % NaCl solution. It can be found that SS can maintain its superhydrophobic property within 3 days. Though its contact angle falls to below 150 ° after an immersion of 4 days, it can maintain around 140 ° even after an immersion of 20 days. It is indicated that the film is stable in NaCl solution, and the decrease of contact angle with immersion time might be related to the microstructure changes of film.
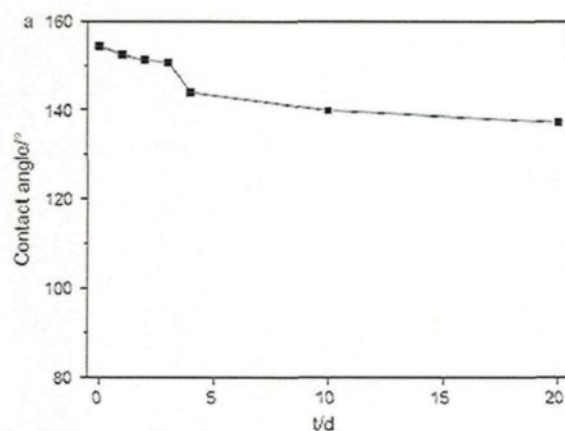
Figure 2.24 The variation of the contact angle of superhydrophobic film coated specimen (SS) as a function of immersion time in NaCl solution.

Yin et al. [90] also studied the stability of superhydrophobic surface by measuring the water contact angle after immersing the surface in the corroded solution. They fabricated superhydrophobic aluminum surface by anodizing technique and the water contact angle of the superhydrophobic surface was found to be around 155 °. However, the water contact angle decreased gradually after immersing in seawater for a period of time, which is accord with that of the study by Wang illustrated previously.
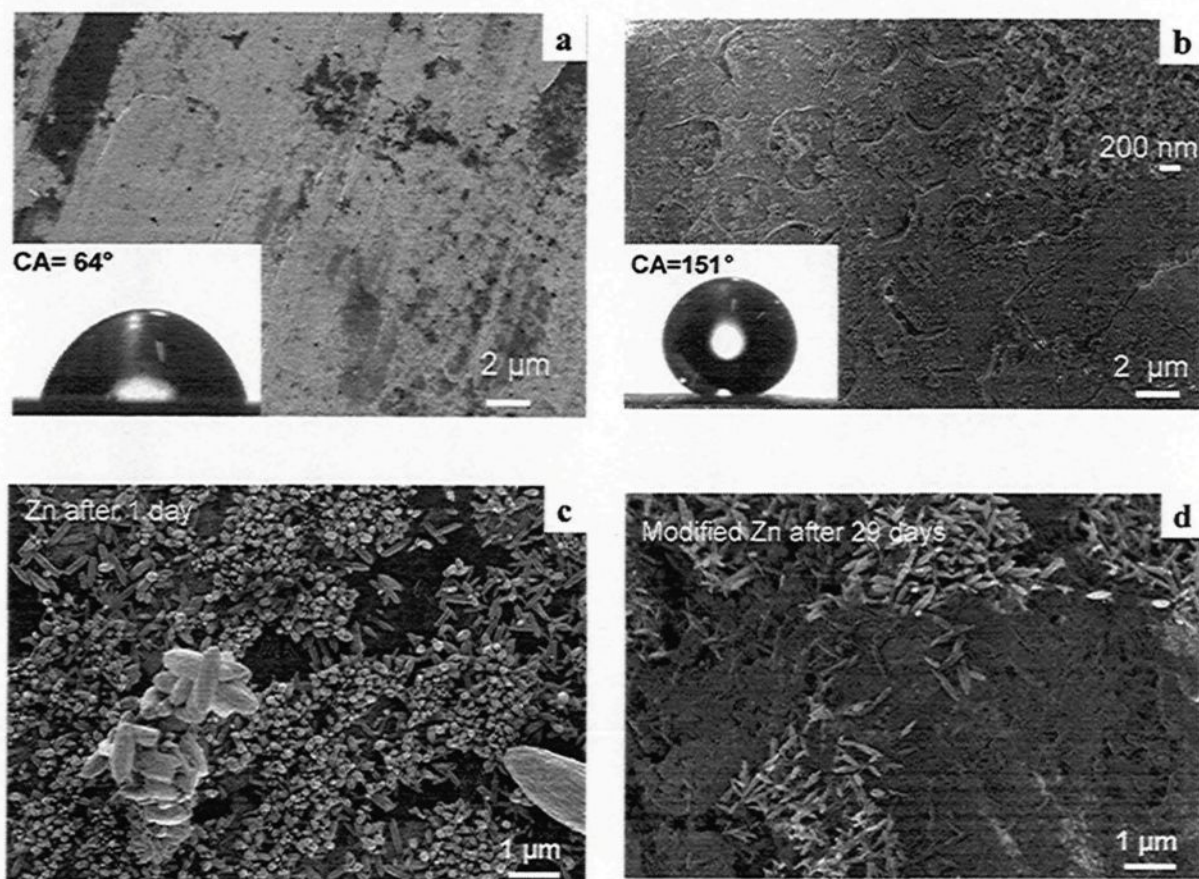
Figure 2.25 SEM images of zinc substrates before (a) and after coating with the perfluorosilane polymer (b). The insets correspond to water contact angles (droplet volume 6 μL) and zoom-in modified zinc. (c) SEM images of unmodified zinc and (d) zinc coated with a superhydrophobic film (B) after immersion in a 3 % NaCl aqueous solution for 1 and 29 days, respectively.

The morphology of surfaces after immersing in the corrosive solution has been compared with that of before immersing in Liu's study [91]. Stable superhydrophobic films with a contact angle of 151° were prepared by them on zinc substrates by a simple immersion technique into a methanol solution of hydrolyzed 1H, 1H, 2H, 2H- perfluorooctyltrichlorosilane [$CF_3(CF_2)_5(CH_2)_2SiCl_3$, PFTS] for 5 days at room temperature followed by a short annealing at 130 °C in air for 1 h. Fig. 2.25 displayed the SEM images of (a) zinc substrate and (b) the substrate after coating with the superhydrophobic polymer (hydrolyzed 1H, 1H, 2H, 2H- perfluorooctyltrichlorosilane [$CF_3(CF_2)_5(CH_2)_2SiCl_3$, PFTS]). The increase of the roughness of the modified surface as well as

the formation of the low-surface-energy materials (-CF$_2$, -CF$_3$, -CH$_2$) on the surface lead to the superhydrophobicity.

After immersing in 3 % NaCl solution for 1 day, the formation of a dense film of ZnO structures all over the zinc surface, indicating the zinc substrate is easily corroded after 1 day immersing. However, the oxide structures can be only seen in certain areas on the superhydrophobic surface immersed in the same solution for 29 days, indicating the superhydrophobic surface can resist corrosion much better than that of bare zinc substrate. The authors supposed the presence of the defect in the superhydrophobic layer may be responsible for the few oxide appearance on the superhydrophobic surface.

T. Liu et al. [92] investigated the mechanism of anticorrosion of superhydrophobic surfaces. The structure of super-hydrophobic surface has been simulated simply and elementarily to the interface model (fig. 2.26). The super-hydrophobic surface composed of hills (solid portion of the surface) can easily trap gas within the 'valleys' between the hills [13]. Therefore, the Cl$^-$ can hardly reach the bare surface for the obstructive effect of 'air valleys'. Furthermore, another important reason why the modified surface can improve the anticorrosion of copper is 'capillarity'. As we know, when a vertical cylindrical tube is placed in liquid, the liquid rises and forms a concave surface called a meniscus if the tube is hydrophilic; otherwise the liquid is depressed if the tube is hydrophobic. The height of the water column within the tube can be calculated by the following equation:

$$h = \frac{2\gamma \cos \theta}{\rho g R}$$

(Equation 2.7)

where R is the radius of the cylindrical tube, θ contact angle, γ surface tension and ρ is density of liquid. The capillary descend (h < 0) is very obvious when the pore diameter (R) is shorter than 3 μm and contact angle is 158 ° (in their study). Then water transport against gravity is easy in such porous structure. As a result, the seawater can be pushed out from the pores of the superhydrophobic film.
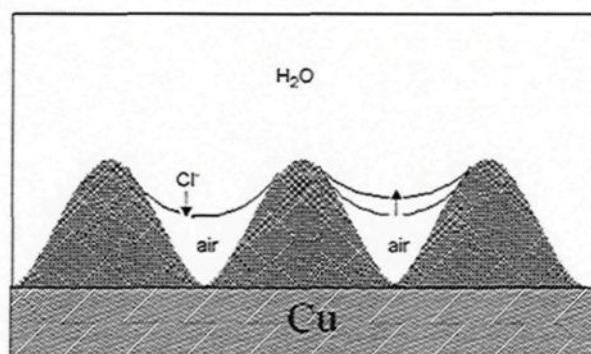
Figure 2.26 Model of the interface between super-hydrophobic surface and sterile seawater.

2.3.2   Electrochemical technique- Potentiodynamic polarization

Potentiodynamic polarization curves are very popular to be used to investigate the corrosion behaviors of materials. In a study by He et al., aluminum surfaces were anodized and further passivated using myristic acid [78]. These surfaces were then tested for electrochemical corrosion in sterile seawater (the seawater which is 3.2 wt. % NaCl solution with a pH 8.02 was boiled for 20 min). The superhydrophobic surface produced positive results mainly on the aluminum anodic reaction, whose current were reduced by about three orders of magnitude (shown in figure 2.27) as compared to the superhydrophilic counterpart. It also shows that the corrosion potential increased about 0.2 V after myristic acid modification which suggested that the myristic acid film retarded the dissolution of aluminum between the interface of the aluminum surface and seawater.

44
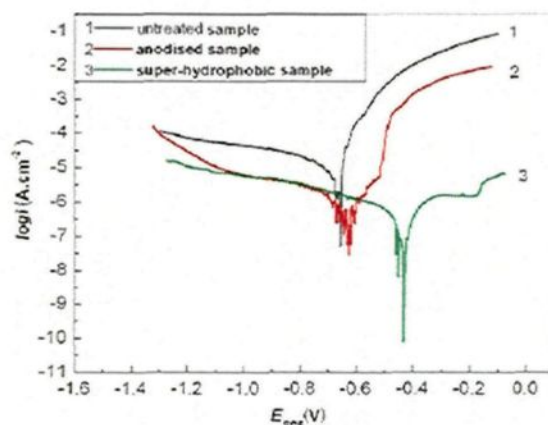
Figure 2.27 Potentiodynamic polarization curves of untreated, anodized and superhydrophobic samples for 24 h in sterile seawater at 2 mV s^{-1}.

A study by T. Ishizaki et al. reported corrosion behaviors on magnesium alloys [88]. In their study, a crystalline CeO_2 film was vertically formed on magnesium alloy and passivated by fluoroalkyl-silane (FAS). The FAS-coated CeO_2 film presented superhydrophobicity providing a water contact angle of greater than 150 °. Figure 2.28 shows the difference in the behavior of a water drop placed on a superhydrophilic surface covered with CeO_2 film and a superhydrophobic surface after FAS coating. The shape of water droplet on the as-prepared surface composed of CeO_2 nanosheets indicated the surface shows superhydrophilic. However, the water droplet is hardly sticky on the CeO_2 nanosheet surface after FAS coating.
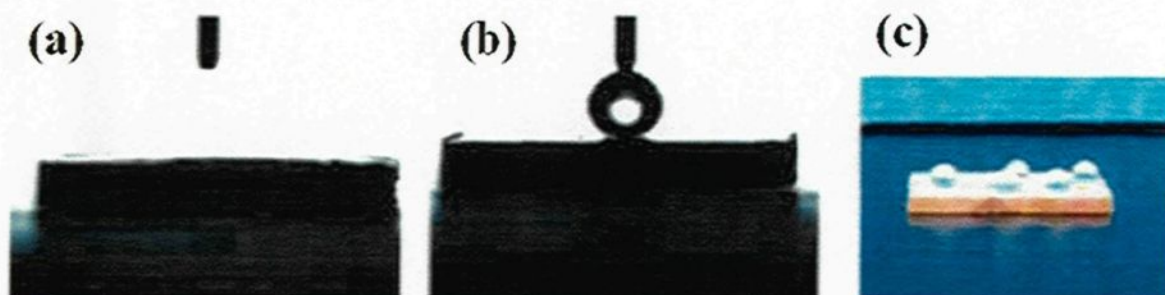
Figure 2.28 (a) Shape of water droplet on the as-prepared surface composed of CeO_2 nanosheets; (b) Water droplet behavior on the CeO_2 nanosheet surface after FAS coating; (c) Digital photograph image of the shape of water droplets on the superhydrophobic surface.

The behavior of that superhydrophobic surface is then analyzed by electrochemical technique, as compared with that of bare magnesium alloy. Figure 2.29 shows potentiodynamic curves of (a) a bare magnesium alloy and (b) a superhydrophobic surface on a magnesium alloy. It can be seen from figure 2.29 that the corrosion potential, E_{corr}, of the superhydrophobic surface is more positive than that of the bare magnesium alloy which may be because of the protective film on the substrate. The corrosion current density, i_{corr}, of the superhydrophobic film decreases by greater than 1 order of magnitude as compared with that of the uncoated one, which indicates that, the superhydrophobic film of the bare material improved the corrosion resistance.
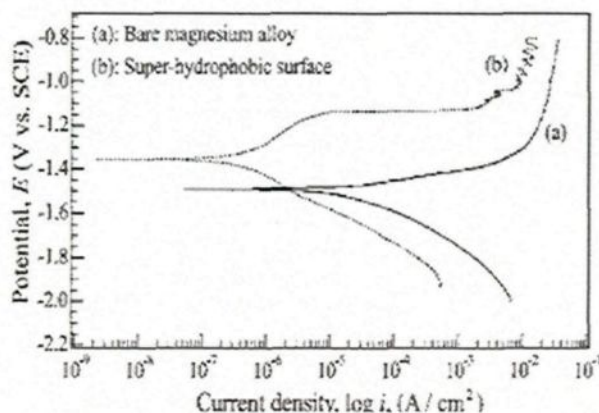
Figure 2.29 Potentiodynamic curves of (a) a bare magnesium alloy and (b) a superhydrophobic surface on a magnesium alloy.

CHAPTER 3

EXPERIMENTS

3.1 Material synthesis

3.1.1 Surface cleaning

Prior to any treatment or modification, the as-rolled substrates of copper and AA6061 aluminum alloy (Al 97.9 wt. %, Mg 1.0 wt. %, Si 0.60 wt. %, Cu 0.28 wt. %, Cr 0.20 wt. %) were thoroughly degreased and cleaned. Copper substrates were initially ultrasonically degreased in a soap solution for 30 minutes as well as with de-ionized water for 10 minutes followed by oxide removal by immersing in 10 vol. % HNO_3 and rinsing in ethanol. Then the copper samples were dried for 10 hours at 70 °C. Aluminum alloy substrates were ultrasonically degreased in a soap solution for 30 minutes followed by ultrasonically rinsing in de-ionized water for 10 minutes. Then the aluminum samples were dried for 10 h at 70 °C.

3.1.2 Fabrication of superhydrophobic copper surfaces

One-inch-square copper substrates were cleaned by the method mentioned previously. The cleaned substrates were immersed in a 0.01 M stearic acid solution for certain period of time and the DC voltage from 5 V to 30 V was applied. The anodic and cathodic copper plates were separated by a distance of 1.5 cm. The electrochemical modification device for the fabrication of superhydrophobic copper surfaces is shown in fig. 3.1. The surface of the anodic copper electrode turns blue due to the application of DC voltage. The modified anodic copper electrode was then dried for 10 h at 70 °C.
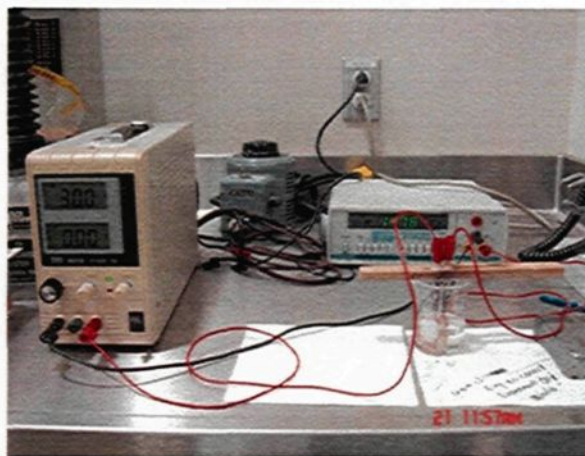
Figure 3.1 The electrochemical modification device (CURAL, Chicoutimi) for fabricating superhydrophobic copper surfaces.

3.1.3 Fabrication of superhydrophobic aluminum alloy surface

3.1.3.1 One-step process electrochemical modification

One-by-two-inch aluminum alloy substrates (AA6061) were cleaned by the method mentioned in the section of 3.1.1. The cleaned substrates were immersed in a 0.01 M stearic acid solution for certain period of time and the DC voltage from 5 V to 30 V was applied. The anodic and cathodic aluminum alloy plates were separated by a distance of 1.5 cm. It's the same device with the fabrication of superhydrophobic copper surfaces. The modified anodic aluminum alloy electrode was then dried for 10 h at 70 °C.

3.1.3.2 Chemical etching technique

One-by-two-inch aluminum alloy substrates are cleaned by the method mentioned in the section of 3.1.1. The cleaned substrates were immersed in 1 M NaOH solution for different times ranging from 1 to 30 min. All the etched samples were ultrasonically cleaned with deionized water

to remove any residual dust particles from their pores. The etched clean samples were dried in an oven at 70 °C for 10 h followed by passivation by 0.01 M stearic acid solution via immersing the samples in 0.01 M stearic acid solution for 30 minutes. The chemical etched aluminum alloys after passivation were then dried for 10 h at 70 °C.

3.1.3.3 Copper deposition on aluminum alloy followed by electrochemical modification with stearic acid molecules

Copper films were deposited on the cleaned AA6061 aluminum alloy substrates (one by two inches) with using an aqueous solution of 0.1 M CuSO4 and 0.1 M NaClO4 as used by Sarkar et al. [59] under potentials ranging from 0 to -1 V for a deposition time of 2- 90 minutes. The copper coated aluminum alloy substrates were electrochemically modified in ethanolic stearic acid solution for 30 minutes at 30 V.

3.2 Surface analysis

3.2.1 Surface microstructures

3.2.1.1 Morphology analysis

A scanning electron microscope (SEM/EDS, JEOL JSM 6480 LV, CURAL, Chicoutimi) was used for morphological characterizations, as shown in fig. 3.2. SEM measurements provide a two dimensional image of the morphological features of the surface as well as the chemical composition of the material via energy dispersive X-ray analyses.

Figure 3.2 The scanning electron microscope (SEM/EDS, JEOL JSM 6480 LV, CURAL, Chicoutimi)

3.2.1.2   Topography analysis

An optical profilometer was used to measure the roughness of surfaces, as shown in fig. 3.3

(MicroXAM-100 HR 3D surface profilometer, CURAL, Chicoutimi).

Figure 3.3 An optical profilometer (MicroXAM-100 HR 3D surface profilometer, CURAL, Chicoutimi).

3.2.1.3   Image analysis

Figure 3.4 Optical microscope and image analysis system (Clemex, CURAL, Chicoutimi).

The optical microscope equipped with a digital camera (Nikon ME 600) and an image analysis system (CLEMEX JS-2000, PE4.0, CURAL, Chicoutimi) allows the examination and quantitative analysis of the microstructure, as illustrated in figure 3.4. In our study, ten SEM images of each copper coated aluminum alloy sample prepared in a specific potential were analyzed using Clemex software to determine the number density of the copper particles and their interparticle distances. These methods were applied to describe and quantitatively analyze the microstructures.

3.2.2   Chemical composition analysis

In addition to the EDS introduced above, X-ray diffractometer (XRD) in CURAL, UQAC as shown in fig. 3.5 was also used to identify the crystalline properties of the different materials.
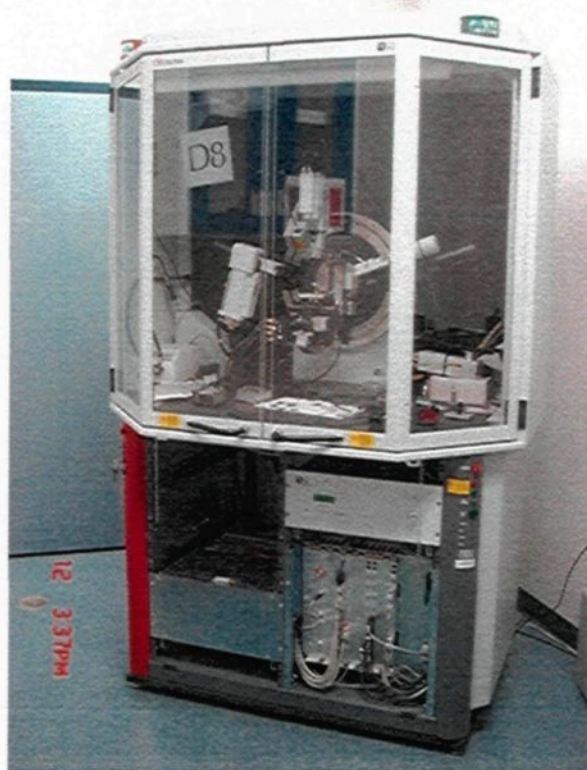
Figure 3.5 X-ray diffractometer (XRD) in CURAL, Chicoutimi

3.2.3   Wettability measurements

A contact angle goniometer (First Ten Angstrom contact angle goniometer, GRTB, University, Chicoutimi) is used to characterize the wetting characteristics of the different surfaces prepared by measuring static contact angles of water drops on these surfaces as well as by measuring the contact angle hysteresis by measuring the advancing and receding contact angles of a water drop advancing in one direction on a surface. The difference between the advancing and receding contact angles provides the contact angle hysteresis. A water drop of volume 10 uL is suspended from the syringe needle and brought into contact with the modified surfaces using a computer controlled device. The advancing and receding contact angles are measured by holding the needle stationary and moving the sample in one direction.
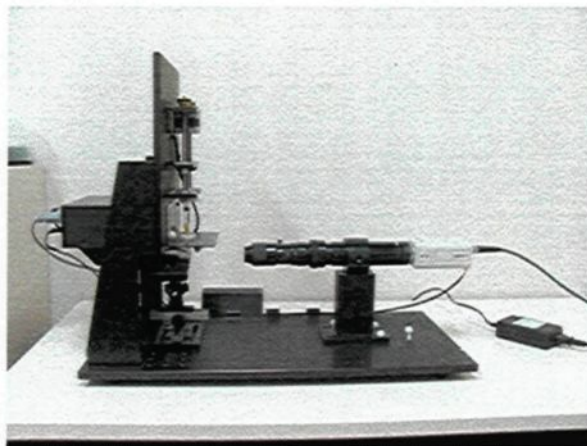
Figure 3.6 A contact angle goniometer (First Ten Angstrom contact angle goniometer, GRTB, University, Chicoutimi).

3.2.4 Corrosion test on the superhydrophobic copper and aluminum alloy surfaces

The corrosion resistance properties of superhydrophobic surfaces were investigated by immersing the samples in 3.5 wt. % NaCl solution and studying them in electrochemical technique-potentiodynamic polarization.

Superhydrophobic copper surfaces fabricated by immersing in 0.01 M stearic acid for 3 h at 30 V were exposed in 3.5 wt. % NaCl solution for 1- 120 h in order to analyze the stability of the superhydrophobic copper surfaces. The device was shown in fig. 3.7.

Figure 3.7 Homemade device (CURAL, Chicoutimi) of the corrosion behavior analysis by immersing the treated samples in the NaCl solution for a range of time.

Another corrosion test on superhydrophobic copper surfaces fabricated by immersing in 0.01 M stearic acid for 2 h at 30 V is immersing the surfaces in 0.5- 3.5 wt. % NaCl solution for 12 h to verify the effect of the corroded solution concentration on the corrosion behavior of the superhydrophobic copper surfaces.

Further, potentiodynamic polarization curve was obtained to compare the corrosion behaviors among copper substrate, hydrophobic copper surface prepared by immersing for 2 h at 5 V and superhydrophobic copper surface prepared by immersing in stearic acid for 2 h at 30 V. The electrochemical device was shown in fig. 3.8.

Figure 3.8 The electrochemical device for obtaining potentiodynamic polarization curves (Aluminum Technology Centre (NRC-ATC), Chicoutimi).

Superhydrophobic aluminum alloy surfaces, fabricated by copper deposited on aluminum alloy substrate for 10 minutes at -0.8 V in 0.1 M $CuSO_4$ and $NaClO_4$ mixed solution followed by electrochemically modification with 0.01 M stearic acid for 30 minutes at 30 V, were immersed in 3.5 wt. % NaCl solution for 1- 120 h to analyze the stability of the superhydrophobic film on aluminum alloy surfaces. The experimental device is the same as that of corrosion test for superhydrophobic copper surfaces shown in fig. 3.7. Furthermore, the similar electrochemical experiment by the equipment shown in fig. 3.8 has also been done to investigate the corrosion behaviors of superhydrophobic aluminum alloy surfaces as compared with their hydrophilic counterparts.

CHAPTER 4

PREPARATIONS OF NANOSTRUCTURED SUPERHYDROPHOBIC COPPER SURFACES

4.1 Introduction

A one-step electrochemical deposition process was applied to fabricate nanostructured superhydrophobic surface on cleaned copper surface via immersing the copper surfaces in stearic acid solution for certain period of time under certain potential. The experimental parameters such as the coating time, applied potential and the concentration of stearic acid solution are investigated in this project and are discussed in the following sections 4.2, 4.3 and 4.4, respectively.

4.2 Effect of modification time on the property of the superhydrophobic copper surfaces

4.2.1 The microstructures of the modified surfaces: Effect of the modification time

SEM studies of the copper surfaces reveal the evolution of different morphological features as a result of the application of 30 V DC on the copper electrodes immersed in the stearic acid solution with varying time, namely, 0.5 h, 1 h, 1.5 h, 2 h and 3 h, as shown in figure 4.1(a- e). A reaction between the anodic copper and the ethanolic stearic acid electrolyte due to an applied DC voltage results in the formation of flower-like morphological pattern on the anodic copper surface as shown by a high magnification SEM image in figure 4.1(f). It can be seen that a closely packed uniform

56

coating (figure 4.1(a)) is obtained on the surface prepared with 0.5 h of coating time. The formation of micro-size particles appears on the copper surface when the time of coating was increased to 1 h.

It is however, evident from figure 4.1(e) that prolongation of coating time to an increased 3 h resulted in the formation of a rough surface with features revealing flower-like microstructures of ~ 50- 100 μm. The SEM image of the individual flower-like microstructure (figure 4.1(f)) showed that each flower is composed of several tiny nanofibres clustered together to resemble a flower. It can be seen in figure 4.1(e) that these micro-nanoflowers are distributed randomly resulting in a micro-nanorough surface comparable to that of the lotus leaves promoting entrapment of air beneath a water drop placed on its surface [93]. The insets of fig. 4.1(a- e) present the shape of water drops on the respective surfaces in order to compare the superhydrophobicity of each surface visually. Recently, we have demonstrated the formation of flower-like silver films formation on copper surface by electroless deposition process [55].
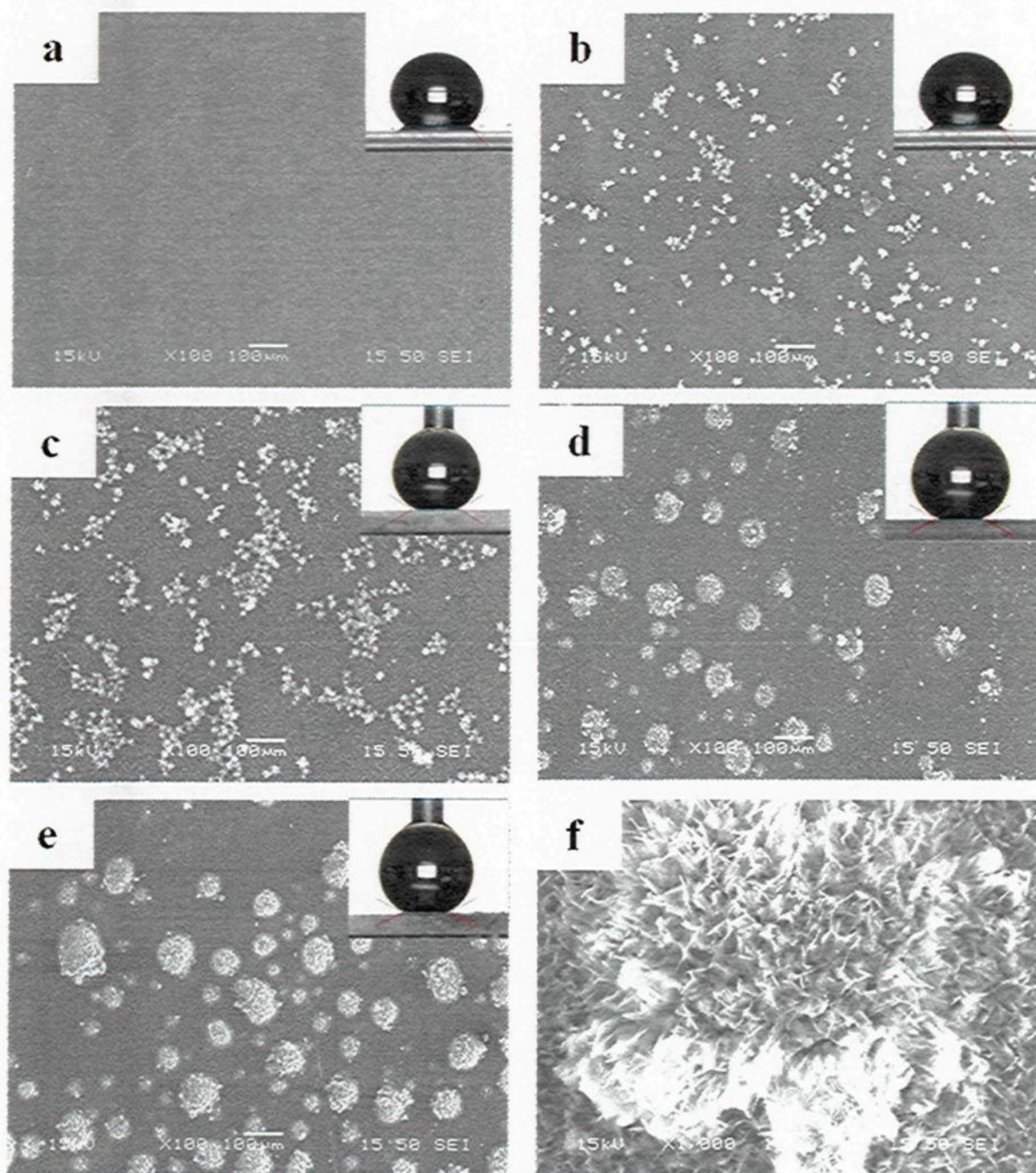
Figure 4.1 SEM image of the anodic surface of the copper electrode after the application of DC voltage in ethanolic stearic acid solution. Inset shows the drop of water on the sample surfaces. (a) 0.5 h; (b) 1 h; (c)1.5 h; (d) 2 h; (e) 3 h; (f) Morphology of the particles with 3 h. Insets of 4.1(a-e) shows images of a water drop placed on the respective surfaces.

4.2.2 Mechanism of the formation of flower-like copper stearate micro-nano particles

SEM studies of electrochemical modified anodic copper surfaces reveal a continuous growth process of flower-like particles. Figures 4.2(a- c) show the presence of different forms and sizes of flower-like particles on the surface of a same sample modified with stearic acid in the application of 30 V DC for 3 h. Figure 4.2(a) shows a uniform surface with tiny fibers distributed homogeneously along with the formation of a flower-like particle of diameter around $\sim 10 \mu$m. This nucleation centre is labeled as "a" which is whiter than the rest of the surface and composed of a few nanofibres.

In another region of the same surface as shown in figure 4.2(b), a larger flower-like particle is found having a diameter of ~ 20 μm diameter and it is labeled as "b". The number of nanofibres is more in the particle "b" as compared to the particle "a". Furthermore, figure 4.2(c) shows the presence of more than four flower-like particles in another region of the same surface. The particles are labeled as "c", "d", "e" and "f". The sizes as well as the number of nanofibres are different in these particles. After observing all the flower-like particles ("a"-"f") in the figures 4.2(a-c), a possible growth mechanism is proposed. The occurrence of the nucleation sites is random and a few nanofibres initially assembled together to form a nucleation of the flower-like particle on the surface. With the increase of time, more nanofibres are assembled together around the nucleation sites to produce larger flower-like particles. Lee et al. [94] show the formation of random disturbed nucleation sites with varying sizes in the bioactive and degradable ceramic/polymer composite films.
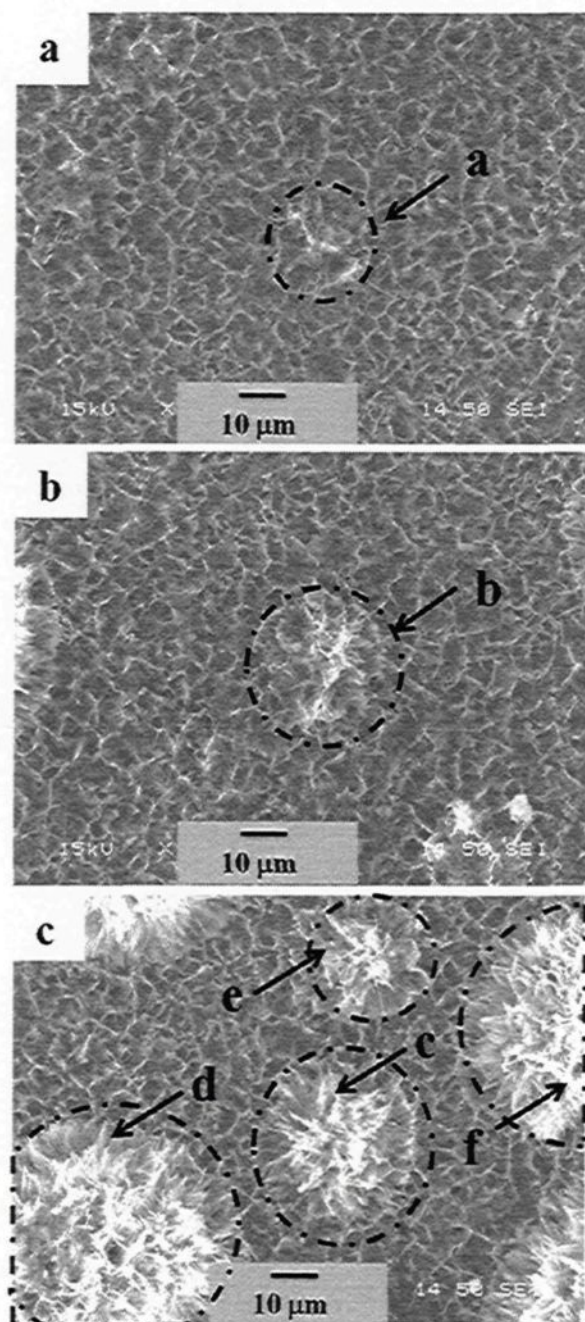
Figure 4.2 The different number and size of the formation of flower-like particles

4.2.3 The chemical composition of the modification films: Effect of the modification time

Further analyses of the surfaces were carried out using X-ray diffraction (XRD). Figure 4.3 shows the XRD patterns of the different surfaces as compared to a clean copper substrate recorded in the lower angle of 2θ range of $3 - 11$ °. The four distinct peaks appearing in the spectra are assigned to copper stearate $(CH_3(CH_2)_{16}COO)_2Cu$ [95] resulting from a reaction between stearic acid $(CH_3(CH_2)_{16}COOH)$ and copper upon application of DC voltage. The intensity of copper stearate peaks are found to increase with the increase of deposition time due to the increase of thickness. This observation is complementary with the SEM analysis (figure 4.1(a- e)), where an increase in the time of applied voltage results in an increase in the dimensions of the flower-like micro-nanostructures. The appearance of the copper stearate peaks in the XRD patterns confirms the presence of low surface energy methylated $(CH_3$ and $CH_2)$ components on the copper surfaces.
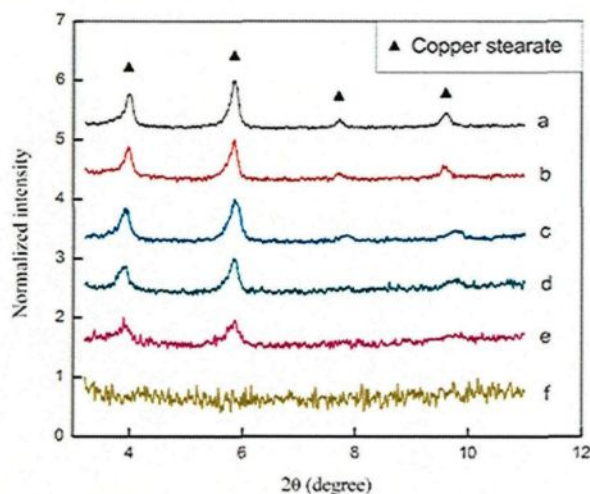
Figure 4.3 XRD patterns of copper sample with the application of DC voltage for (a) 3 h; (b) 2 h; (c) 1.5 h; (d) 1 h; (e) 0.5 h; (f) pure copper substrate.

61

4.2.4 The superhydrophobicity of the modified surfaces: Effect of the modification time

Presence of flower-like micro-nanorough morphology and the low surface energy copper stearate together transform the copper surfaces to superhydrophobic. The wetting characteristics of these surfaces were characterized by measuring the water contact angles and contact angle hysteresis. Variations of the water contact angle (CA) and the contact angle hysteresis (CAH) of copper coating surfaces as a function of coating time were shown in figure 4.4(a) and (b). By increasing the coating time, contact angle increased in the application of each DC voltage. At 5 V and 10 V, the contact angle was measured to be increased just from 129 ± 3 ° and 132 ± 1 ° to the maximum of 138 ± 3 ° and 144 ± 1 ° when coating for 3 h, respectively. However, when 20 V DC was applied, the contact angle was found to be increased from 133 ± 2 ° to 138 ± 1 ° and arrived 156 ± 2 ° when the reaction retained to 3 h, much larger than that of 5 V and 10 V. It can be seen clearly that the surface exhibited superhydrophobicity as soon as the applied voltage increased to 20 V for 3 h immersing time. However, superhydrophobic phenomena observed on copper surfaces after 2 h immersing time under the application of 25 V DC, where the contact angle was found to be 152 ± 1 °. Superhydrophobicity at 25 V was arrived at a shorter time than that of 20 V. With the further increased of DC voltage of 30 V, the contact angle increased rapidly from 138 ± 1 ° to 155 ± 2 ° when reaction time increased from 0.5 h to 1.5 h. Further increase of immersion time of 3 h at 30 V, the CA remains constant. The contact angle value is powerful to confirm applied potential of 30 V leads to the superhydrophobic phenomena appeared faster than that of other lower potentials. However, the contact angle values all increase with the increase of the coating time at whatever potentials.

Figure 4.4 (b) showed the CAH of samples prepared at 5 V with coating times of 0.5 h to 3 h, where contact angle hysteresis decreased from 64 ° to 52 °. Due to these high CAH, water drops stuck to the stearic acid modified surfaces prepared at 5 V. Contact angle hysteresis for samples prepared at 30 V are shown in fig. 4.4(b). It is found that the CAH decreases from 33 ° to 1 ° with variation of the coating time of 0.5 h to 3 h. Evidently, with a high value of CAH water drop stuck to the copper surfaces that are prepared at 30 V for 0.5 h but a roll off properties are observed when the coating time was increased to 1.5 h. Safaee et al. [52] has also ever reported the variation of the contact angle and contact angle hysteresis over a range of coating times for three values of initial Ag^+ concentrations. It is found that the superhydrophobicity is obtained with CA as high as 156 ° and contact angle hysteresis as low as 5 °.

The increase in water contact angle and the decrease in contact angle hysteresis at 3 h of time of application of DC voltage can be attributed to the co-existence of the micro-nanorough surface morphology with increased dimensions of the flower-like micro-nanofeatures (figure 4.1(e)) and the increased intensity of low surface energy copper stearate (figure 4.2), together reducing affinity of water toward the surface. Recently Sarkar et al., reported the formation of superhydrophobic copper surfaces with the deposition of silver films by galvanic exchange reaction both in one-step [96] and two-steps processes [52]. In the present study, the one-step process employed to obtain superhydrophobic copper surfaces is much simpler than we reported earlier [96].
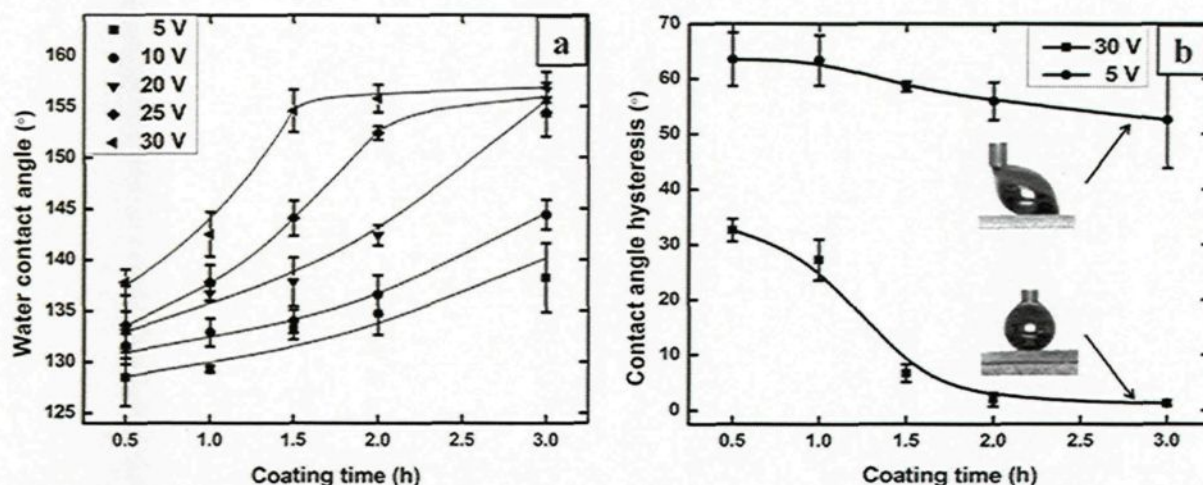
Figure 4.4(a) Water contact angle and (b) contact angle hysteresis of anodic copper electrode with the application of 5 V and 30 V DC voltage respectively in an ethanolic stearic acid solution. The insets show the water drops on the copper surfaces coated in 5 V and 30 V for 3 h.

4.3 Effect of DC potential on the superhydrophobic properties of copper surfaces

4.3.1 The microstructures of the modified surfaces: Effect of the modification potential

Figures 4.5(a- d) show the SEM images of copper surfaces modified electrochemically using stearic acid for 2 h under the application of DC voltages of 5 V, 20 V, 25 V and 30 V featuring micro-nanosized flower-like particles formation on the anodic copper plate. It can be seen that the size and the density of flower-like particles are increased with the increase of DC voltage. When the applied voltage was equal or lower than 20 V (figure 4.5(a- b)), the copper surfaces were reasonably smooth, as seen by SEM, and the water drop stuck to the surfaces providing a water contact angle below of 142 ° as shown in the inset of figure 4.5(a- b). However, the formation of micro-nanoparticles appeared when the voltage increased to 25 V (figure 4.5(c)) giving the contact angle of 152 ° (inset of figure 4.5(c)). Likewise, the flower-like microstructures were obtained at a

64

potential of 30 V (fig. 4.5(d)) and the water drops roll off those surfaces easily with the contact

angle of 156 ° (inset of figure 4.5(d)). The particles with flower-like patterns were distributed

randomly all over the copper surfaces creating two-tier micro-nanorough surfaces comparable to

that of the lotus leaves structure, resulting in superhydrophobicity.
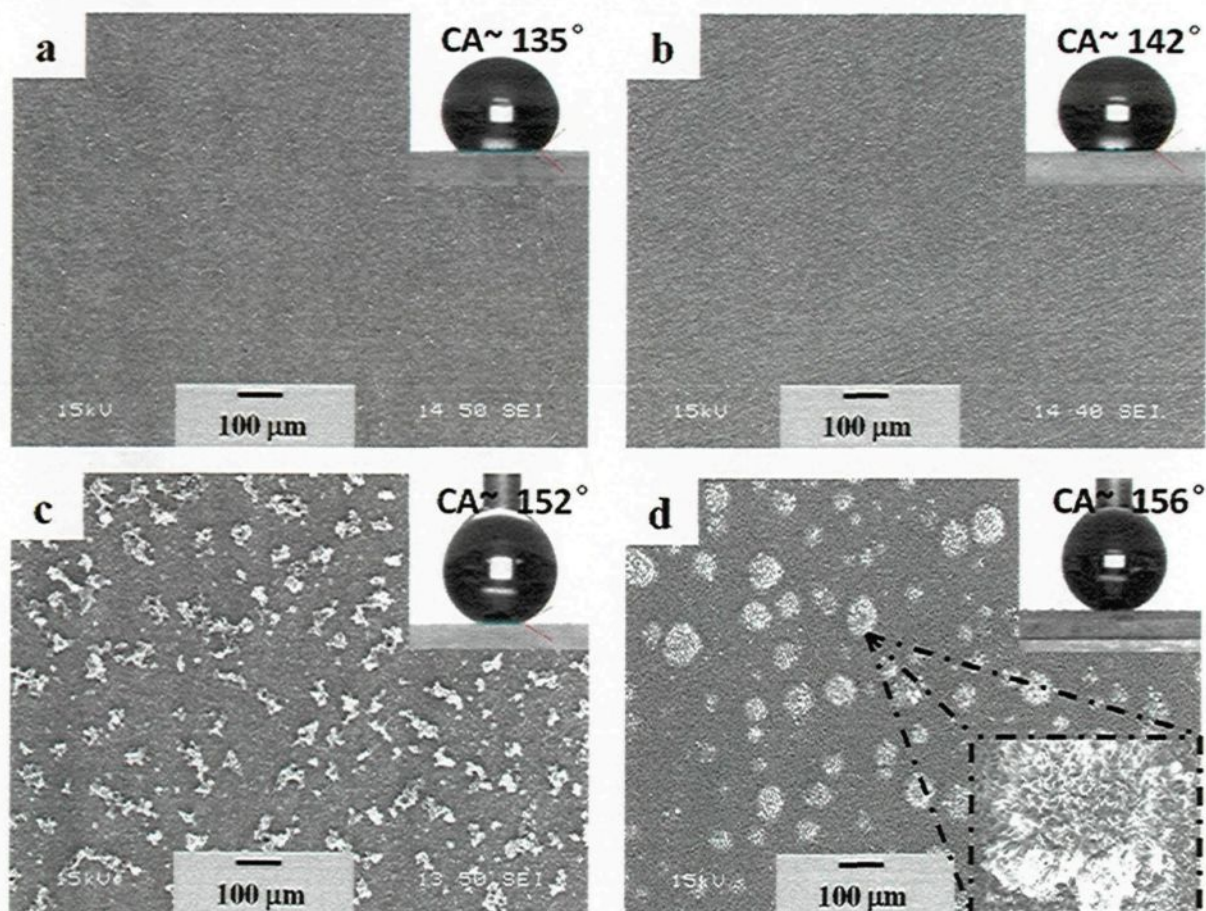
Figure 4.5 SEM images of anodic copper surface coated for 2 h in the application of different voltage. (a) 5 V. (b) 20 V. (c) 25 V. (d) 30 V. Inset of (d) shows the magnified image of one of the flower-like particles. The insets also show the water drop images on the copper surfaces coated with copper stearate at the respective voltages.

In our recent work, we have demonstrated that the reasonably smooth copper stearate surface

deposited at 30 V for 30 minutes provides a contact angle of 134 °. However, we find that smooth

copper stearate surface prepared at 5 V for 30 minutes provides a contact angle of 128 °, similar to

smooth Teflon surface, indicating that copper stearate is a low surface energy compound. Hence, a smooth coating of copper stearate on any microstructure surface with adequate roughness can be used to achieve superhydrophobicity.

4.3.2 The chemical composition of the modified films: Effect of the modification potential

The compositional and structural analyses of the surfaces were carried out using X-ray diffraction (XRD). Fig. 4.6 shows the low angle (2 θ range of 3 - 11 °) XRD patterns of the different surfaces prepared in the application of various DC voltages for 2h. The XRD pattern is very similar as presented in section 4.2.3 (fig 4.3) and the four peaks appears in the spectra are assigned to be copper stearate $(CH_3(CH_2)_{16}COO)_2Cu$ [95] resulting from a reaction between stearic acid $CH_3(CH_2)_{16}COOH$ and copper due to the applied voltage. It confirms the presence of low surface energy methylated (CH_3 and CH_2) components on the copper surfaces as before.
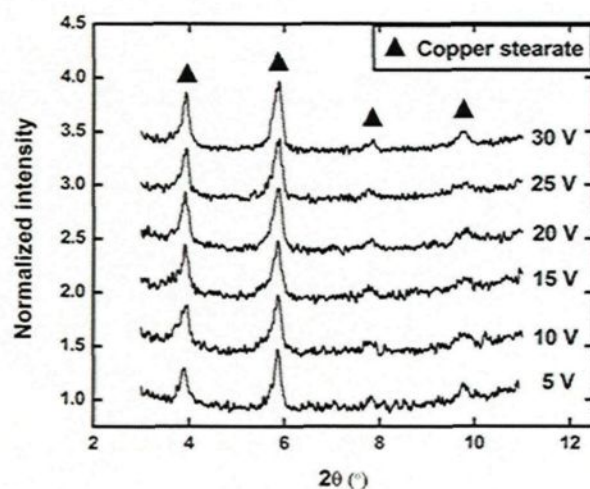
Figure 4.6 XRD patterns of the anodic surface of the copper electrode after the application of different voltage application when copper substrate immersed in stearic acid solution for the same time (2 h, 5-30V).

4.3.3 The superhydrophobicity of the modified surfaces: Effect of the modification potential

Figure 4.7 shows the variation of water contact angle as a function of the applied potential when the surfaces were immersed in stearic acid solution for a time of 0.5 h, 1.5 h, 2 h and 3 h. It is clear from the figure as well as from the table 4.1 that the water contact angles increase gently from 129 ± 3 ° to 138 ± 1 ° at the voltages of 5 and 30 V, respectively, for the samples electrochemically modified for 0.5 h. By increasing the electrochemical modification time of 1.5 h, the water contact angles increase gently up to 20 V. In this immersion time, a contact angle of 144 ± 2 ° is achieved at the modification voltage of 25 V and a contact angle of 155 ± 2 ° with superhydrophobic properties is achieved at a critical voltage of 30 V. By increasing the modification time of 2 h, the superhydrophobic surface with water contact angle of 152 ± 1 ° is achieved at a critical voltage of 25 V. Further increasing the modification time to 3 h, the superhydrophobic surface with water contact angle of 156 ± 2 ° is achieved at a critical voltage of 15 V. It has been observed that the critical voltage to achieve superhydrophobic surfaces can be reduced by increasing the deposition time. Similarly, the critical time to achieve superhydrophobic surfaces can be reduced by increasing the deposition potential. Many researchers investigated the variation of water contact angle with the variation of coating time with potential for the electrochemically deposited films. Zhang et al. [97] studied the variation of water contact angles on the surfaces of dendritic gold clusters as a function of the duration of electrochemical deposition of a constant voltage. They found the contact angles increase gradually with the time of electrochemical deposition. Further, they also pointed out that applied higher negative potential can increase the process of enrichment of the anions to the

electrode interface and lead to the formation of discrete gold aggregates. However, they never

illustrated that the longer coating time may bring superhydrophobic property at lower potentials.
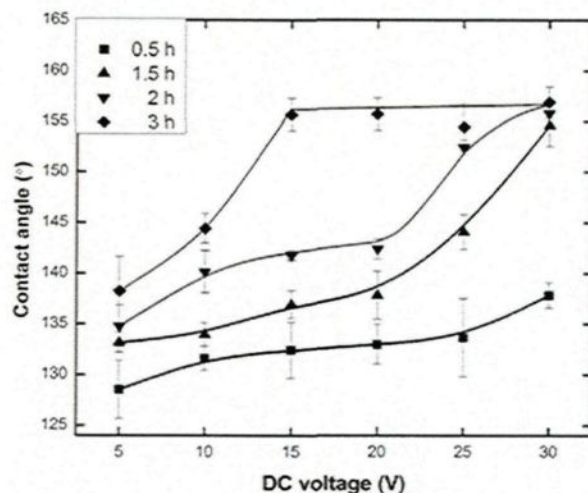
Figure 4.7 The variation of water contact angle of anodic copper electrode as a function of the application of voltage for 0.5 h, 1.5 h, 2 h and 3 h reaction time, respectively.

Table 4.1 The variation of water contact angle (°) as a function of the applied DC voltage as well as the time of modification.

Coating time (h) \ DC voltage (V)	5	10	15	20	25	30
0.5.	129 ± 3	132 ± 1	132 ± 3	133 ± 2	134 ± 4	138 ± 1
1.5	133 ± 1	134 ± 1	137 ± 1	138 ± 2	144 ± 2	155 ± 2
2	135 ± 2	140 ± 2	142 ± 1	142 ± 1	152 ± 1	156 ± 1
3	138 ± 3	144 ± 1	156 ± 2	156 ± 2	154 ± 2	157 ± 2

4.3.4 The roughness of the modified surfaces: Effect of the modification potential

Fig. 4.8(a) depicts the variation of surface roughness of copper surfaces modified by stearate

acid with the application of different DC voltage for 2 h. In order to analysis the relationship

between roughness and water contact angle, fig 4.8(b) shows the variation of water contact angle as a function of roughness of surfaces fabricated in the same condition as figure 4.8(a). The surface roughness of 5 V potential applied copper stearate film is found to be only 0.86 ± 0.13 μm as shown in fig. 4.8(a). The roughness of copper stearate film increased to 1.63 ± 0.34 μm at 10 V. At 15 V, the roughness further increases to 2.42 ± 0.71 μm and up to 2.53 ± 0.3 μm at 20 V. However, the increase of the potential to 25 V leads to an obvious leap to 4.82 ± 0.59 μm and arrived 6.44 ± 0.33 μm at 30 V. It can be also observed in figure 4.8(a) that the speed of the increase of roughness with the increasing potential between 20 to 30 V is faster than that of 5- 20 V. Further, it has been observed that the water contact angle increases with the increase of the surface roughness linearly with a slope of 3.99 °/μm. A roughness of 4.82 μm was essential in our study to obtain a surface with water contact angle of 152 ± 1 ° giving rise to superhydrophobicity.
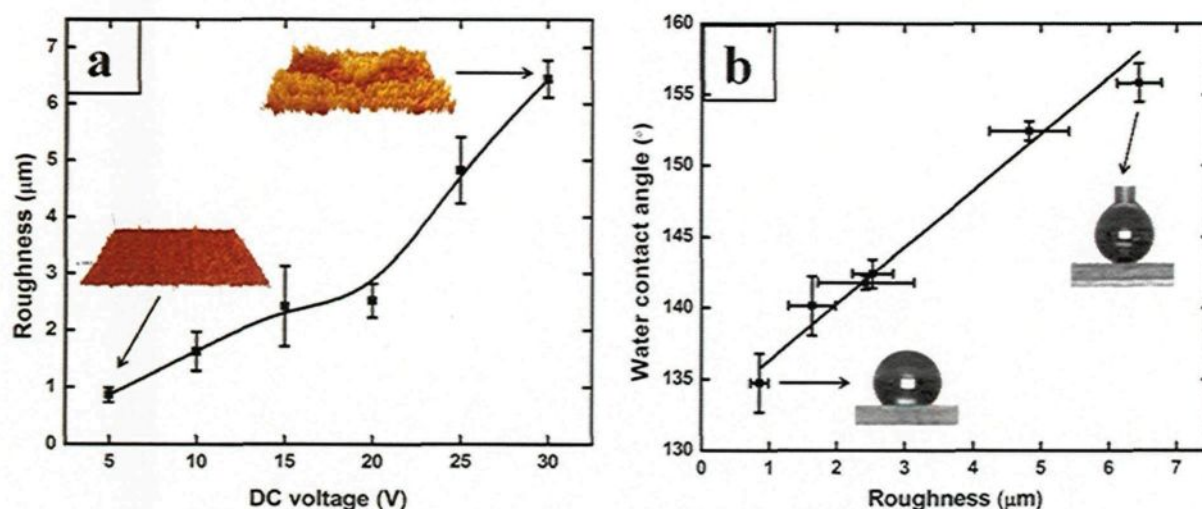
Figure 4.8 The variation of roughness vs. deposition potential, (b) variation of water contact angle vs. surface roughness on the stearic acid modified copper film deposited on aluminum surfaces. The inset of (a) shows the 3D images of the rough surfaces and (b) shows the images of water drops (-0.2 V & -0.8 V).

4.4 Effect of the stearic acid concentration on the superhydrophobic properties of copper surfaces

4.4.1 The microstructures of the modified surfaces: Effect of the stearic acid concentration

Morphological study of the anodic copper electrode in different concentration of ethanolic stearic acid solution was carried out by scanning electron micrographs. SEM micrographs shown in figure 4.9 are obtained from different concentration of stearic acid modified copper electrode in the application of 20 V DC for 30 min. It can be seen from the SEM images (fig. 4.9(a) to (d)) that the concentration of stearic acid solution is strongly responsible for the morphology of anodic copper electrode surfaces. When the concentration is low (0.01 M), the copper stearate film distributed non-uniformly on the copper substrate, which can be identified by EDS analysis in different areas of the modified copper surface, as presented in figure 4.10(a) as well as table 4.2. In the area (c), only copper signals are appeared in the EDS analysis after modification with 0.01 M stearic acid solution at 30 V for 30 minutes. In the area (d) on the other hand, the EDS analysis shows the appearance of the elements of copper, carbon and oxygen, confirming the formation of copper stearate after the modification with 0.01 M stearic acid solution at 30 V for 30 minutes. It can be concluded that the copper surface can't be covered by the flower-like particles by the low concentration (0.01 M) of stearic acid solution. The increasing of the concentration of the stearic acid solution (0.02 M) leads to the formation of large number of micro-sized clustered–particles, besides the copper stearate films are more compact than that of fig. 4.9(a). The background coverage of the coated lamellar particles is obviously increased with the increase of the concentration from 0.01 M to 0.02 M.
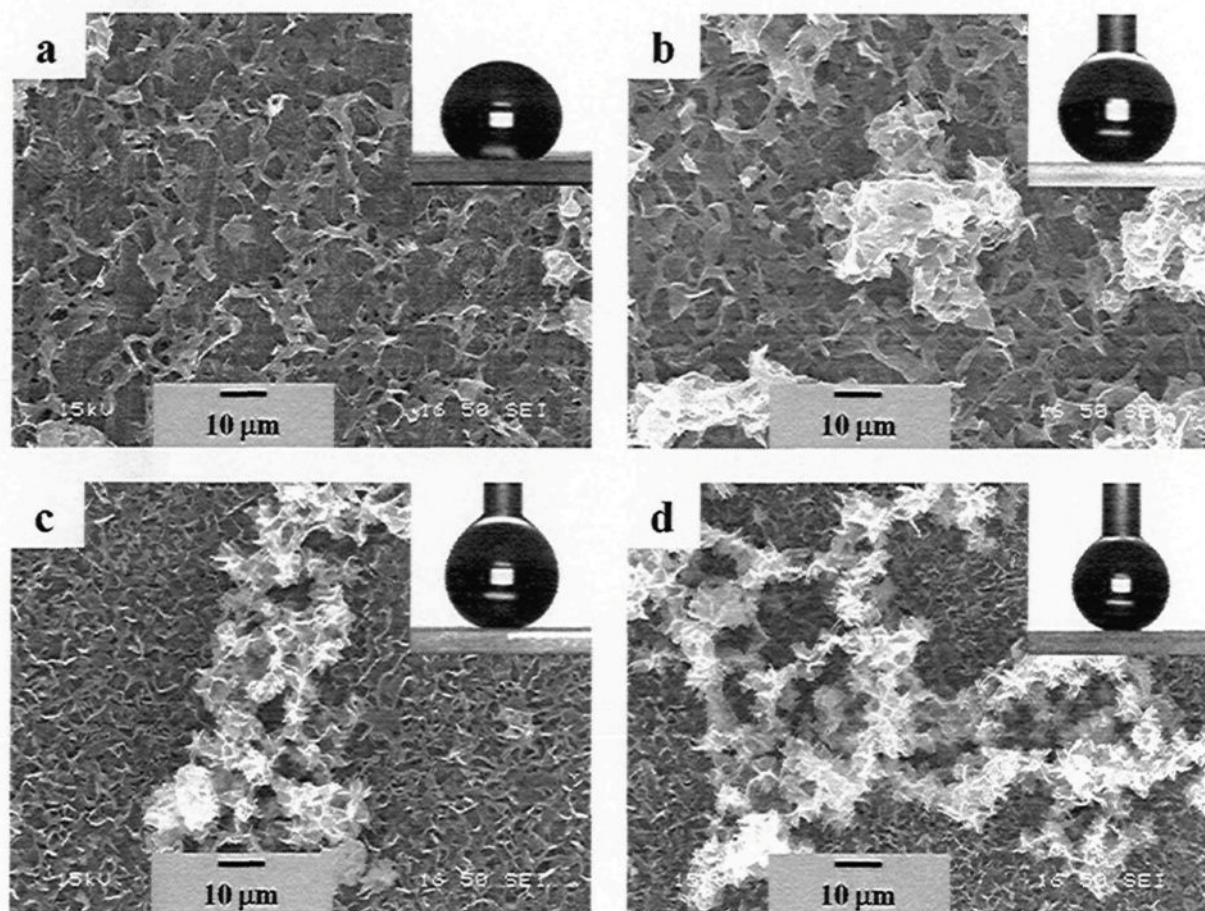
Figure 4.9 SEM images of the anodic surface of the copper electrode after the application of 20 V DC voltage in different concentration ethanolic stearic acid solution for 0.5 h. (a) 0.01 M; (b) 0.02 M; (c) 0.05 M; (d) 0.1 M. The insets show the water drops on the coated surface prepared by stearic acid solution of respective concentration.

It can be seen from figure 4.9(c) that the copper surfaces are completely covered with the copper stearate films when the concentration is increased to 0.05 M. In this concentration, a series of much smaller micro-sized structures appeared on the top of the compact structure as a second layer. The size and of the branches of the second layer was found to increase with the increase of the concentration of 0.1 M. It can be concluded that the higher concentration of stearic acid leads to the increase of the higher coverage of copper stearate on the copper surface as well as helps to the formation of flower-like particles. It is well known that the number of the nucleation sites on a surface depends on the concentration of the solution [98], and higher concentration leads to higher

71

number of nucleation sites. Therefore, the morphologies of the different surfaces are different due to the concentration of the solution as well as their superhydrophobic (wetting) properties according to the Cassie Baxter model [13]. N. L. Tarwal et al. [99] and Shinde et al. [100] have also discussed about the effect of the concentration on the nucleation on glass substrates. Further, the roughness of the surfaces increased due to the formation of large number of nucleation sites and their sizes.
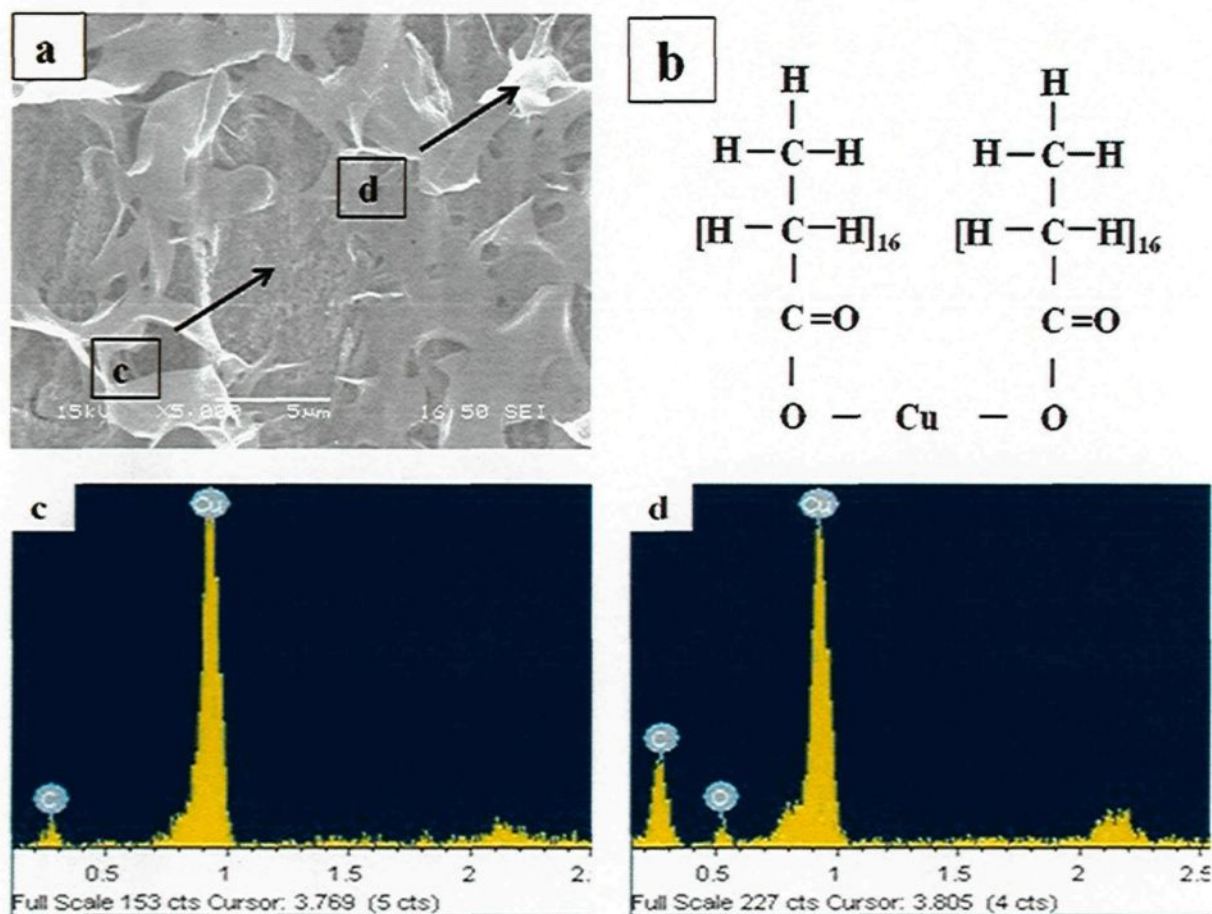
Figure 4.10(a) SEM image and (c), (d) EDS spectrum acquired from different morphologies on copper coating film made by immersing copper substrate in stearic acid solution for 0.5 h in application of 20 V DC voltage; the EDS spectrum of (c) and (d) chose the field shown in (a); (b) shows the molecule of copper stearate.

Table 4.2 The chemical composition of EDS result obtained from fig. 4.10

Elements	Point c (atomic %)	Point d (atomic %)
Cu	100	13.34
C	0	76.71
O	0	9.95

4.4.2 The chemical composition of the modified surfaces: Effect of the stearic acid concentration

The structure of the anodic copper surface was analyzed by using X-ray diffraction (XRD). Figure 4.11 shows the XRD patterns of different copper surfaces modified by ethanolic stearic acid solution of different concentration recorded in the lower angle of 2θ ranges of $3 - 11°$. In the previous section, we have reported that XRD patterns of different anodic surfaces after the application of 30 V DC in an ethanolic stearic acid solution (0.01 M). The four distinct peaks are assigned to copper stearate $(CH_3(CH_2)_{16}COO)_2Cu$, (the molecule was shown in fig. 4.10 (b)) [95], which coming from the reaction between copper and stearic acid $(CH_3(CH_2)_{16}COOH)$ in the application of 20 V DC voltage and the four peaks are perfectly consistent with that of previous work. It can be seen that the intensity of the four peaks increase obviously with the increasing concentration of the solution due to the increase of the nucleation sites and possible of the increase of thickness of the copper stearate films. The behavior is quite complementary with the SEM images shown in figure 4.9 (a-d), where the number of laminated structure increases with the increasing concentration of stearic acid in the solution. Further, the appearance of the copper stearate peaks in the XRD patterns confirms the presence of low surface energy methylated $(CH_3$ and $CH_2)$ components on the copper surfaces.
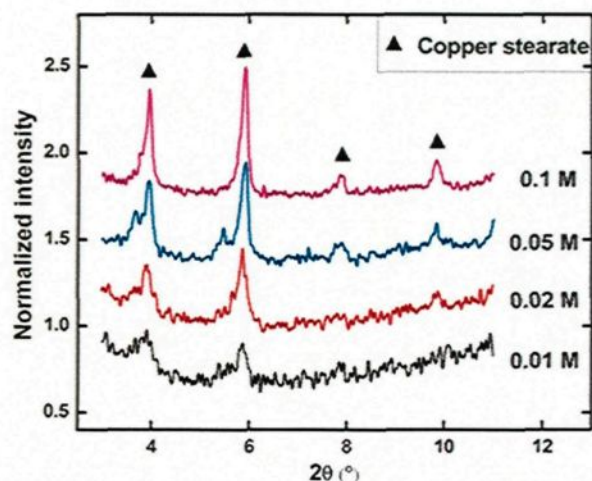
Figure 4.11 XRD patterns of the anodic surface of the copper electrode after the application of 20 V DC voltage in ethanolic stearic acid solutions of different concentration from 0.01 M to 0.1 M.

4.4.3 The superhydrophobicity of the modified surfaces: Effect of the stearic acid concentration

The wetting characteristics of the surface were analyzed by the water contact angle measurement. Figure 4.12 shows the variation of water contact angle of the modified copper surfaces as a function of the concentration of stearic acid solution at 30 V for 30 min. A water contact angle value of 133 ± 2 ° is obtained on the surface modified by 0.01 M stearic acid that is increased to 154 ± 3 ° with water roll off properties on the surface after modification with 0.02 M stearic acid solution. The water contact angle increased slightly to 157 ± 1 ° when the concentration of the stearic acid is 0.1 M. The insets of fig. 4.12 show the shape of water drops on the modified copper surface by different concentration of stearic acid in the solution, in order to compare the superhydrophobicity on the respective surfaces visually. The repelling of water on these surfaces is because of the formation of micro-nanorough surface morphology on the copper substrate as presented in figure 4.9 and the increased intensity of low surface energy copper stearate as presented in figure 4.11.

74
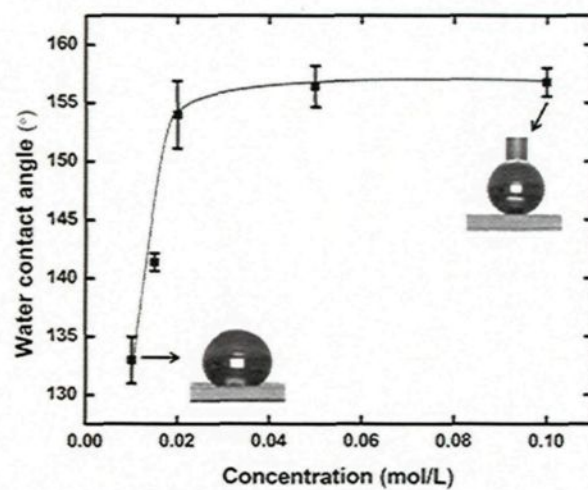
Figure 4.12 Water contact angle of different concentration stearic acid used to modify copper substrates in 20 V for 0.5 h.

CHAPTER 5

PREPARATIONS OF NANOSTRUCTURED SUPERHYDROPHOBIC ALUMINUM ALLOY SURFACES

5.1 Introduction

A one-step electrochemical deposition process has been applied to fabricate nanostructured superhydrophobic surface on cleaned copper surface via immersing the surface in stearic acid solution under certain potential. The same method was also applied on cleaned AA6061 aluminum alloy substrate as illustrated in section 5.2 to prepare superhydrophobic aluminum alloy surfaces. However, this method fails to demonstrate superhydrophobic aluminum alloy surfaces. Therefore, two new methods were adopted to prepare superhydrophobic aluminum alloy surfaces. In the first method, aluminum alloy surfaces were etched with NaOH solution followed by passivation with stearic acid solution (section 5.3).

In the second method, copper film was firstly deposited on aluminum alloy surface followed by electrochemically modification with stearic acid solution for 30 minutes at 30 V. The detail of the preparation of aluminum alloy surfaces in this method has been given in the following sections 5.4.1, 5.4.2 and 5.4.3.

5.2 Fabrication of superhydrophobic aluminum alloy surfaces by one-step electrochemical deposition

The same methodology of one-step procedure to fabricate superhydrophobic copper surfaces was also used to obtain superhydrophobic aluminum alloy surfaces. Figure 5.1 shows the variation

76

of water contact angles on electrochemically modified anodic aluminum alloy surfaces at 30 V for the variation of time from 0.5 h to 3 h. The water contact angles remain nearly the constant at 105 ± 1.5 ° and independent on the time of modification. As this method fails to show superhydrophobic properties (CA more than 150 °) on aluminum alloy surfaces we used chemical etching followed by passivation as given below.
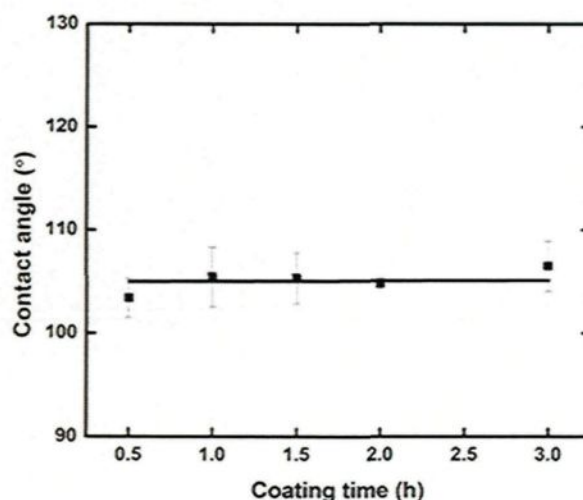
Figure 5.1 Water contact angle of anodic aluminum alloy electrode at 30 V DC voltage for 0.5 h, 1h, 1.5 h, 2 h and 3 h, respectively.

5.3 Fabrication of superhydrophobic aluminum alloy surfaces by chemical etching followed by passivation

5.3.1 The morphologies of the modified aluminum alloy surfaces

Fig. 5.2(a, c and e) shows the SEM images in different magnifications of the aluminum alloy surface after chemical etching in 1 M NaOH solution for 4 minutes followed by passivation with stearic acid (0.01 M) for 30 minutes. Fig 5.2(b, d and f) shows the SEM images in different magnifications of the aluminum alloy surface after chemical etching in 1 M NaOH solution for 20 minutes followed by passivation with stearic acid (0.01 M) for 30 minutes. It is clear from fig. 5.2

77

that the etch pits are formed on the aluminum alloy surface after etching with NaOH solution. The etch patterns are formed due to this preferential etching which effectively change the surface morphology and shows superhydrophobicity after passivation with stearic acid solution [61]. Further, it is observed from comparing to the morphologies by etching different time (a vs. b and c vs. d) that the longer etching time results in the increased roughness of the aluminum alloy surfaces. The aluminum alloy surface etched for 4 minutes was not covered by stearic acid completely after passivation. However, the stearic acid distributed uniformly on the aluminum alloy surface which was initially etched for 20 minutes. The higher coverage of the stearic acid on the 20 minutes etched surface as compared to 4 minutes etched surfaced due to higher roughness associated with the longer time of etching.
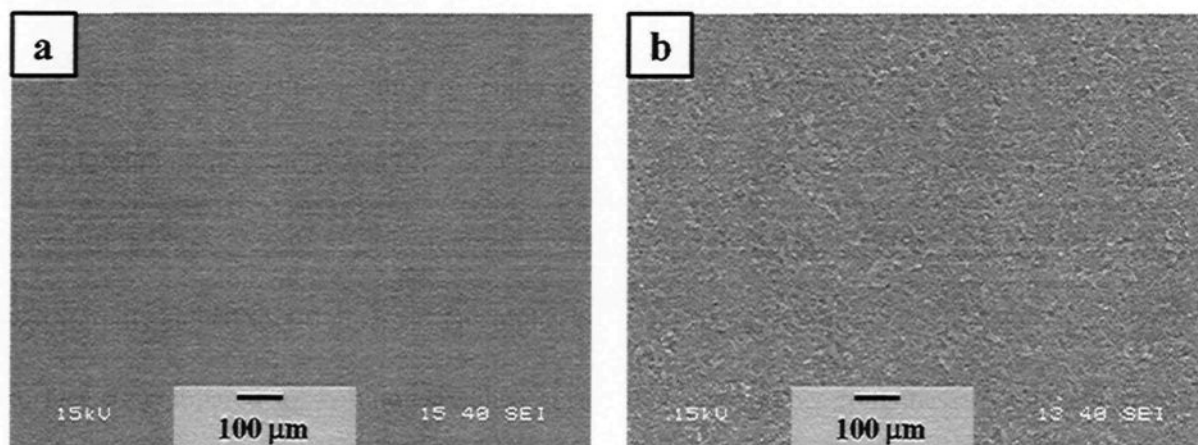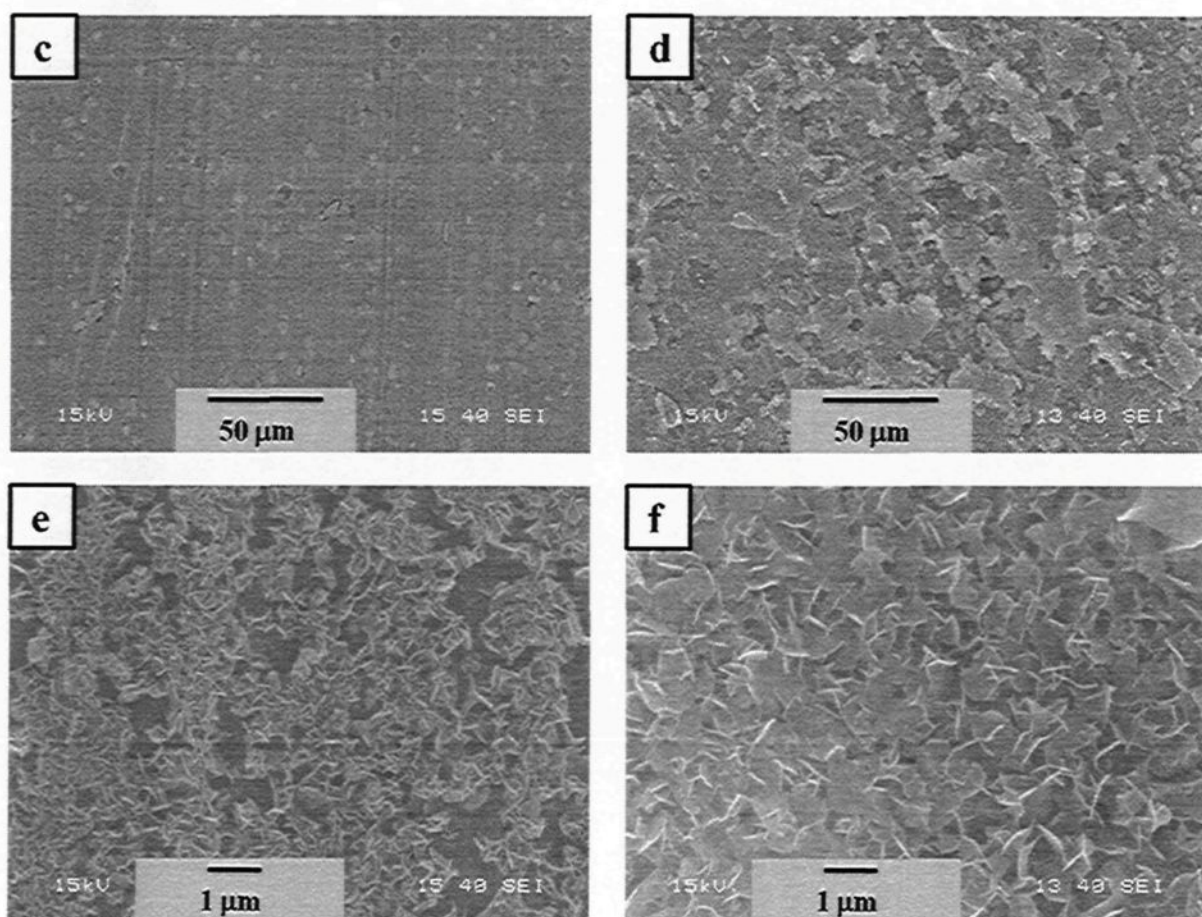
Figure 5.2(a, c and e) The SEM images in different magnifications of aluminum alloy surface etched for 4 minutes followed by passivation with stearic acid for 30 minutes. (b, d and f) show the SEM images in different magnifications of aluminum alloy surface etched for 20 minutes followed by passivation with stearic acid for 30 minutes.

5.3.2 The wettability of the modified surfaces

Fig. 5.3 shows the variation of water contact angle as a function of the etching time of the aluminum alloy surface in NaOH solution followed by passivation with stearic acid solution for 30 minutes. It is clear to observe that the stearic acid coated as-received AA6061 aluminum alloy substrate showed a contact angle of 103 ± 2 °. The water contact angle is found to increase to 153 ± 1 ° after etching for 2 minutes followed by passivation with stearic acid, showing water rolling off properties. It can be concluded that chemical etching for 2 minutes followed by passivation with

stearic acid for 30 minutes is necessary for the obtaining of superhydrophobicity on the aluminum alloy surface. The contact angle is 160 ± 2 ° with the 4 minutes etching time after passivation and then almost constant. The insets of Fig. 5.3 show the shapes of water drop on the aluminum alloy surfaces after 0 min, 2 min and 30 min chemical etching followed by passivation with stearic acid for 30 minutes for visualizing the values of contact angles. The similar relationship between water contact angle and the etching time has also been reported by Sarkar et al. [61].Compared with their study, which shows minimum of 2.5 minute of etching time with 14.8 wt. % of HCl solution followed by rf-sputtered Teflon coatings, we need slightly shorter etching time than their work to obtain superhydrophobic surfaces.
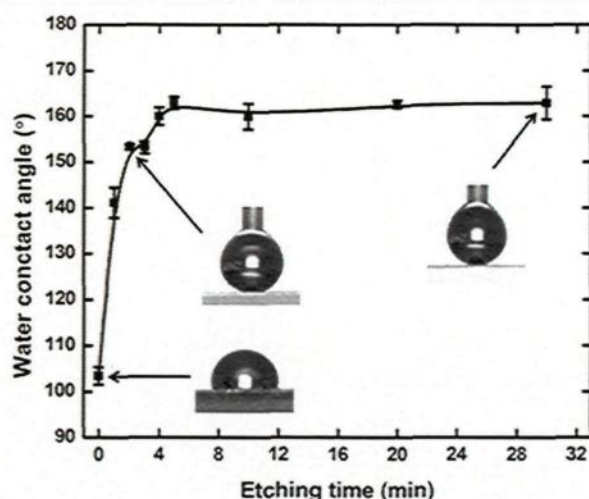
Figure 5.3 The variation of water contact angle as a function of the etching time of the aluminum alloy surface in NaOH solution followed by passivation with stearic acid solution for 30 minutes.

Figure 5.4 shows the variation of thickness of the aluminum alloy substrates with the etching time. The thickness of the as-received aluminum alloy substrate is 1.610 ± 0.005 mm. The thickness of the aluminum alloy substrates decreased with the etching time obviously, though the decrease value is only ~ 0.02 mm even after etching for 5 minutes, as shown in fig. 5.4. After 10 minutes of etching period, the thickness reduced to 1.577 ± 0.008 mm, which further reduced to 1.518 ± 0.002

mm after a prolongation of etching period to 30 minutes.
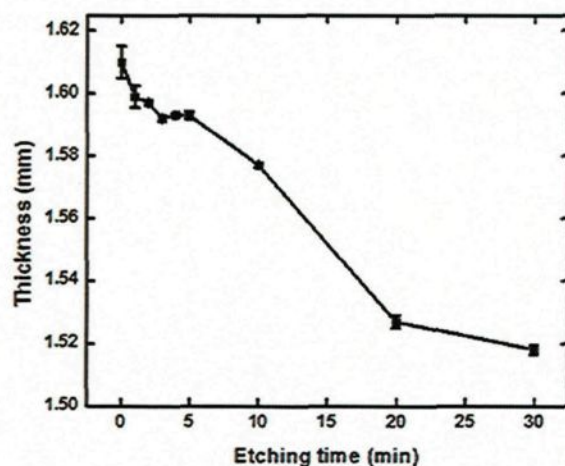
Figure 5.4 Variation of the thickness of aluminum alloy substrates with the etching time.

In Sarkar's work, it was also found that the thickness of the aluminum alloy substrate decrease with the increasing etching time [61]. The thickness of the aluminum alloy substrates is lost ~ 0.3 mm after 5 minutes in their study, which is much higher than that of ~ 0.017 mm with the same etching time in the present study. However, in the chemical etching process, aluminum alloy is lost from the surface which is not desirable for the benefit of the aluminum alloy industries. Therefore, we have adopted a second method. In this method, copper film was firstly deposited on aluminum alloy surface followed by electrochemically modification with stearic acid solution for 30 minutes at 30 V. In this method, the surfaces of aluminum alloy will be protected with additional layers of copper and copper stearate without losing the aluminum alloy substrate.

5.4 Fabrication of superhydrophobic aluminum alloy surfaces with copper deposition on aluminum alloy followed by electrochemical modification with stearic acid molecules

An attempt was made to obtain superhydrophobic aluminum alloy surfaces via similar procedure as it was performed on copper surfaces as presented in the chapter 4. However, because stearic acid modified aluminum alloy surfaces did not show the superhydrophobic properties, the aluminum alloy surfaces were firstly coated with copper films and further modified electrochemically by stearic acid molecules to achieve low surface energy copper stearate. The morphologies, chemical composition and surface wettability are found to be dependent on the aluminum alloy deposition time in the $CuSO_4$ solution, the deposition potential and the concentration of $CuSO_4$ solution, as discussed in section 5.4.1, 5.4.2 and 5.4.3.

5.4.1 Effect of the deposition potential of copper on aluminum alloy surfaces on the properties of superhydrophobic aluminum alloy surfaces

5.4.1.1 The microstructures of copper deposition on aluminum alloy surfaces as well as those surfaces after modification with stearic acid molecules

The SEM images of copper films deposited on aluminum alloy substrates are illustrated in Figure 5.5(a), (c), (e) and (g), respectively. Furthermore, the SEM images of the stearic acid modified copper surfaces are shown in Figure 5.5(b), (d), (f) and (h). It is found that, the electrodeposited copper films are composed of microdots of copper which is identified by EDS (spectrum not shown) as well as by XRD analysis. By means of image analysis technique, the

82

surface density of copper microdots (shown in table 5.1 as well as in figure 5.6) is found to be

4.5×10^4 cm^{-2} and the average distance between the microdots (nearest neighboring particles) is

26.66 μm for the film deposited at -0.2 V. Figure 5.6 also shows that an increase in the negative

potential to -0.4 V resulted in the increase of the number density to 8.3×10^4 cm^{-2} and the decrease of

the distance between neighboring particles to 18.69 μm. However, the sharp increase of the number

density of copper particles on aluminum alloy substrate appeared at -0.6 V, where the number

density and interparticle distance on copper film are 2×10^5 cm^{-2} and 13.15 μm, respectively. The

particle density further increases with the increase of negative potential and at -0.8 V the number

density of the particle is found to be 2.9×10^5 cm^{-2}. Moreover, the sizes of the microdots are found to

reduce with increase in negative deposition potentials. According to the Volmer-Weber growth

mode, in case of electrochemical deposition process, the number of the nucleation cites increases

with the increase of the negative deposition potential [101]. Therefore, it can be concluded that the

increase of the negative potential is responsible for the increase of the number density of the copper

microdots and consequently, the decrease in the distances between them in the present study. The

following equation can be used to express the density of the microdots as a function of the

deposition potential as presented in fig. 5.6(a):

$$N=\exp(-3.45V+9.99) \qquad \text{(Equation 5.1)}$$

where N is the number density of the microdots and V is the deposition potential. A plot of the

logarithm of particle density vs. deposition potential evidently shows a linear relation. Khelladi et al.

[102] also have observed a similar linear relationship between the deposition potential and the

logarithm of the particles density while depositing copper on n-Si (1 0 0) electrodes.

83

Table 5.1 The number density and inter-particle distance for copper film deposited on aluminum alloy substrates at different potentials.

Applied DC Voltage (V)	Number density of particles (number/cm^2)	Inter-particle distance (μm)	Roughness (μm)	Contact Angle (degree)
0.0	$1.1 \times 10^4 \pm 2.5 \times 10^3$	51.31 ± 22.67	2.39 ± 0.23	115 ± 1
-0.2	$4.5 \times 10^4 \pm 4.9 \times 10^3$	26.66 ± 9.71	3.15 ± 0.65	130 ± 5
-0.4	$8.3 \times 10^4 \pm 4.6 \times 10^3$	18.69 ± 6.62	4.24 ± 0.46	143 ± 4
-0.6	$2 \times 10^5 \pm 7.1 \times 10^3$	13.15 ± 4.00	6.20 ± 0.97	157 ± 1
-0.8	$2.9 \times 10^5 \pm 2.8 \times 10^4$	11.03 ± 3.33	6.77 ± 0.70	157 ± 1
-1.0	$2.4 \times 10^5 \pm 2.5 \times 10^4$	8.66 ± 2.59	7.02 ± 0.33	157 ± 1

We have observed that the aluminum alloy surfaces modified by ethanolic stearic acid solution under the influence of DC voltage did not show the superhydrophobic properties as we observed in the case of copper surfaces. In order to obtain superhydrophobic properties on aluminum alloy surfaces, the copper coated aluminum alloy surfaces were further electrochemically modified in ethanolic stearic acid solution at 30 V for 30 minutes. The stearic acid modified copper microdots were decorated with nanofibres resembling micro-nanostructured flower-like particles after stearic acid modification as shown in figures 5.5 (b, d, f and h). The flower-like morphologies formed on copper microdots coated aluminum alloy substrates are very similar to those obtained from the electrochemically modified pure copper surfaces reported previously by us. Further, it is interesting to note that the surface coverage on the stearic acid modified surfaces is higher covering nearly the whole area at higher negative potential as compared to a lower coverage at lower negative potential. The higher coverage might be due to the shorter interparticle distances between the copper micro-dots and the coalescence of the branches of copper stearate, a composition of copper and stearic acid, initiating from individual copper microdots in the empty space.
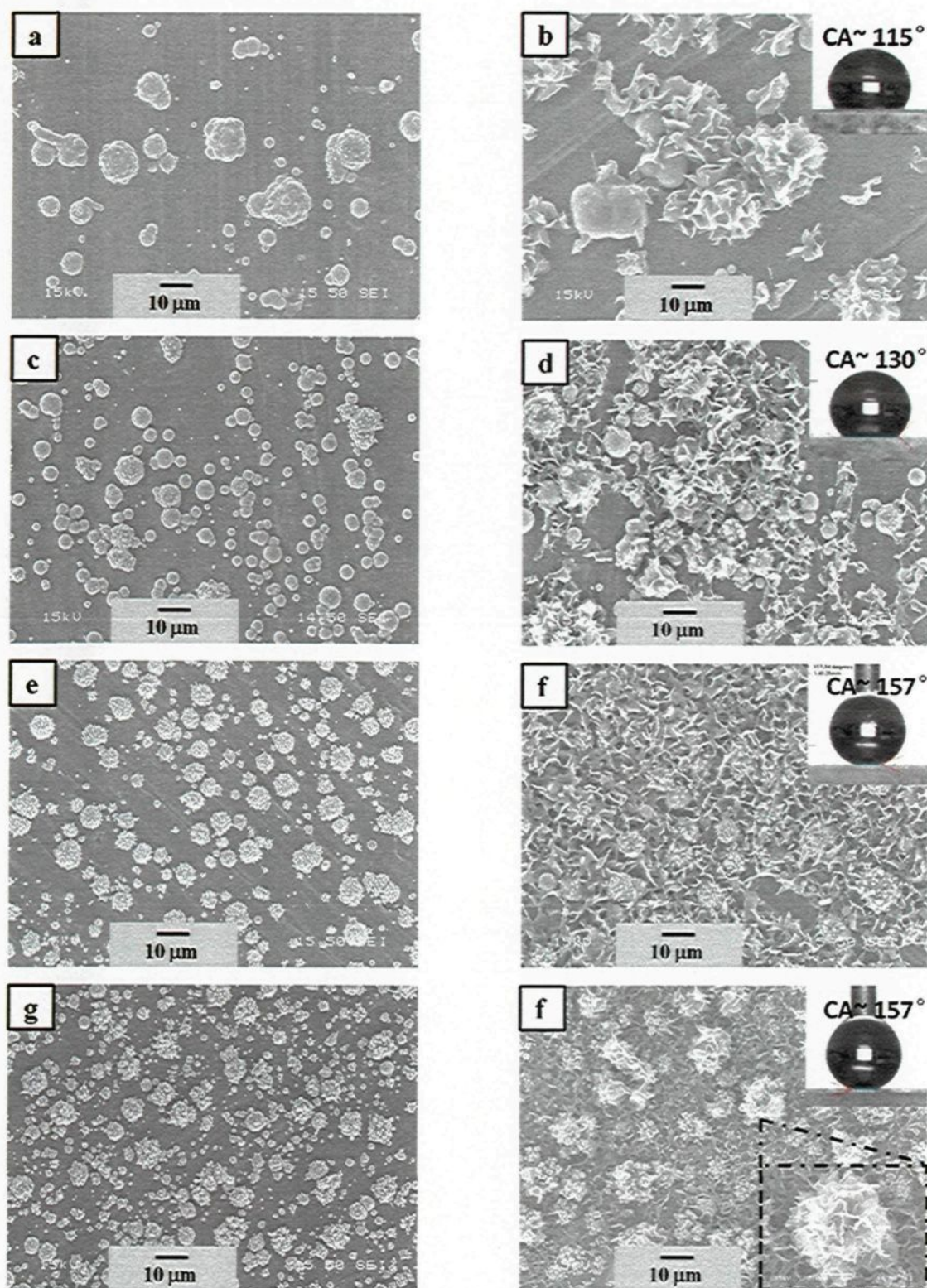
Figure 5.5 SEM images of copper films coated aluminum alloy substrates for 10 min at (a) -0.2 V, (c) -0.4 V, (e) -0.6 V and (g) -0.8 V and their surfaces after modified with stearic acid for 30 minutes at 30 V, namely, (b) -0.2 V, (d) -0.4 V, (f) -0.6 V and (h) -0.8 V, respectively. The insets of (b, d, f and h) show the water drop

images on the respective surfaces.
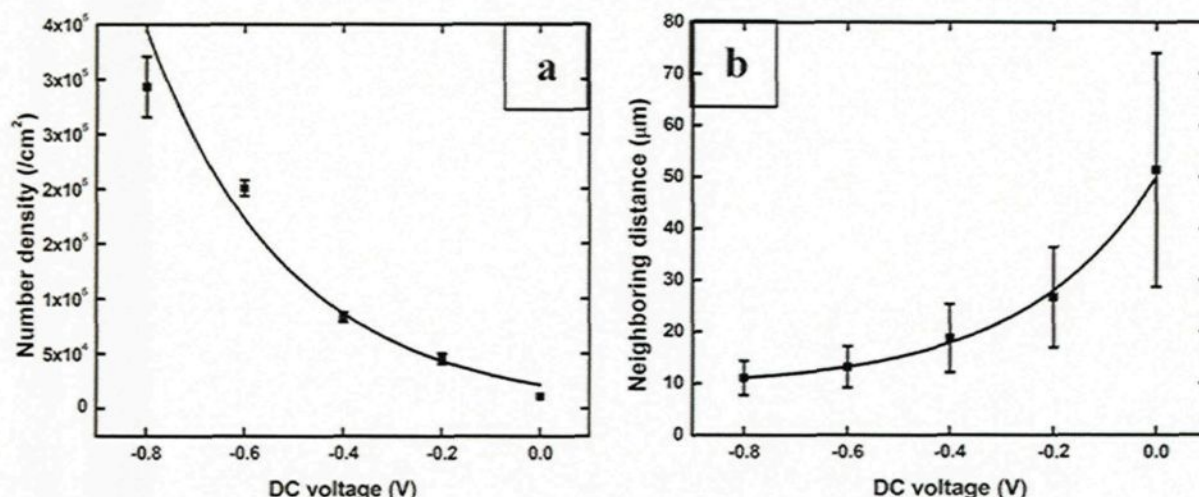
Figure 5.6 The number density of the copper microdots as a function of deposition potential and (b) The distance between the copper microdots as a function of deposition potential.

5.4.1.2 The chemical composition of the modified films

Figure 5.7(a) shows the XRD patterns of the copper films deposited on the aluminum alloy substrates with the application of different DC voltage of -0.2 V, -0.4 V, -0.6 V and -0.8 V in the 2 θ scan range of 35 - 55 ° showing the characteristic peaks at 38.47 ° and 44.72 ° correspond to Al (1 1 1) and Al (2 0 0), respectively arising from the aluminum alloy substrate [103] and the characteristic peaks of Cu (1 1 1) and Cu (2 0 0) at 43.32 ° and 50.45 °, respectively [104] confirming the copper deposition on aluminum alloy substrates. What's worth to note is the tiny peak at 43.32 ° on aluminum alloy substrate resulted from copper from AA6061 aluminum alloy. Figure 5.7(a) also shows that the peak intensity of Cu (1 1 1) increases and the peak intensity of Al (1 1 1) decreases with the increase of negative potential showing that the amount of copper deposition is higher at larger negative potential, which is complementary with the observation from SEM images of large

86

number of copper micro-dots deposition with the increase of large negative potential on aluminum alloy substrates.

Figure 5.7(b) shows the low angle (2 θ=3 $^\circ$ - 11 $^\circ$) XRD patterns of the electrochemically modified copper films composed of micro-dots of copper on aluminum alloy substrates in ethanolic stearic acid solution. Figure 5.7(b) also displays the low angle XRD pattern of the aluminum alloy substrate as well as our recently published copper stearate film (CuSA) prepared by electrochemically modified copper substrate in ethanolic stearic acid solution [95]. The copper stearate $(CH_3(CH_2)_{16}COO)_2Cu$ resulting from the reaction between stearic acid $(CH_3(CH_2)_{16}COOH)$ and copper under the application of DC voltage and it shows four distinct peaks at low angle XRD pattern as shown in Figure 5.7(b). On the other hand aluminum alloy substrates show a broad peak at 9.45 $^\circ$ might be due to the precipitate in the AA6061 aluminum alloy. The four copper films deposited at -0.2, -0.4, -0.6 and -0.8 V on aluminum alloy substrates and further modified electrochemically by stearic acid also show the four characteristics peaks of copper stearate. As the copper stearate consists of methylated (CH_2 and CH_3) components, the electrochemical modification by stearic acid of the copper films reduces the surface energy of the copper coated aluminum alloy substrates.
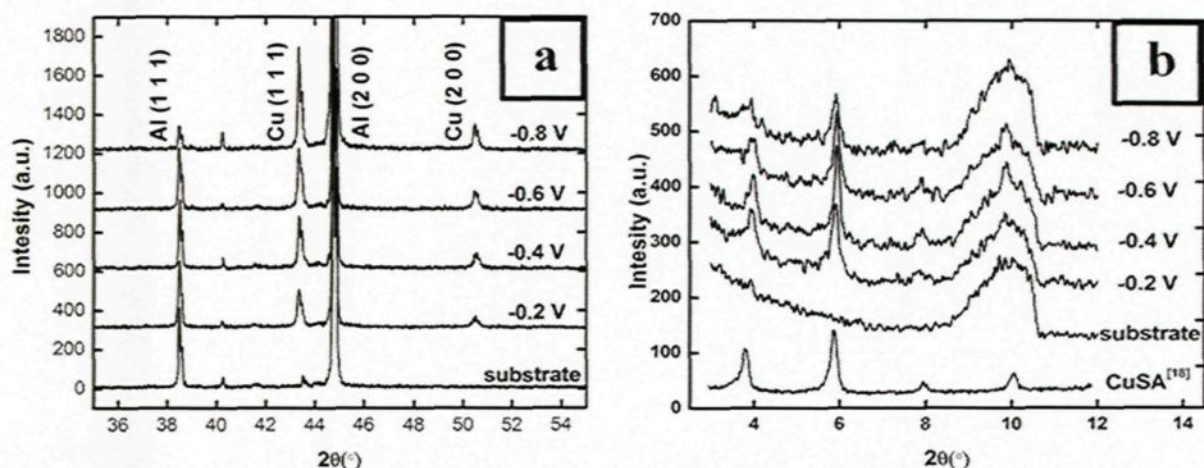
Figure 5.7(a) High angle XRD patterns of copper films deposited on aluminum alloy substrates for the duration of 10 min in the application of various voltages (as shown in the figure) followed by electrochemical modification in ethanolic stearic acid solution and (b) low angle XRD patterns of (a). CuSA is the XRD pattern of copper stearate films.

5.4.1.3 The wettability and roughness of the modified surfaces

Figure 5.8(a) and (b) depict the variation of surface roughness and water contact angle of electrodeposited copper film followed by electrochemical modification in ethanolic stearic acid solution. The surface roughness electroless deposited copper films (applied voltage equal to zero) is found to be 2.39 ± 0.23 μm as shown in fig 5.8(a) and the water contact angle on the surface is found to be 115 ± 1 ° as shown in fig 5.8(b) The roughness of the copper films increased to 3.15 ± 0.65 μm and the water contact angle also increased to 130 ± 5 ° for the copper films deposited at -0.2 V. At -0.4 V, the roughness further increases to 4.24 ± 0.46 μm and the water contact angle consequently also increases to 143 ± 4 °. At -0.6 V, the roughness further increases linearly with a slope absolute value of 2.45 μm/V to 6.20 ± 0.97 μm and the water contact angle found to be 157 ± 1 ° on that surface demonstrating superhydrophobicity. It can be also observed in the Fig. 5.8(a) that the speed of the increase of roughness with the increasing potential reduces to 2.33 μm/V between -0.6 to -1.0 V. The obtained roughness at -0.8 V is 6.77 ± 0.70 μm and the water contact angle on

this surface is remain the same as 157 ± 1 °. The roughness increases slightly to 7.02 ± 0.33 μm keeping the same water contact angle on the surface of copper films deposited at -1.0 V. It has been observed that the water contact angle increases with the increase of the surface roughness. An optimum roughness of 6.20 ± 0.97 μm was essential in our study to obtain a surface with water contact angle of 157 ± 1 ° giving rise to superhydrophobicity. Our observations have very good agreement with the studies of Rawal et al. [105], where they fabricated hydrophobic zirconium oxynitride films by reactive RF magnetron sputtering and found that water contact angle increased with the increase of surface roughness.
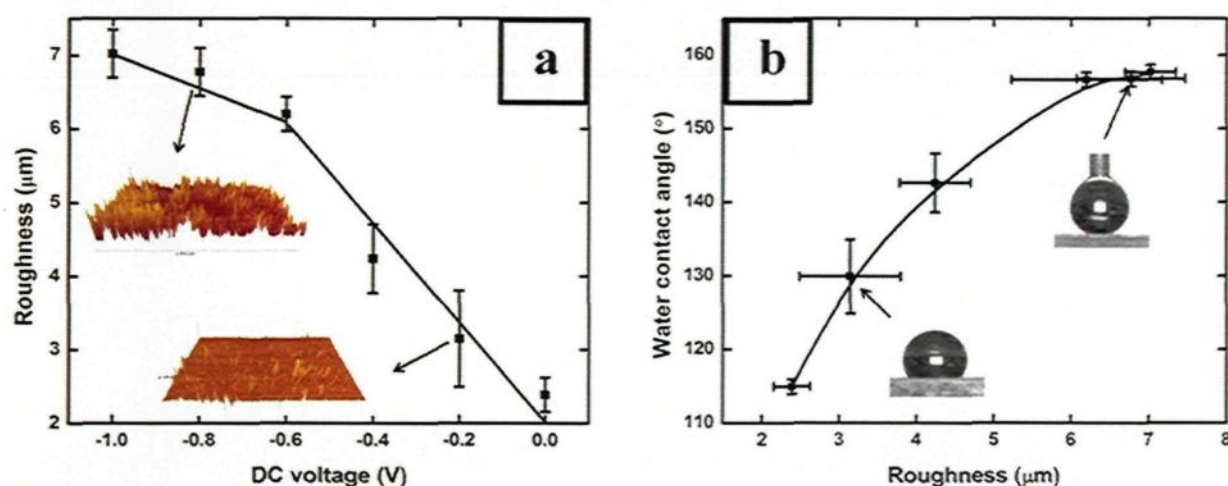
Figure 5.8(a) The variation of roughness vs. deposition potential, (b) variation of water contact angle vs. surface roughness on the stearic acid modified copper film deposited on aluminum alloy surfaces. The inset of (a) shows the 3D images of the rough surfaces and (b) shows the images of water drops (-0.2 V & -0.8 V).

5.4.2   Effect of the deposition time of copper on aluminum alloy surfaces on the superhydrophobic properties of aluminum alloy surfaces

We have found that superhydrophobic properties depend on the time of electrochemical modification of copper electrodes for a fixed potential. In the previous section we have shown that the morphological as well as superhydrophobic properties of aluminum alloy surfaces depend on

89

the copper deposition potentials for a fixed deposition time. In this section we will discuss the role of the deposition time on the superhydrophobic properties.

5.4.2.1 The microstructures of the copper deposited aluminum alloy surfaces as well as those surfaces after modification with stearic acid molecules

The figure 5.9 shows the SEM images of the morphological evolution of copper films deposited on aluminum alloy (fig. 5.9(a), (c), (e), (g) and (i)) and their further modification with stearic acid molecules (figures 5.9(b, d f, h and j). The electrodeposited copper films are composed of microdots of copper whose density and morphology changes drastically with the increase of deposition time as evident from the SEM images. The morphology of the surface changed from the circular particles (shown in fig. 5.9(a) to the fractal (foliar) shape (fig. 5.9(g)) with the increasing deposition time. The stearic acid modified microdots as well as the fractal-like structures decorated with nanofibres after stearic acid modification as observed previously in the copper films deposited in various potentials (fig. 5.5). The insets in fig. 5.9(b), (d), (f), (h) and (j) show the water drop on the modified aluminum alloy surfaces.
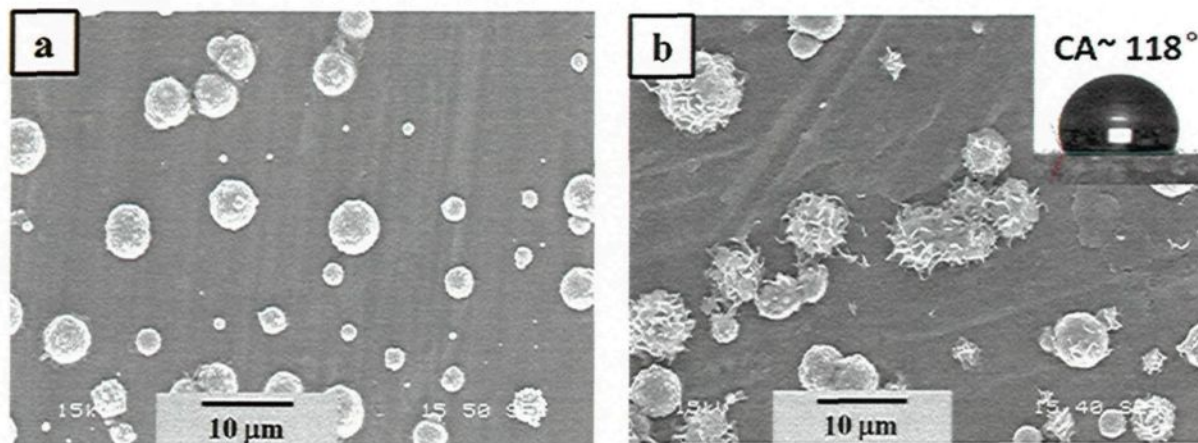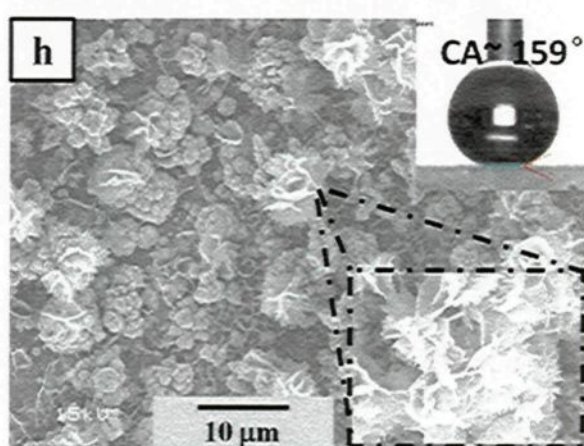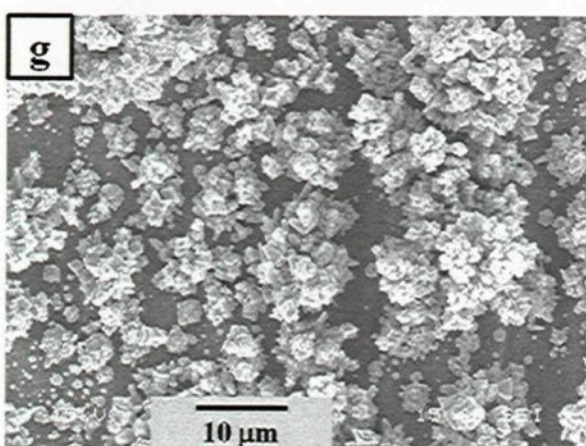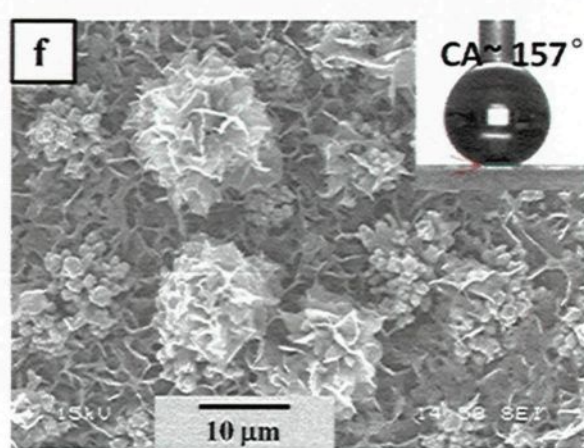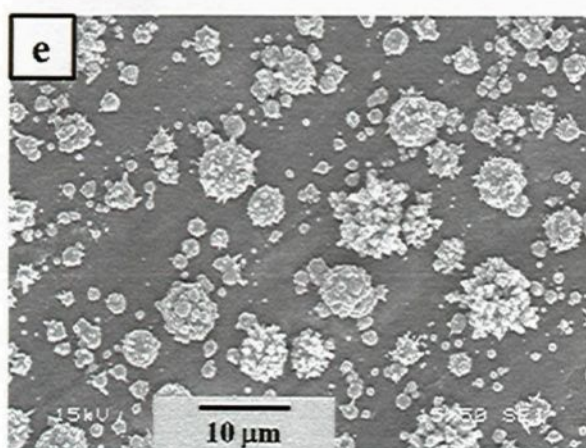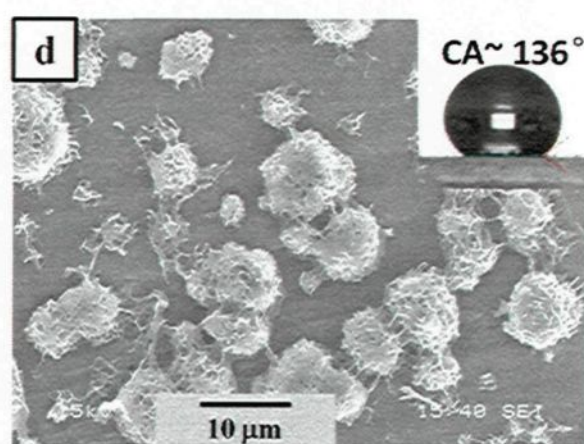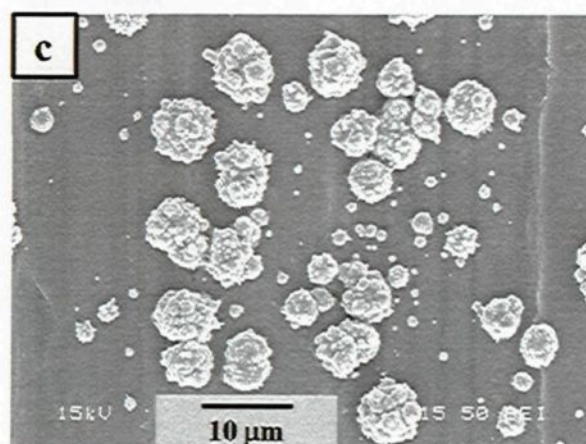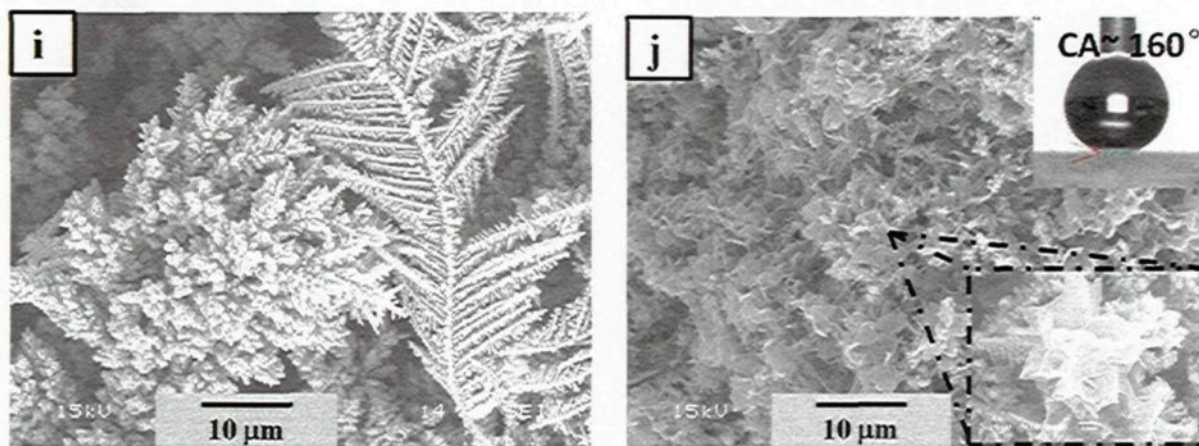
Figure 5.9 SEM images of copper deposited on aluminum alloy for different deposition time in the application of 0.8 V DC voltage (a) 2 min, (c) 5 min, (e) 10 min, (g) 30 min, (i) 90 min and their surfaces after modified with stearic acid for 30 minutes at 30 V, namely, (b) 2 min, (d) 5 min, (f) 10 min, (h) 30 min and (j) 90 min, respectively. The insets of fig. 5.9(b& d& f& h& j) show the water drop images on the respective surfaces.

5.4.2.2 The wettability of the modified surfaces: Effect of copper deposition time

We have shown that the existence of flower-like micro-nanorough morphology and the low surface energy copper stearate films together alter a hydrophilic copper surface to a superhydrophobic copper surface. The variation of water contact angle of the copper deposited aluminum alloy surface for a range of time followed by stearic acid modification as a function of the deposition time are shown in fig. 5.10. A contact angle value of only 118 ± 3 ° is obtained on the surface with copper deposition time of only for 2 minutes that is increased to 157 ± 1 ° with water roll off properties on the surface with copper deposition time of 10 minutes. The water contact angle increased slightly to 160 ± 1 ° when the copper deposition time is increased to 90 minutes. The inset of fig. 5.10 shows the shape of water drops for the two different time of deposition, namely 2 min and 90 min. The tendency of water contact angle variation in this case is agreement with that of copper deposited aluminum alloy surfaces at various potential as shown in the previous section.
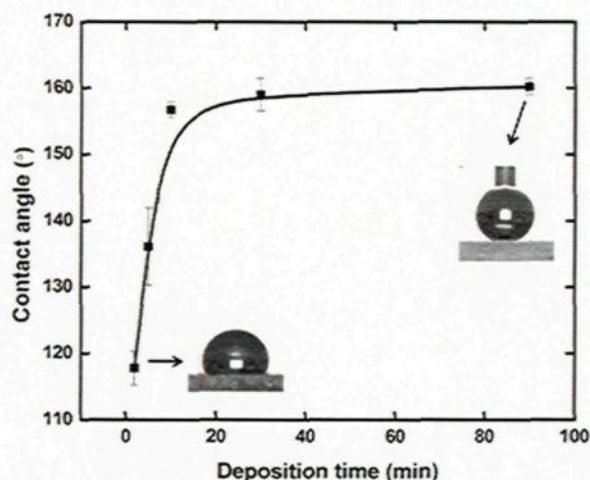
Figure 5.10 Variation of water contact angle on the stearic acid modified copper film deposited on aluminum alloy surfaces for various deposition time at -0.8 V followed by electrochemical modification by stearic acid at 30 V for 30 minutes. The insets show the water drop on the modified surfaces.

5.4.3 Effect of the concentration of deposition solution on the properties of superhydrophobic aluminum alloy surfaces

5.4.3.1 Microstructures of modified aluminum alloy surfaces

Fig. 5.11 shows the SEM images of the copper deposited aluminum alloy surfaces at -0.8 V for 10 minutes in the different concentration of $CuSO_4$ and $NaClO_4$ mixed solution followed by electrochemical modification with 0.05 M/L stearic acid solution for 30 minutes at 30 V. The electrodeposited copper films are composed of microdots of copper whose number density increase with the increase of the concentration of $CuSO_4$ as evident from the SEM images. The stearic acid modified microdots decorated with nanofibres after stearic acid modification and the formation of copper stearate on the copper deposited aluminum alloy surface increases with the increase of the concentration of $CuSO_4$ as observed in fig. 5.11. Furthermore, more fibers of the copper stearate clustered together and the neighboring distance of the clusters decreased obviously with the

93

increase of the concentration of the stearic acid solution.
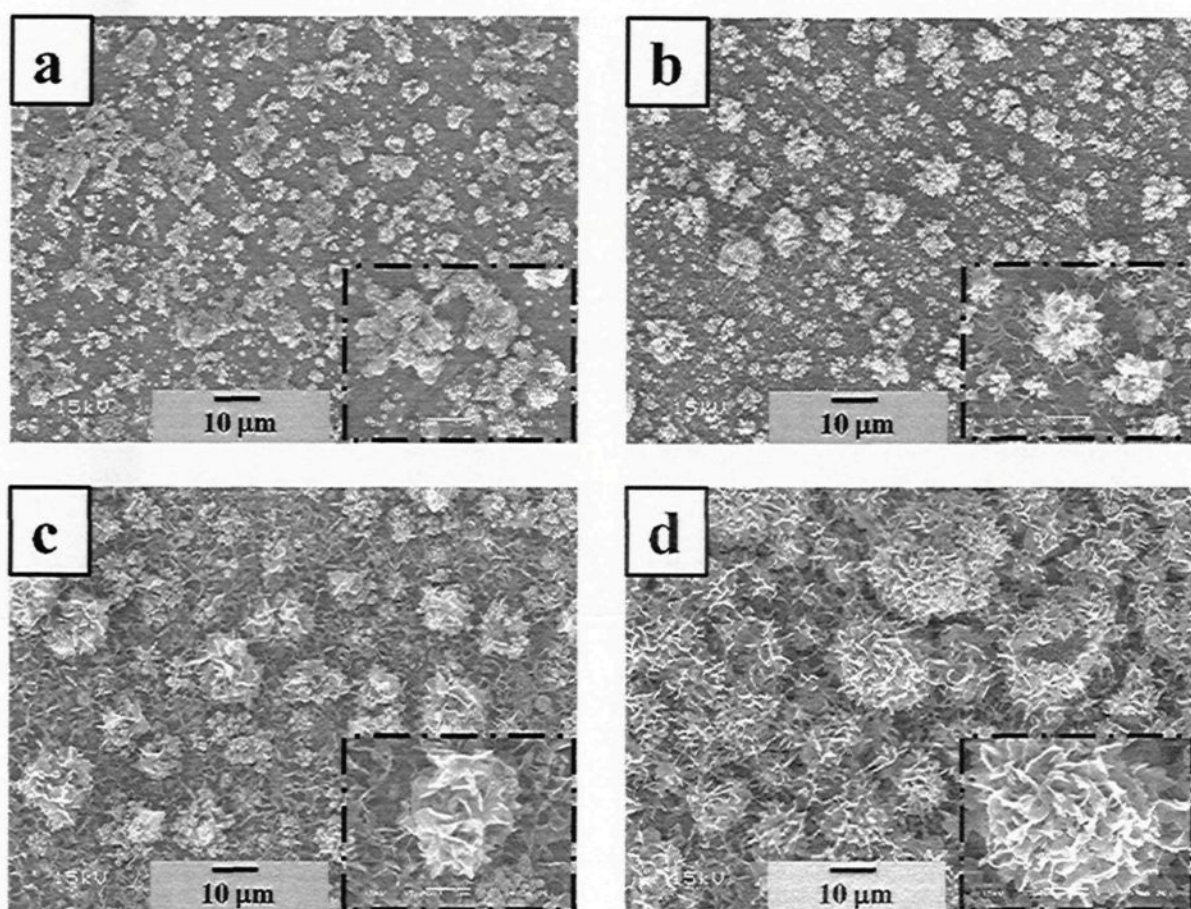
Figure 5.11 SEM images of the copper deposited on aluminum alloy surfaces by immersing in $CuSO_4$ solution of different concentrations followed by electrochemical modification with stearic acid molecules at 30 V for 30 minutes. (a) 0.01 M; (b) 0.05 M; (c) 0.1 M; (d) 0.5 M.

5.4.3.2 Wettability

Fig. 5.12 shows the variation of the water contact angles of the copper plated aluminum alloy substrate in the different concentration of $CuSO_4$ and $NaClO_4$ mixed solution at -0.8 V for 10 minutes followed by stearic acid modification. A contact angle value of 48 ± 1 ° is obtained on the surface of stearic acid modified copper films on aluminum alloy substrate with copper deposition solution containing 0.01 M $CuSO_4$.is the CA increased to 151 ± 2 ° with water roll off properties on

94

the surface with copper deposition solution containing 0.05 M CuSO₄ The water contact angle

increased slightly to 157 ± 1 ° when the concentration of the CuSO₄ solution increased to 0.5 M.

The insets of Fig.5.12 show the shape of water drops for the two different concentration of CuSO₄,

namely 0.01 M/L and 0.5 M/L. The tendency of water contact angle variation in this case is

agreement with that of copper deposited aluminum alloy surfaces at various potential as well as for

various deposition times as shown in the previous section. It is well agreement with the variation of

water contact angle as a function of the concentration of stearic acid solution when anodic copper

electrodes were modified by different concentration stearic acid under the potential, which

concluded that the increase of the concentration leads to the large number of nucleation of copper

on aluminum alloy substrates, which is responsible for the higher value of the water contact angles.
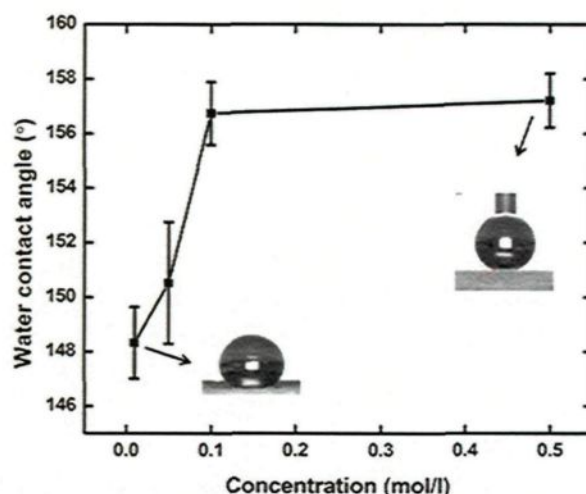
Figure 5.12 The variation of water contact angle as a function of the concentration of CuSO₄ solution of the copper deposited aluminum alloy surfaces at -0.8 V for 10 minutes followed by electrochemical modification with stearic acid for 30 V at 30 minutes.

CHAPTER 6

CORROSION TESTS ON SUPERHYDROPHOBIC COPPER AND ALUMINUM ALLOY SURFACES

6.1 Introduction

The superhydrophobic copper and aluminum alloy surfaces have been fabricated by electrochemical deposition technique as illustrated in the chapter 4 and chapter 5. The durability of these superhydrophobic copper and aluminum alloy surfaces was investigated by immersing them in 3.5 wt. % NaCl solution for a period of time of 1h to 120 h. The NaCl solution immersed superhydrophobic surfaces were further analyzed by measuring the water contact angle, morphology, chemical composition both by XRD as well as EDS. Furthermore, the electrochemical technique- potentiodynamic polarization is also used to determine the corrosion behaviors of superhydrophobic copper surface, hydrophobic copper surface as well as the bare copper surfaces in the NaCl solution by means of corrosion current density and polarization resistance.

6.2 Corrosion test on superhydrophobic copper surfaces

6.2.1 Effect of the immersion time in NaCl solution on the wettability of superhydrophobic copper surfaces

The durability of superhydrophobic copper surfaces were investigated by measuring the water contact angle after immersing in the NaCl solution. Figure 6.1 presents the variation of water contact angle of superhydrophobic copper surfaces as a function of the immersion time in 3.5 wt. % NaCl solution. The superhydrophobic copper surface was fabricated by placing the copper

electrodes in an ethanolic stearic acid solution for 3 h in the application of 30 V DC forming copper stearate providing a water contact angle is 157 ± 2 °. The water contact angle reduces to 152 ± 2 ° with roll off properties on the superhydrophobic surface that was immersed in the NaCl solution for one hour. The further increase of immersion time to 24 h, the water contact slightly reduced to 150 ± 1 ° keeping the superhydrophobic properties. It is found that the superhydrophobic copper surfaces with copper stearate coatings is resistance to corrosion against high concentrated NaCl solution at least for 24 h. Further increase of the immersion time to 48 h, the water contact angle on the superhydrophobic surface reduced to 131 ± 5 °. The water contact angle on the surfaces decreased continuously with the increase of the immersion time and reached 126 ± 6 ° after 120 h. Further, it is interesting to note from figure 6.1 that the error bars for 48- 120 h surfaces are much larger than that of 1- 24 h. It is indicated that the corrosion extent of longer time immersed surfaces isn't as uniform as that of 1- 24 h, which can be confirmed by SEM analysis. The superhydrophobic copper surface with copper stearate is stable in the strong NaCl solution to a certain extent, and the loss of superhydrophobicity with the immersion time might be related to the loss of copper stearate and the change of the microstructure of the surfaces. Some researchers also studied the corrosion protection of copper by fabricating superhydrophobic film on the surface [106,107,108], among which, Wang et al. reported that superhydrophobic film was fabricated by potentiostatic electrolysis method on copper and then placed in 3.5 wt. % NaCl solution for 20 days and the water contact angle was found to decrease to 140° [89].
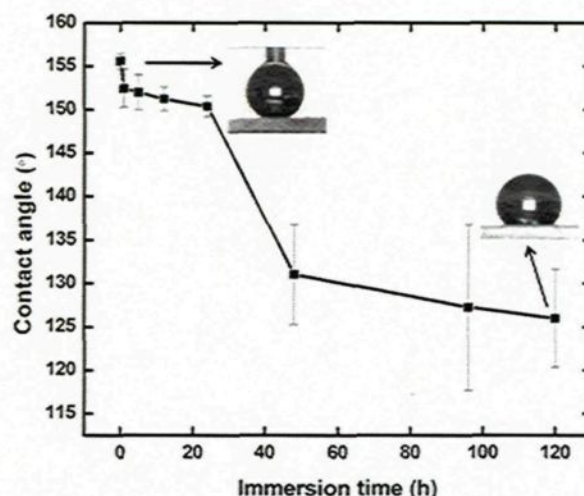
Figure 6.1 Water contact angle of copper stearate modified copper surface after immersing in the 3.5 wt. % NaCl corrosive solution in different times.

In order to investigate the loss of superhydrophobic properties, scanning electron microscope (SEM) was used to analyze the morphologies of superhydrophobic copper surface before (as discussed in section 4.2) and after immersing in the 3.5 wt. % NaCl solution for 120 h.

Figure 6.2(a) and (b) show the microstructure of superhydrophobic copper surface and its flower-like particle, respectively. It has been reported in the section of 4.2 that the reaction between copper and stearic acid under 30 V for 3 h resulted in the formation of a rough surface with features revealing flower-like microstructures of ~50- 100 μm. The SEM image of the individual flower-like microstructure (Fig. 6.2(b)) showed that each flower is composed of several tiny nanofibres clustered together to resemble a flower. However, the morphologies of the superhydrophobic copper surface changed obviously after immersing in the NaCl corrosive solution for 120 h as compared in fig. 6.2(c) with (a). Fig. 6.2(c) illustrates that the flower-like particle, as present in (a), was disappeared completely, on the contrary, several new smaller particles of ~ 2 μm appeared on the surface after immersing for 120 h. It is well known that the corrosion processes of copper in NaCl solution comprise the anodic dissolution of copper and cathodic reduction of oxygen [23,89]. The

98

anodic dissolution of copper is shown in the following equations:

$$Cu \rightarrow Cu^+ + e^-$$ (Equation 6.1)

$$Cu^+ + Cl^- \rightarrow CuCl$$ (Equation 6.2)

$$CuCl + Cl^- \rightarrow CuCl_2^-$$ (Equation 6.3)

And the cathodic reduction of oxygen is as follow:

$$O_2 + 4e^- + 2H_2O \rightarrow 4OH^-$$ (Equation 6.4)
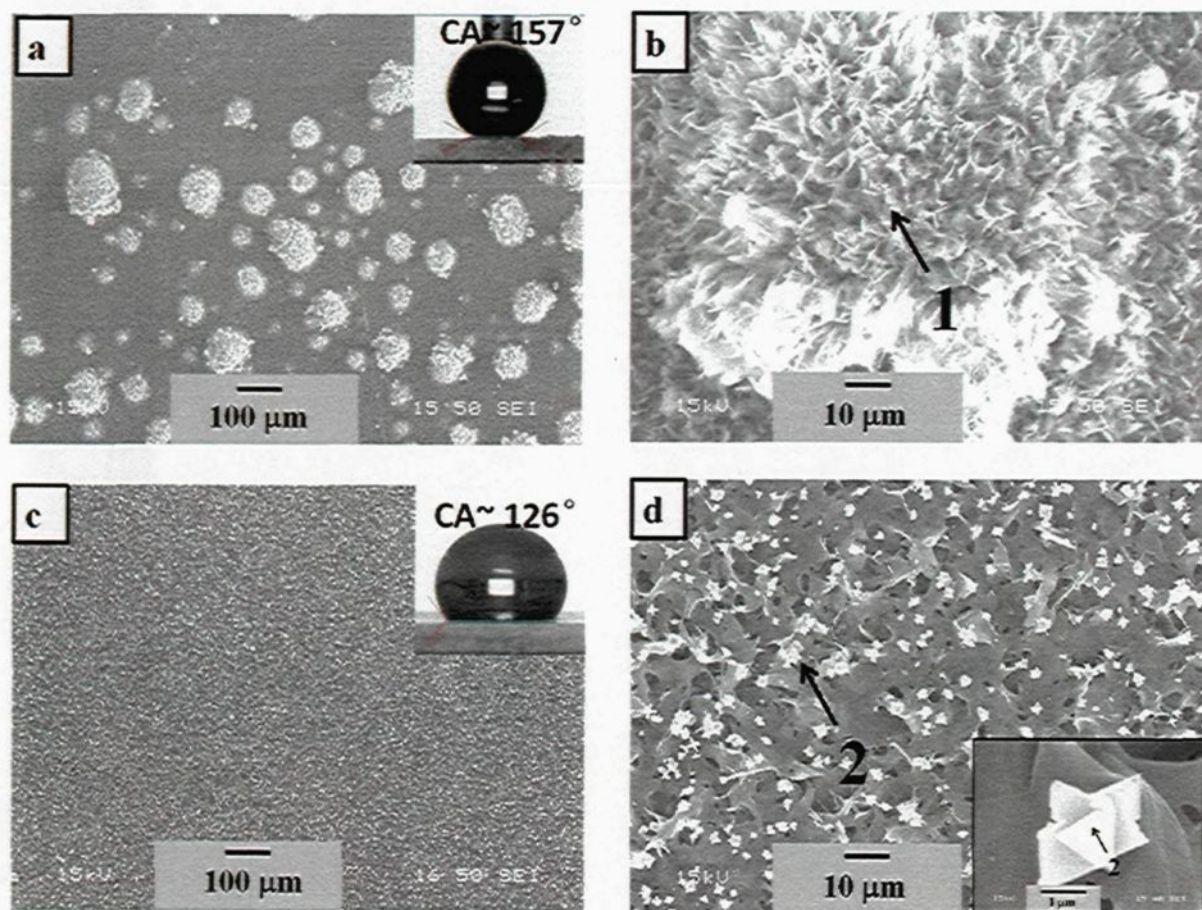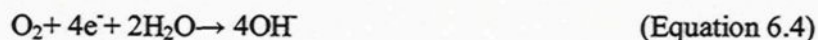
Figure 6.2(a) SEM micrographs of superhydrophobic copper surface which is fabricated by immersing copper substrate in stearic acid for 3h at 30 V DC voltage and (b) the magnified flower-like particle; (c) SEM micrographs of modified superhydrophobic copper surface after corrosion in NaCl solution for 120 h and (d) the magnified particle.

99

According to the eq.6.1-6.4 as well as the EDS results as shown in fig. 6.3 and table 6.1, the new observed smaller particles (corrosion product) were composed by elements of copper and chlorine, which is responsible to the decrease of the water contact angle of the copper superhydrophobic surfaces after immersion in 3.5 wt. % NaCl solution. Yan et al. [109] and Wang et al. [110] also studied the corrosion protection of copper by immersing their surfaces in the NaCl solution. They both utilized the equations of corrosion process of copper in NaCl solution, but they didn't analyze the different morphologies before and after the corrosion. In our report, however, the SEM images are used to compare the difference of the morphologies clearly. Ferreira et al. [111] studied copper corrosion in buffered and non-buffered synthetic seawater. They mentioned that when the concentration of chloride is lower than 5.84 wt. %, the final corrosion production is Cu_2O_3. Some other researchers, such as Brian et al., Milosev et al., Parkins et al. and Niu et al. [112], have investigated the corrosion, passivation and transpassive corrosion of copper in the presence of aggressive anions, ie. HCO^{3-}, Cl^- or SO_4^{2-}.

Table 6.1 The chemical composition of EDS result obtained from figure 6.2.

Element	Point 1 (Atomic %)	Point 2 (Atomic %)
C	87.34	59.33
O	7.85	28.77
Cu	4.80	8.23
Cl	0.00	3.67
Total	100	100
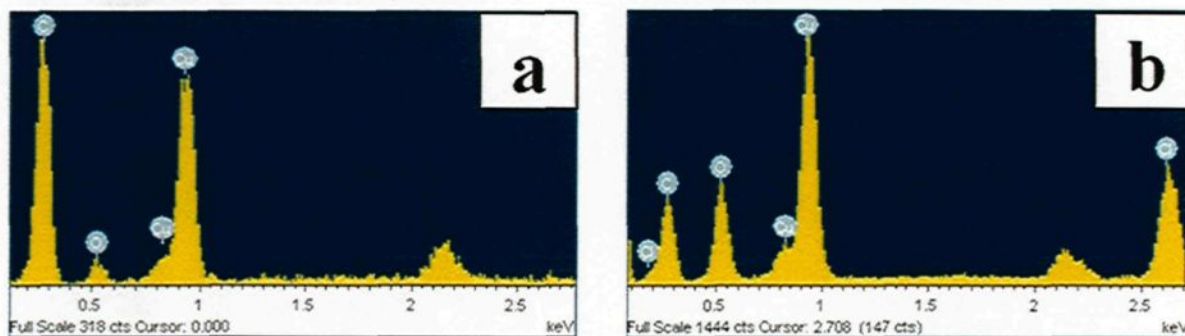
Figure 6.3(a) EDS observation of superhydrophobic copper surface as shown in point 1 and (b) the surface after immersion for 120 h as shown in point 2.

6.2.2 Effect of the potential of copper surface modification on the corrosion prevention properties

Figure 6.4 shows the potentiodynamic polarization curves of the bare copper surface, copper stearate presence hydrophobic and superhydrophobic copper surfaces. The hydrophobic and superhydrophobic copper surface was fabricated by immersing copper substrate in ethanolic stearic acid solution for 2 h in the application of only 5 V and 30 V, respectively. The water contact angles of these two surfaces were found to be 135 ° and 156 °, respectively. The corrosion current density (j_{corr}) of the copper surface is found to be 8×10^{-6} A/cm^2. The corrosion current density is reduced to 2×10^{-6} A/cm^2 on the hydrophobic surface which is 4 times smaller than the copper surface. Interestingly, the corrosion current density reduced to 5×10^{-7} A/cm^2 on the superhydrophobic copper surface which is 16 times smaller as compared to the copper surface. Therefore, it could be concluded that the stearic acid modified copper surfaces exhibit anticorrosion properties as compared to a bare copper surface and this property is better for the superhydrophobic copper surface than the hydrophobic copper surface.

Moreover, Table 6.2 shows the relationship between water contact angle and polarization resistance of bare copper surface, hydrophobic and superhydrophobic copper surfaces. The calculation of the polarization resistance from potentiodynamic polarization curves has been presented in the annex I. It is clear from the table 6.2 that the copper substrate with the low water contact angle of 94 ° provides very low polarization resistance of 1 KΩ. The hydrophobic copper surface with smooth copper stearate having water contact angle of 135 ° provides higher polarization resistance of 5 KΩ. In the case of the superhydrophobic surface having water contact angle of 156 ° shows the increased polarization resistance increased of 37 KΩ. The increase of the superhydrophobic properties was found to lead to the increase of the polarization resistance (Rp) as shown in table 6.2. The original data for calculating the polarization resistance as well as the graph has been presented in appendix. It is well known that the polarization resistance is an important parameter to evaluate the anti-corrosion strength of materials. Larger the polarization resistance is better the protection against the corrosion. It seems that the increase in polarization resistance of the surfaces was obtained due to the coating film passivation and barrier properties of the superhydrophobic coating. Amini's et al. [113] used sodium dodecyl sulfate (SDS) for phosphate coating on an AZ31 magnesium alloy surface to improve the anti-corrosion properties. They found that the increase in SDS concentration helped to decrease in corrosion current (i_{corr}) and the increase in Rp. Therefore, it can be conclude from their studies that the phosphate coating was beneficial to obtain higher corrosion resistance properties to the magnesium alloy surfaces.
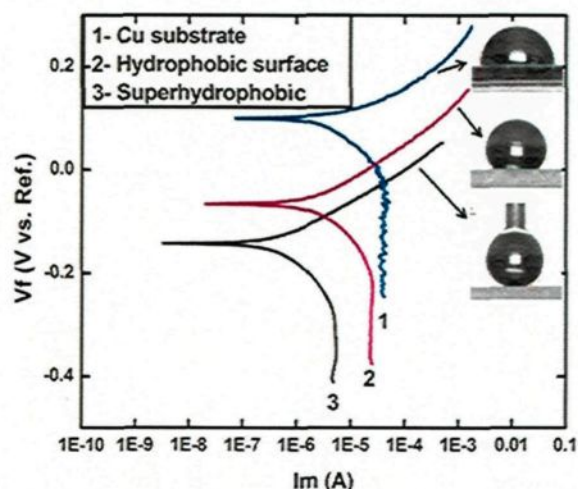
Figure 6.4 Potentiodynamic curves of (1) copper surface, (2) hydrophobic copper surface (formation of copper stearate on copper surface in the application of 5 V) and (3) superhydrophobic copper surface (formation of copper stearate on copper surface in the application of 30 V). The insets show the water drops on each surface.

Table 6.2 The corrosion current and polarization resistance obtained from fig. 6.4 and the water contact angle for each surface.

Surface code	Water contact angle (°)	Corrosion current (A/cm^2)	polarization resistance Rp (KΩ)
Copper substrate	94	8×10^{-6}	1
Hydrophobic surface (2 h at 5 V)	135	2×10^{-6}	5
Superhydrophobic surface (2 h at 30 V)	156	5×10^{-7}	37

6.3 Corrosion test on superhydrophobic aluminum alloy surfaces

Similar to superhydrophobic copper surfaces, the durability of superhydrophobic aluminum alloy surfaces were investigated measuring the water contact angles after immersing them in a high

concentrated 3.5 wt. % NaCl solution. Figure 6.5 shows the variation of water contact angle of superhydrophobic aluminum alloy surfaces as a function of the immersion time. The superhydrophobic aluminum alloy surfaces were fabricated by copper deposition at -0.8 V for 10 minutes followed by electrochemical modifications by stearic acid solution as describes in the sections 5.4.1. The as-prepared superhydrophobic aluminum alloy surface shows a water contact angle of 157 ± 1 ° with roll of properties. The superhydrophobic surfaces immersed in the NaCl solution up to 10 h retain their superhydrophobic properties. The figure 6.5 shows the water contact angle decreased to 152 ± 2 ° after 10 h of immersion. Further increase of the immersion time to 24 h, the water contact angle reduces to 148 ± 7 ° and the surface loss its superhydrophobic properties. The water contact angle of the superhydrophobic surfaces decreased continuously with the increase of the immersing time and reached to 144 ± 2 ° after 48 h of immersion. Finally, it fell to 51 ± 30 ° after the superhydrophobic surface was immersed in the NaCl corrosive solution for 120 h. The superhydrophobic aluminum alloy surface becomes hydrophilic aluminum alloy surface. The relationship between the water contact angle of superhydrophobic aluminum alloy surface with their immersing time in the corrosive solution was investigated by Y. S. Yin et al. [8]. In their study, superhydrophobic aluminum alloy surfaces were prepared by chemically adsorbed myristic acid onto the anodized aluminum alloy surfaces. Sea water was used as the corrosive solution. They observed that the water contact angle of the superhydrophobic aluminum alloy surface decreased to 130 ° after immersing for 24 h.
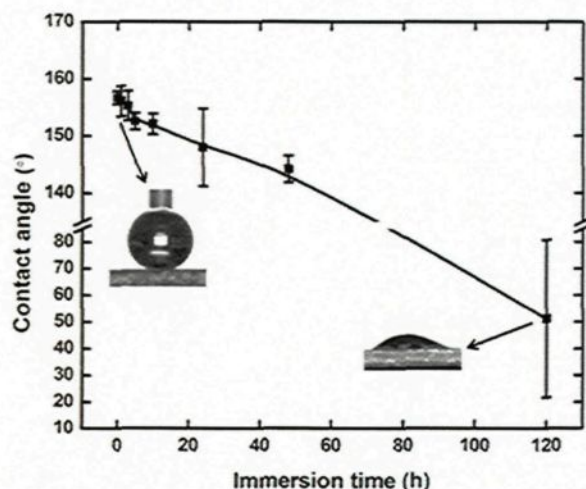
Figure 6.5 Water contact angle of copper plated superhydrophobic aluminum alloy surface after corrosion for a range of time.

It is significant to investigate the reason behind the loss of superhydrophobic properties of the aluminum alloy substrates in the corrosive NaCl solution (3.5 wt. %). The morphological as well as chemical composition changes of the superhydrophobic surfaces were analyzed using SEM and EDS after immersing them in the NaCl solutions.

Figure 6.6(a) and (b) show the copper deposited on aluminum alloy surface for 10 minutes at -0.8 V and the same surface after electrochemical modification with stearic acid solution for 30 minutes at 30 V, respectively. It has been reported in the section of 5.4 as well as seen in figure 6.6(a) and (b) that the electrodeposited copper films are composed of microdots of copper and the stearic acid modified microdots decorated with nanofibres after stearic acid modification. However, some new material appeared and covered on the superhydrophobic aluminum alloy surface after immersion in NaCl solution for 120 h as seen in figure 6.6(c). The chemical composition of the new material was confirmed by the EDS analysis as shown in fig. 6.7 and the chemical reaction during the corrosion process is shown in eq. (6.5- 6.7). The elemental analysis of point 1

(superhydrophobic aluminum alloy surface) and point 2 (superhydrophobic aluminum alloy surface after immersing in the NaCl solution for 120 h) are determine from the EDS spectra of figure 6.7 and presented in table 6.3. The content of Al and O atoms in the flower-like structure on the superhydrophobic surface is found to be 0.65 at. % to 8.62 at. %, respectively. The Al and O atomic percentages increase to 5.59 % to 35.07 %, respectively on the similar flower-like structure after immersing the superhydrophobic aluminum alloy surface in the NaCl solution for 120 h. The enhancement of both Al and O atomic percentage as well as the chemical reaction associated with the corrosion reactions suggest that the possible new compound on the surface might be the $Al(OH)_3$. It has been also observed that the atomic percentages of C as well as Cu are reduced in the corroded surface as compared to superhydrophobic surfaces. The reduction of C and Cu might be associated with the loss of copper stearate coatings either by chemical reactions or by dissociation in the NaCl solutions. It could be visualized that, firstly, the loss of copper stearate from the superhydrophobic aluminum alloy surfaces destroy the essential morphology and finally the formation of $Al(OH)_3$ on the surfaces increase the surface energy. These two effects together transform a superhydrophobic aluminum alloy surface to a hydrophilic aluminum alloy surface.
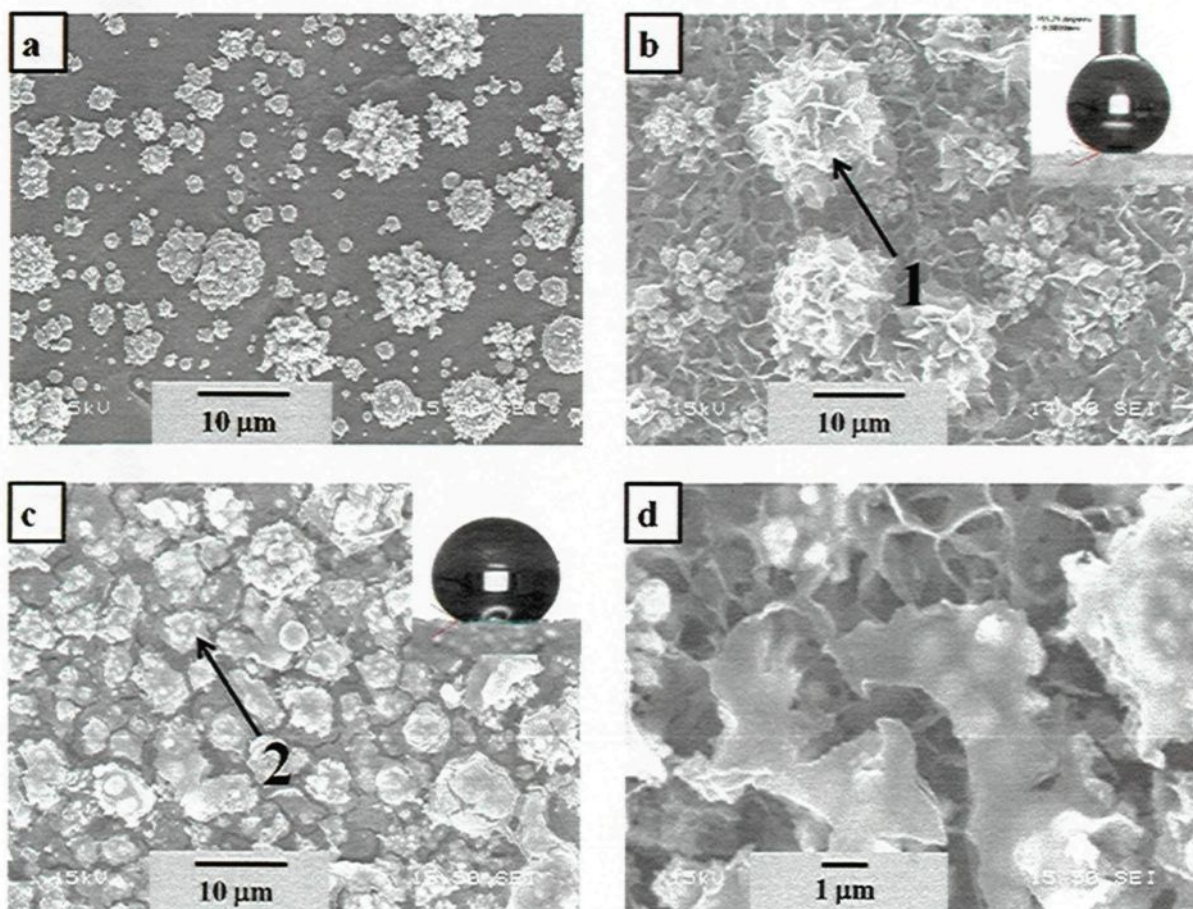
Figure 6.6 SEM images of (a) copper deposited on aluminum alloy for 10 min at -0.8 V followed by electrochemical modification with stearic acid for 30 min at 30 V shown in (b); (c) shows the surface (b) were immersed in NaCl for 120 h and its magnified image (d).
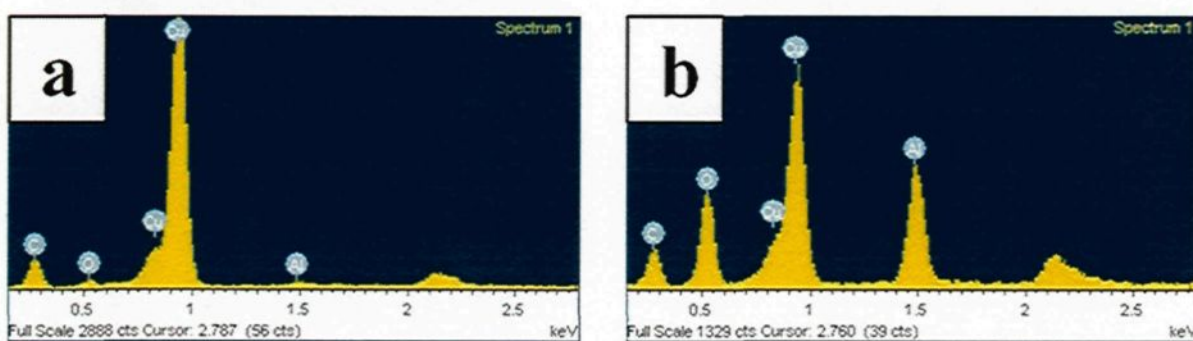
Figure 6.7 EDS observation of superhydrophobic aluminum alloy surface after immersion for 120 h with (a) the particle existed before corrosion and (b) the new particle after corrosion.

Table 6.3 The chemical composition of point (1) (superhydrophobic aluminum alloy surface) and point (2) (superhydrophobic aluminum alloy surface after immersion for 120 h) as determine from the EDS spectra of Figure 6.7.

Element	Point (1) (Atomic %)	Point (2) (Atomic %)
C	70.11	44.07
O	5.59	35.07
Al	0.65	8.62
Cu	23.65	12.24
Total	100	100

$$Al \rightarrow Al^{3+} + 3e^- \qquad \text{(Equation 6.5)}$$

$$O_2 + 4e^- + 2H_2O \rightarrow 4OH^- \qquad \text{(Equation 6.4)}$$

$$Al^{3+} + 3OH^- \rightarrow Al(OH)_3 \qquad \text{(Equation 6.6)}$$
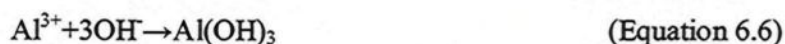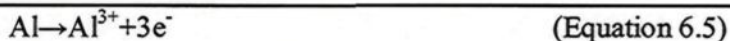
Both of the home-made corrosion tests of the superhydrophobic copper and aluminum alloy surfaces are a kind of galvanic corrosion. Galvanic corrosion occurs when two different metals electrically contact each other and are immersed in an electrolyte. In order for galvanic corrosion to occur, an electrically conductive path and an ionically conductive path are necessary. It is worth to mention that it affects a galvanic couple where the more active metal corrodes at an accelerated rate and the more noble metal corrodes at a retarded rate. Galvanic corrosion is often utilized in sacrificial anodes. It is well known that copper is more noble than aluminum alloy, therefore, when copper deposited aluminum alloy was immersed in NaCl solution, aluminum alloy is used as a sacrificial anode in the copper and aluminum system, so the aluminum alloy is more preferred to be destroyed whereas copper is protected as the cathode. This is one of the most important reasons which leads to the breakdown of the superhydrophobic copper deposited aluminum alloy surface.

CHAPTER 7

CONCLUSIONS AND FUTURE RECOMMENDATIONS

7.1 Conclusions

7.1.1 Preparation of superhydrophobic copper surfaces

The one-step deposition process has been utilized to prepare superhydrophobic copper surfaces. In this process, the copper electrodes were immersed in the stearic acid solution and applied a DC voltage. Morphological and structural analyses of the anodic electrodes show that the surface composed of micrometer size flower-like particles of copper stearate. The anodic copper electrode shows superhydrophobic properties with water contact angle of 157 ± 2 $^{\circ}$ with the rolling off properties of water drops.

Furthermore, the critical potential to achieve superhydrophobic surfaces is found to be the function of time as well as critical time is found to be function of deposition potentials. The critical potential is found to be 25 V for the deposition time 2 h and the critical time is 1.5 h for the deposition potential of 30 V. The increase of the concentration of stearic acid leads to the increase of the formation of copper stearate on the copper surfaces as well as the increase of the water contact angle on the surfaces.

7.1.2 Preparation of superhydrophobic aluminum alloy surfaces

The same methodology of one-step procedure to fabricate superhydrophobic copper surfaces was also used to obtain superhydrophobic aluminum alloy surfaces. The variation of water contact angles on electrochemically modified anodic aluminum alloy surfaces at 30 V remain nearly the

same as 105 ° and independent on the time of modification. However, this method fails to demonstrate superhydrophobic aluminum alloy surfaces. Therefore, two new methods were adopted to prepare superhydrophobic aluminum alloy surfaces. In the first method, aluminum alloy surfaces were etched with NaOH solution followed by passivation with stearic acid solution.

The chemical etching method was also applied to fabricate the superhydrophobic aluminum alloy surfaces. It was found that minimum of 2 minutes of etching using 1 M NaOH solution followed by 30 minutes passivation with stearic acid was necessary to obtain superhydrophobic aluminum alloy surfaces.

In the chemical etching process, aluminum alloy is lost from the surface which is not desirable for the benefit of the aluminum alloy industries. Therefore, we have adopted a second method. In this method, copper film was firstly deposited on aluminum alloy surface followed by electrochemically modification with stearic acid solution for 30 minutes at 30 V.

Superhydrophobic aluminum alloy surfaces have been fabricated by means of electrodeposition of copper on aluminum alloy surfaces followed by electrochemical modification using stearic acid organic molecules. Scanning electron microscopy (SEM) images show that the electrodeposited copper films follow island growth mode in the form of microdots and their number densities increase with the increase of the negative deposition potentials. At an electrodeposition potential of -0.2 V the number density of the copper microdots are found to be 4.5×10^4 cm^{-2} that are increased to 2.9×10^5 cm^{-2} at a potential of -0.8 V. Systematically, the distances between the microdots are found to be reduced from 26.6 μm to 11.03 μm with the increase of negative electrochemical potential from -0.2 V to -0.8 V. The X-ray diffraction (XRD) analyses have

110

confirmed the formation of copper stearate on the stearic acid modified copper films. The roughness of the stearic acid modified electrodeposited copper films is found to increase with the increase in the density of the copper microdots. A critical copper deposition potential of -0.6 V in conjunction with the stearic acid modification provides a surface roughness of 6.2 μm with a water contact angle of 157° resulting superhydrophobic properties on the aluminum alloy substrates.

7.1.3 The corrosion protection property of the superhydrophobic copper and aluminum alloy surfaces

As a conclusion of the corrosion test, we have studied the anti-corrosion properties of superhydrophobic copper and aluminum alloy surfaces by immersing them in the high concentrated (3.5 wt. %) NaCl solution and examined their water contact angles after the immersion. We have also performed refined anti-corrosion test of the superhydrophobic copper surfaces by electrochemical impedance spectroscopy. Both the surfaces show anti-corrosion properties for a certain number of hours in 3.5 wt. % NaCl solution. However, superhydrophobic copper surfaces are more stable than superhydrophobic Al surfaces as prepared in our studies.

7.2 Future recommendations

Applied higher potential (both the potential in one-step process for the fabrication of superhydrophobic copper surface and the applied potential of the copper deposition on aluminum alloy surface) may improve the thickness of the copper stearate film, which may decrease the gap of the coating films on the copper (or aluminum alloy) surfaces and improve the prevention of corrosion on the materials.

Longer modification time (both the deposition time in one-step process for the fabrication of superhydrophobic copper surface and the copper deposition on aluminum alloy surface) may improve the thickness of the copper stearate film, which may decrease the gap of the coating films on the copper (or aluminum alloy) surfaces and improve the prevention of corrosion on the materials.

The material which is more active than Al could be used to instead of the copper film to be the sacrificial anode in order to protect the aluminum alloy which is as the cathode in the new material and aluminum alloy system. Because copper is more noble than aluminum alloy, the aluminum alloy surface is more preferred to be destroyed with deposition of the copper film. The protection of the aluminum alloy surface could be done by depositing a material as the sacrificial anode on the aluminum alloy surface, which is more active than aluminum alloy. The superhydrophobic film could be fabricated on the new material to reduce the contact area between the new material and water or some other environments.

In addition to stearic acid, some materials with-COOH, such as melissic acid, may be applied to prepare superhydrophobic surfaces. Some new coatings can also be used to fabricate superhydrophobic copper and aluminum alloy surfaces, such as silane. Another example is the materials with $-CF_3$ terminated reagents which usually have low surface energy.

Aluminum alloys can also be anodized, formed a thin oxide film on the aluminum alloy surface, to increase corrosion resistance, to increase surface hardness, and to allow dyeing (coloring), improved lubrication, or improved adhesion. The superhydrophobic surface can be fabricated on the anodization of aluminum alloy surface. Micro-nanoporous oxide layer was formed

on the aluminum alloy surface after anodizing process, and such micron-nanostructures can be then modified by low surface energy materials to reduce the surface energy. The formation of the micro-nanostructures as well the low surface energy can lead to the superhydrophobicity of the surface.

PUBLICATIONS

1 "A one-step process to engineer superhydrophobic copper surfaces", Y. Huang, D. K. Sarkar and X.-Grant Chen, Materials Letters 64 (2010) 2722

2 "Fabrication of superhydrophobic surfaces on aluminum alloy via electrodeposition of copper followed by electrochemical modification", Y. Huang, D. K. Sarkar and X.-Grant Chen, Nano-Micro Letters 3 (2011) 160

3 "Preparation of nanostructured superhydrophobic copper and aluminum surfaces", Y. Huang, D. K. Sarkar and X.-Grant Chen, Advanced Materials Research 409 (2012) 497. (Also oral presentation by Y. Huang and proceedings at Thermec 2011: International conference on advanced materials, held on August 1-5, 2011, Quebec city, Canada)

4 "Fabrication of nanostructured superhydrophobic copper by a one step process" Y. Huang, D. K. Sarkar and X.-Grant Chen, p 486-1 to 4, proceeding international conference on nanotechnology fundamentals and applications, held on August 4-6, 2010, Ottawa, Canada.

5 "Corrosion resistance nanostructured superhydrophobic coatings on metal surfaces", Y. Huang, D. K. Sarkar and X.-Grant Chen, Poster presentation by Y. Huang at Journée des étudiants du RÉGAL, October 26, 2010, Quebec city (Received the prize from Aluminum association of Canada).

6 "Protection of metal and alloy surfaces using corrosion resistance nanostructured superhydrophobic coatings", Y. Huang, D. K. Sarkar and X.-Grant Chen, oral and poster

presentation by Y. Huang at Journée des étudiants du RÉGAL, October 03, 2011, Montreal

(Received the best oral speaker, the price of conference)

REFERENCES

1 D. Quéré, *Rep. Prog. Phys.* 68 (2005) 2495.

2 W. Barthlott and C. Neinhuis, *Planta* 202 (1997) 1.

3 S. J. Yuan, S. O. Pehkonen, B. Liang et al., *Corrosion science* 53 (2011) 2738.

4 T. Ishizaki and M. Sakamoto, *Langmuir* 27 (2011) 2375.

5 L. N'u'nez, E. Reguera, F. Corvo, E. Gonzalez, C. Vazquez, *Corros. Sci.* 47 (2005) 461.

6 L. Bacarella, J.C. Griess, *J. Electrochem. Soc.* 120 (1973) 459.

7 J.P. Ferreira and J.A. Rodrigues, *J. Solid State Eletrochem.* 8 (2004) 260.

8 Y.S. Yin, T. Liu, S.G. Chen, T. Liu and S. Cheng, *Applied Surface Science* 255 (2008) 2978.

9 S. E. Potts, L. Schmalz et al., *Journal of the Electrochemical Society* 158 (2011) C132.

10 X.F. Gao and L. Jiang, *Nature*, 432 (2004) 36.

11 Z.J. Wei, W.L. Liu, D. Tian, C.L. Xiao and X.Q. Wang, *Applied Surface Science* 256 (2010) 3972.

12 R.N. Wenzel, *Industrial & Engineering Chemistry* 28 (1936) 988.

13 A.B.D. Cassie and S. Baxter, *Trans. Faraday Soc.* 40 (1944) 546.

14 F. Liu, Y.P. Liu, L. Huang, X.H. Hu, B.Q. Dong, W.Z. Shi, Y.Q. Xie and X. Ye, *Optics Communications* 284 (2011) 2376.

15 P. G. de Gennes, *Rev. Mod. Phys.* 57 (1985) 827.

16 T. Young, *Phil. Trans.* 84 (1805), edited by Peacock, 1, 432.

17 R. E. Jr. Johnson and R. H. Dettre, *Adv. Chem. Ser.* 43 (1964) 112.

18 M. Nosonovsky and B. Bhushan 2008 *Multiscale Dissipative Mechanisms and Hierarchical Surfaces—Friction, Superhydrophobicity, and Biomimetics* (New York: Springer)

19 A. Scardino, R. De Nys, O. Ison, W. O'Connor, P. Steinberg, *Biofouling* 19 (2003) 221.

20 J. D. J. S. Samuel, P. Ruther, H.-P. Frerichs, M. Lehmann, O. Paul, *J. Ruhe, Sens. Actuators, B* 110 (2005) 218.

21 A. Singh, L. Steely, *H. R. Allcock, Polym. Prepr. (ACS, Div. Polym. Chem.)* 46 (2005) 599.

22 H. Gau, S. Herminghaus, P. Lenz, R. Lipowsky, *Science* 283 (1999) 46.

23 T. Liu, Y. Yin, S. Chen, X. Chang, S. Cheng, *Electrochim. Acta* 52 (2007) 3709.

24 K. Satoh, H. Nakazumi, *J. Sol-Gel Sci. Technol.* 27 (2003) 327.

25 T. Kako, A. Nakajima, H. Irie, Z. Kato, K. Uematsu, T. Watanabe, K. Hashimoto, *J. Mater. Sci.* 39 (2004) 547.

26 A. Nakajima, K. Hashimoto, T. Watanabe, *Monatshefte fur Chemie* 132 (2001) 31.

27 D. K. Sarkar and M. Farzaneh, *Journal of Adhesion Science and Technology* 23 (2009) 1215.

28 B. Bhushan, Y.C. Jung and K. Koch, *Langmuir* 25 (2009) 3240.

29 R. Furstner, W. Barthlott, C. Neinhuis and P. Walzel, *Langmuir* 21 (2005) 956.

30 A. Nakajima, K. Hashimoto, T. Watanabe, K. Takai, G. Yamauchi and A. Fujishima, *Langmuir* 16 (2000) 7044.

31 D. Nystrom, J. Lindqvist, E. Ostmark, P. Antoni, A. Carlmark, A. Hult and E. Malmstrom, *ACS Appl. Mater. Interfaces* 1 (2009) 816.

32 R.L. Townsin, *Biofouling* 19 (2003) 9.

33 C. S. Gudipati, J. A. Finlay, J. A. Callow, M. E. Callow and K. L. Wooley, *Langmuir* 21 (2005) 3044.

34 A. Marmur, *Biofouling* 22 (2006) 107.

35 H. Zhang, R. Lamba and J. Lewis, *Sci. Technol. Adv. Mater.* 6 (2005) 236.

36 J. Li, J. Fu, Y. Cong, Y. Wu, L.J. Xue and Y.C. Han, *Applied Surface Science* 252 (2006) 2229.

37 M. Thieme, R. Frenzel, S. Schmidt, F. Simon, A. Hennig, H. Worch, K. Lunkwitz and D. Scharnweber, *Advanced Engineering Materials* 3 (2001) 691.

38 V. Stelmashuk, H. Biederman, D. Slavinska, J. Zemek and M. Trchova, *Vacuum* 77 (2005) 131.

39 S. H. Kim, J. H. Kim, B. K. Kang, and H. S. Uhm, *Langmuir* 21 (2005) 12213.

40 D. Schondelmaier, S. Cramm, R. Klingeler, J. Morenzin, C. Zilkens and W. Eberhardt, *Langmuir* 18 (2002) 6242.

41 E. Hosono, S. Fujihara, I. Honma and H. Zhou, *Journal of the American Chemical Society* 127 (2005) 13458.

42 V. R. Shinde, C. D. Lokhande, R. S. Mane and S. H. Han, *Applied Surface Science* 245 (2005) 407.

43 H. Liu, L. Feng, J. Zhai, L. Jiang and D. B. Zhu, *Langmuir* 20 (2004) 5659.

44 F. Shi, Z. Wang and X. Zhang, *Advanced Materials* 17 (2005) 1005.

45 N. Saleema and M. Farzaneh, *Applied Surface Science* 254 (2008) 2690.

46 J. Zhang, Y. Mo, M. B. Vukmirovic, R. Klie, K. Sasaki and R.R. Adzic, *The Journal of Physical Chemistry B* 108 (2004) 10955.

47 N. Zhao, F. Shi, Z. Wang and X. Zhang, *Langmuir*, 21 (2005) 4713.

48 X. H. Xia, C. M. A. Ashruf, P. J. French and J. J. Kelly, *Chemistry of Materials* 12 (2000) 1671.

49 S. J. Huo, X. K. Xue, Q. X. Li, S. F. Xu, and W. B. Cai, *The Journal of Physical Chemistry* B 110 (2006) 25721.

50 X. F. Wu and G. Q. Shi, *Nanotechnology* 16 (2005) 2056.

51 C. Wang, Y. Song, J. Zhao and X. Xia, *Surface Science* 600 (2006) 38.

52 A. Safaee, D. K. Sarkar and M. Farzaneh, *Applied Surface Science* 254 (2008) 2493.

53 C. D. Gu, H. Ren, J. P. Tu and T. Y. Zhang, *Langmuir* 25 (2009) 12299.

54 Y. Y. Song, Z. D. Gao, J. J. Kelly and X. H. Xia, *Electrochem. Solid-State let.* 8 (2005) 148.

55 D. K. Sarkar and N. Saleema, *Surface& Coatings Technology* 204 (2010) 2483.

56 JCPDS: Cu2O （01-077-0199）

57 JCPDS: Ag (03-065-8428)

58 Q. Chen, C. C. Perry, B. G. Frederick, P. W. Murray and S. Haq, N. V. Richardson, *Surf. Sci.* 446 (2000) 63.

59 D. K. Sarkar, X. J. Zhou, A. Tannous, and K. T. Leung, *J. Phys. Chem.* B 107 (2003) 2879.

60 S. Wang, L. Feng, H. Liu, T. Sun, X. Zhang, L. Jiang and D. Zhu, *Chem. Phys. Chem* 6 (2005) 1475.

61 D. K. Sarkar, M. Farzaneh and R. W. Paynter, *Materials Letters* 62 (2008) 1226.

62 L. N. Pan, H. R. Dong and P. Y. Bi, *Applied Surface Science* 257 (2010) 1707.

63 N. Saleema, D. K. Sarkar, R. W. Paynter and X.-G. Chen, *Applied Materials & Interfaces* 2 (2010) 2500.

64 N. Saleema, M. Farzaneh and R. W. Paynter, *Materials Letters* 63 (2009) 233.

65 J. D. Brassard, D. K. Sarkar and J. Perron, *ACS Appl. Mater. Interfaces* 3 (2011) 3583.

66 D. K. Sarkar, M. Farzaneh and R.W. Paynter, *Applied Surface Science* 256 (2010) 3698.

67 D. Kim, W. Hwang, H.C. Park, K.-H. Lee, Curr. *Appl. Phys.* 8 (2008) 770-773.

68 H. Wang, D. Dai, X. Wu, *Appl. Surf. Sci.* 254 (2008) 5599–5601.

69 S. Hohne, C. Blank, A. Mensch, M. Thieme, R. Frenzel, H. Worch, M. Muller and F. Simon, *Macromol. Chem. Phys.* 210 (2009) 1263.

70 C. S. Lim, M. H. Hong, A. S. Kumar, M. Rahman and X. D. Liu, *Int. J. Mach. Tools Manuf.* 46 (2006) 552.

71 I. Etsion, *Journal of Tribology-Transactions of ASME* 127 (2005) 248.

72 M. F. Chen, Y. P. Chen, W. T. Hsiao and Z. P. Gu, *Thin Solid Films* 515 (2007) 8515.

73 G. R. B. E. Romer, A. J. Huis in't Veld, J. Meijer and M. N. W. Groenendijk, *CIRP Ann.-Manuf.Technol.* 58 (2009) 201.

74 C. Sun, X. W. Zhao, Y. H. Han and Z. Z. Gu, *Thin Solid Films* 516 (2008) 4059.

75 M. A. Amin, E. R. Abd and A. S. El-Lithy, *Corrosion* 55 (2010) 5996.

76 C. Neinhuis and W. Barthlott, *Annals of Botany* 79 (1997) 667.

77 T. Liu, L. Dong, T. Liu and Y. Yin, *Electrochemica Acta* 55 (2010) 5281.

78 T. He, Y. Wang, Y. Zhang, Q. lv, T. Xu and T. Liu, *Corrosion science* 51 (2009) 1757.

79 T. Liu, Y. Yin, S. Chen, X. Chang and S. Cheng, *Electrochimica Acta* 52 (2007) 3709.

80 G. X. Shen, Y. C. Chen, L. Lin, C. J. Lin and D. Scantlebury, Electrochimica Acta 50 (2005) 5083.

81 O. K. Abiola, N. C. Oforka and S. S. Angaye, *Materials Letters* 58 (2004) 3461.

82 J. H. Sui, Z.G. Zhang and W. Cai, *Nuclear Instruments and Methods in Physics Research B.* 267 (2009) 2475.

83 H. F. Li, Y. B. Wang, Y. Cheng and Y. F. Zheng, *Materials Letters* 64 (2010) 1462.

84 F. Bentiss, M. Traisnel, L. Gengembre and M. Lagrene´e, *Applied Surface Science* 152 (1999) 237.

85 C. J. E. Smith, K. R. Baldwin and M. A. H. Hewns, *Institute of Materials* 2 (1993) 1652.

86 O. K. Abiola, *corrosion Science* 48 (2006) 3078.

87 P. M. Barkhudarov, P. B. Shah, E. B. Watkins, D. A. Doshi, C. J. Brinker and J. Majewski, *Corrosion Science* 50 (2008) 897.

88 T. Ishizaki and N. Saito, *Langmuir* 26 (2010) 9749.

89 P. Wang, R. Qiu, D. Zhang, Z.F. Lin and B.R. Hou, *Electrochimica Acta* 56 (2010) 517.

90 Y. S. Yin, T. Liu, S. G. Chen, T. Liu and S. Cheng, *Applied Surface Science* 255 (2008) 2978.

91 H. Q. Liu, S. Szunerits, W. G. Xu and R. Boukherroub, *Applied Materials and Interfaces* 1 (2009) 1150.

92 T. Liu, S. G. Chen, S. Cheng, J.T. Tian, X. T. Chang and Y. S. Yin, *Electrochimica Acta* 52 (2007) 8003.

93 W. Barthlott and C. Neinhuis, *Planta* 202 (1997) 1.

94 J. C. Lee, S. B. Cho, S. J. Lee and S. H. Rhee, *J. Mater. Sci.* 44 (2009) 4531.

95 Copper stearate JCPDS # [00-055-1622]

96 D. K. Sarkar and R. W. Paynter, *Journal of Adhesion Science and Technology* 24 (2010) 1181.

97 X. Zhang, F. Shi, X. Yu, H. Liu, Y. Fu, Z.Q. Wang, L. Jiang, and X.Y. Li, J. AM. *Chem. Soc.* 126 (2004) 3064.

98 Y. Enomoto, *Acta Metallurgica et Materialia* 38 (1990) 173.

99 N.L. Tarwal and P.S. Patil, *Appl. Surf. Sci.* 256 (2010) 7451.

100 V.R. Shinde, T.P. Gujar and C.D. Lokhande, *Sens. Actuators, B* 120 (2007) 551.

101 M. Volmer and A. Z. Weber, *Phys. Chem.* 119 (1926) 277.

102 M. R. Khelladi, L. Mentar, A. Azizi, A. Sahari and A. Kahoul, *Materials Chemistry and Physics* 115 (2009) 385.

103 JCPDS Al (01-085-1327).

104 JCPDS Cu (01-085-1326).

105 S. K. Rawal, A. K. Chawla, V. Chawla, R. Jayaganthan and R. Chandra, *Mater. Sci. Eng. B* 172 (2010) 259.

106 X. Q. Xu, L. Q. Zhu, W. P. Li and H. C. Liu, *Applied Surface Science* 257 (2011) 5524.

107 I. Milosev, T. Kosec and M. Bele, *Journal of applied electrochemistry* 40 (2010) 1317.

108 S. G. Chen, Y. Chen, Y. H. Lei, et al., *Electrochemistry communications* 11 (2009) 1675.

109 X. Yan and G. Y. Xu, *Surface & Coating Technology* 204 (2010) 1514.

110 C. T. Wang, S. H. Chen, H. Y. Ma, L. Hua and N. X. Wang, J. Serb. *Chem. Soc.* 67 (2002) 685.

111 J. P. Ferreira, J. A. Rodrigues and I. T. E. Fonseca, *J Solid State Eletrochem* 8 (2004) 260.

112 (a) R. L. Brian, A. L. Darren, and C. G. Jayne, *Langmuir* 26 (2010) 14671.

(b) I. Milosev, M. Metikos-Hukovic, M. Drogowska, H. Ménard and L. Brossard, *J. Electrochem. Soc.* 2409, (1992)139.

(c) R. N. Parkins and S. Zhou, *Corrosion Science* 39 (1997) 159.

(d) L. B. Niu, T. Goto, T. Nakane, et al., *Journal of The Janpan Institute of Metal* 74 (2010) 635.

113 R. Amini and A.A. Sarabi, *Applied Surface Science* 257 (2011) 7134.